

Electrical and mechanical magnetization torques

Electrical and mechanical magnetization torques

Proefschrift

ter verkrijging van de graad van doctor
aan de Technische Universiteit Delft,
op gezag van de Rector Magnificus prof. dr. ir. J.T. Fokkema,
voorzitter van het College voor Promoties,
in het openbaar te verdedigen op vrijdag 20 januari 2006 om 10:30 uur
door

Alexey Alexeevich KOVALEV

Engineer Physicist in Applied Mathematics and Physics
Moscow Institute of Physics and Technology, Russia
geboren te Kirov, Rusland.

Dit proefschrift is goedgekeurd door de promotoren:

Prof. dr. ir. G. E. W. Bauer

Prof. dr. A. Brataas

Samenstelling promotiecommissie:

Rector Magnificus	voorzitter
Prof.dr.ir. G. E. W. Bauer	Technische Universiteit Delft, promotor
Prof.dr. A. Brataas	Norwegian University of Science and Technology, promotor
Prof.dr. Yu. V. Nazarov	Technische Universiteit Delft
Prof.dr. P. J. French	Technische Universiteit Delft
Prof.dr. P. J. Kelly	Universiteit Twente
Dr. Y. Tserkovnyak	Harvard University
Dr. L. Lagae	Interuniversitair Micro-Elektronica Centrum

Het onderzoek beschreven in dit proefschrift is financieel ondersteund door de stichting voor Fundamenteel Onderzoek der Materie (F.O.M.).

Published by: A. Kovalev

Printed by: Optima Grafische Communicatie, Rotterdam

E-mail: a.a.kovalev@tnw.tudelft.nl

Cover design: the picture from M. Faraday, Quarterly Journal of Science, Vol XII, 1821

Casimir PhD Series, Delft-Leiden, 2006-02

ISBN: 90-8593-009-X

Keywords: Magnetoelectronics, nanomechanics, spin transfer, magnetization dynamics, magnetovibrational coupling

Copyright © 2006 by A. Kovalev

All rights reserved. No part of the material protected by this copyright notice may be reproduced or utilized in any form or by any means, electronic or mechanical, including photocopying, recording or by any information storage and retrieval system, without written permission of the author.

Printed in The Netherlands

*To my wife, Elvin,
and my parents.*

Preface

Physics has been in my life since childhood. I still remember the moment when I decided to learn all laws of nature. A movie about the famous Russian scientist, Mikhail Lomonosov, gave me an impression that I could finish with that project quite quickly – in 10 years maximum. With a grief – I have to admit – I failed. However, that failure had some positive consequences as well; and one of those is this thesis.

The thesis is based upon my studies conducted between January 2002 and January 2006, under the supervision of Profs. Gerrit Bauer and Arne Brataas, at TU Delft. The research that has gone into this thesis has been entirely enjoyable. That enjoyment is largely a result of the interaction that I have had with my supervisors, colleagues and all other people I have met in Holland.

Many, many people have helped me not to get lost during my PhD! I would like to express my heartiest felt gratitude to my leading supervisor Gerrit Bauer from whom I have derived invaluable personal and scientific benefit. This thesis would not have been possible without him. Although it was painful at times when he forced me to express myself clearer, working with him has always been fun, enlightening and delighting. I am very grateful to Arne Brataas who, as my second supervisor, has helped me with my research and provided a warm atmosphere during my visits to him. I am very much indebted to Yaroslav Tserkovnyak who has always been my good friend and from whom I have learned a lot. Yuli Nazarov has always asked good questions during seminars and discussions. Yaroslav Blanter, Milena Grifoni and Jos Thijssen have helped me many times not only with physics but also with things related to life in the Netherlands. I would exclusively like to thank our group secretary, Yvonne Zwang, for always being helpful.

"What a beautiful color, so dynamical and never the same?" One can say about the sky in Holland. However it is somewhat depressive, and sun is absent most of the time. I guess I would have been in extremely low mood all the time if it had not been for people who had shared my free time. I will always be grateful to Sabrina Rahmanovic, Raymond de Moré, Jasper Lim, Dennise, and Velimir Meded for always being there for me and being my friends. I am very lucky I have met you! I also have many good memories about AEGEE students who do great job for international newcomers to Delft.

The everyday struggle of academic research is a battle won or lost with ones' buddies

in the trenches, not by the generals in the history books. Consider my debt of gratitude to my colleagues, for everything from arguing on philosophical subjects, to advising me on my research. Omar Usmani was always ready to help whenever I had a trouble. Babak Hosseinkhani shared my dinners with quite tasty pizzas that we used to order to the office. I would like to thank Sijmen Gerritsen, Wouter Wetzels, Freek Langeveld, and Miriam Blaauboer for trying to teach me Dutch language. I thank our current and former postdocs – Sigurdur Erlingsson, Antonio DiLorenzo, Daniel Huertas Hernando, Inanc Adagideli, Dmitri Bagrets, Dmytro Fedorets, Henri Saarikoski and Wataru Izumida for giving me many good advices. I am grateful to Oleg Jouravlev for all those moments when he was silent, and I could better concentrate on my work. I acknowledge Floris Zwanenburg for his efforts in organizing spin meetings. Jens Tobiska was always ready to discuss physics whenever I needed it. It has been a very enjoyable experience for me to play football with Hayk Haroutyunyan, Rachid el Boubsi and people from QT group. Let me also mention Fabian Bodoky, Xuhui Wang, Jan Manschot, Izak Snyman, Jeroen Danon, Catherine Fricot, Richard de Visser, Joël Peguiron, Moosa Hatami, and Gabriele Campagnano.

I owe so much to my parents, Alexey Alexeevich, and Antonina Alexandrovna, for giving me life in the first place, for educating me with aspects from both arts and sciences, for unconditional support and encouragement to pursue my interests. Thank you, my high school teachers, Margarita Anatolyevna Prokashva and Pavel Evgenyevich Kanin, who created my chance for academic career. I have a lot of gratitude to my diploma supervisor in Moscow Institute of Physics and Technology, Alexandr Fedorovich Barabanov, who introduced me to the field of theoretical physics.

And last, as they say, but not least, I would like to thank my better half, Elvin, whose imagination and energy never let me be bored, whose passion can cover the whole world and whose cleverness make me wonder. However princesses are more seldom in the modern world, she always reminds me of one. Elvin brings love into my life, and what can be a better motivation to live on and be successful.

Contents

1	Introduction	1
1.1	Nanoelectromechanical systems (NEMS)	5
1.2	Magnetoelectronic circuit theory	7
1.2.1	Landauer-Büttiker formalism	7
1.2.2	Spin resolved version of Landauer-Büttiker formalism	8
1.2.3	Charge and spin currents in FIN multilayer structures	9
1.3	Spin-transfer effect	10
1.4	Spin-flip in diffusive systems	11
1.5	Magnetization dynamics	12
1.6	Magnetomechanical torques	15
1.7	Electro-magnetic and spin-transfer motors	17
1.8	This thesis	19
	References	20
2	Spin transfer in diffusive ferromagnet-normal metal systems with spin-flip scattering	23
2.1	Introduction	24
2.2	Diffusive approach to multilayer systems	25
2.3	Results for systems without spin-flip	28
2.4	Results for systems with spin-flip	31
2.5	Conclusion	34
2.A	Appendix: Circuit theory approach to the diffusive systems	35
2.B	Appendix: Treatment of interfaces	37
	References	38
3	Perpendicular spin valves with ultra-thin ferromagnetic layers	41
3.1	Introduction	42
3.2	Magnetoelectronic circuit theory and diffusion equation for spin valves	43
3.2.1	Magnetoelectronic circuit theory and diffusion equation	44

3.2.2	Extraction of the mixing conductance from experiment and asymmetric spin valves	45
3.2.3	Analysis of symmetric F N F N F structures	48
3.3	Coherent regime	50
3.3.1	Extended magnetoelectronic circuit theory	50
3.3.2	Observation of ferromagnetic coherence in transport experiments	52
3.3.3	Three terminal device for observation of coherence effects	54
3.4	Conclusion	57
3.A	Appendix: Analytical results for F N F N F structure.	57
	References	58
4	Magnetomechanical torques in small magnetic cantilevers	61
4.1	Introduction	62
4.2	System	63
4.2.1	Magnetization motion in a single-domain ferromagnet	63
4.2.2	Small magnetization oscillations and dependence of FMR broadening on shape and crystal anisotropies	64
4.2.3	Nonlinear magnetization oscillations	65
4.2.4	Cantilever oscillations and coupled magneto-mechanical equations	67
4.2.5	Entirely ferromagnetic cantilever	69
4.3	Small magnetization oscillations	71
4.3.1	Magnet at the tip of cantilever	71
4.3.2	Ferromagnetic cantilever	73
4.3.3	Observation	74
4.4	Probing magnetization dynamics by spin-transfer torques	76
4.4.1	Electrical detection of FMR	76
4.4.2	Electrical detection of magnetovibrational mode	77
4.5	Large magnetization cones and magnetization reversal in the presence of coupling	80
4.5.1	Resonant magnetization oscillations and reversal	80
4.5.2	Non-resonant magnetization oscillations and reversal	84
4.6	Conclusion	86
	References	86
	Summary	91
	Samenvatting	95
	Curriculum Vitae	99

List of publications

101

Chapter 1

Introduction

Charge current is the motion of charge. An electron charge current is induced in a conducting wire by an applied voltage. But electrons have also a mass and an intrinsic angular momentum - spin. Then the motion of electrons is associated to a mass current as well as an angular momentum (spin) current. In ferromagnetic metals the density of states for spin-up and spin-down conductance electrons is shifted in energy (Fig. 1.1) due to the exchange field - the mean field resulting from exchange interactions of itinerant electrons. This leads to splitting of all spin 1/2-electrons into two kinds: spin-up and spin-down electrons that are eigen states in the ferromagnet. Electrons from this two channels are scattered differently when sent through a ferromagnet with a difference between the spin-up and spin-down densities of states at the Fermi level. It is then useful to define conductances for spin-up (G_{\uparrow}) and spin-down (G_{\downarrow}) electrons. A current in a ferromagnet can be represented then as split flow of spin-up and spin-down electrons in two channels with different conductances. An unpolarized current results in a spin-polarized current after passing through a ferromagnet, as it follows from the two channel model. The degree of polarization of outgoing current is characterized by the polarization P of a ferromagnet that is defined in terms of the conductances for spin-up (G_{\uparrow}) and spin-down (G_{\downarrow}) electrons, as $P = (G_{\uparrow} - G_{\downarrow}) / (G_{\uparrow} + G_{\downarrow})$ (for example *Fe*, *Co* or *Ni* have a polarization P of 40 to 70% [1]).

The field of magnetoelectronics is based on two important discoveries: giant magnetoresistance effect (GMR) [2] and spin-transfer effect [3, 4]. The GMR effect arises in ferromagnet-normal metal-ferromagnet (FINIF) structures (with current perpendicular to the plane CPP geometry) in which the magnetizations can be switched from anti-parallel to parallel configurations. Usually the switching is achieved by an external magnetic field that acts on a soft magnet with easily rotated magnetization (free layer) while the other magnetization is fixed *e.g.* by a strong anisotropy. The GMR effect can be defined as a very large change in electrical resistance that is observed in a multilayer structure when the relative orientations of magnetizations change as a function of applied field. The

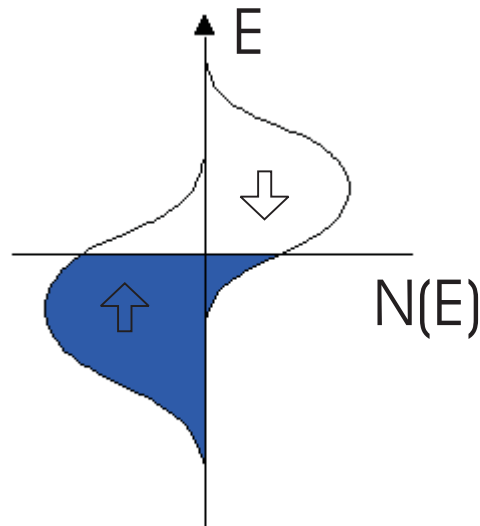


Figure 1.1: A schematic representation of the density of electronic states in a ferromagnet. E , the electron energy; $N(E)$, density of states.

change in electrical resistance can be easily explained by a two resistor model with different resistances in parallel for the spin-up and spin-down electrons (Fig. 1.2). The fixed ferromagnet may be interpreted as a spin polarizer, letting through more spin-up electrons thus creating a spin polarized current collinear to its magnetization. For antiparallel configurations the spin polarized current can not escape the normal metal spacer so easily and thus an imbalance of spin-up and spin-down electrons (spin accumulation) is created in the normal metal.

When the magnetizations of the ferromagnets are not collinear, the situation becomes more complicated and a non-collinear to the free layer spin-current and spin imbalance can appear in the normal metal. For reasons that are explained in Section 1.3, the non-collinear spin current can only partially penetrate the free layer; its transverse component is completely absorbed at the interface. As a direct consequence of angular momentum conservation, the macroscopic magnetization receives a torque equal to the absorbed angular momentum (Fig. 1.3). The spin-transfer torque can then be defined as the angular momentum acquired by the macroscopic magnetization per unit of time due to the interaction with spin-polarized currents.

Since the prediction in 1996 [3, 4], and supporting evidence for its presence starting in 1998 [5, 6], the spin-transfer torque effect has attracted much theoretical [7–11] and experimental [5, 12–16] interest in the phenomenon of current-driven excitations in magnetic multilayers: such as the reversal of layer magnetization with a possibility of steady precessional states [16, 17], or the generation of spinwaves [18]. This interest is sparked by the wish to understand the physics underlying the new phenomenon as well as its potential for devices. Some of these applications are magnetization switching in

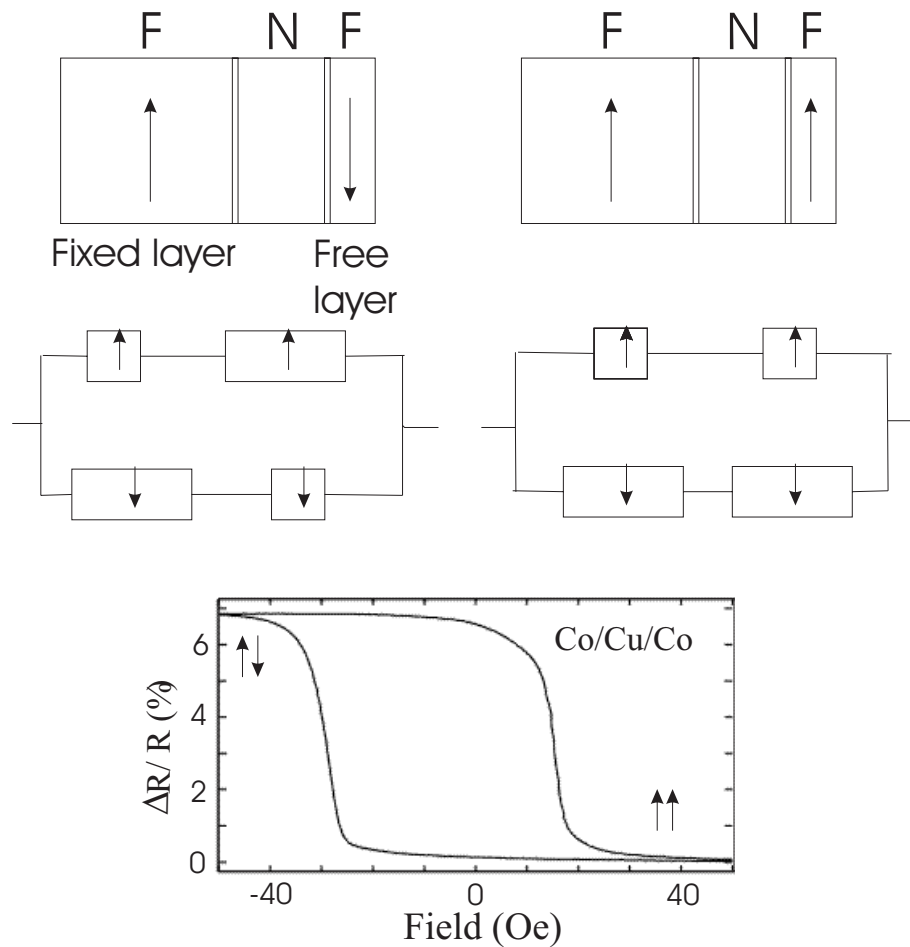


Figure 1.2: The resistance of a ferromagnet-normal metal-ferromagnet structure depends on the magnetic configuration. In the collinear geometry the spin current can be split into two channels. Due to different band structure of the minority and majority-spin bands, the resistances of two channels are different in ferromagnets leading to GMR effect. One magnet is fixed e.g. by anisotropies while the other follows the external magnetic field.

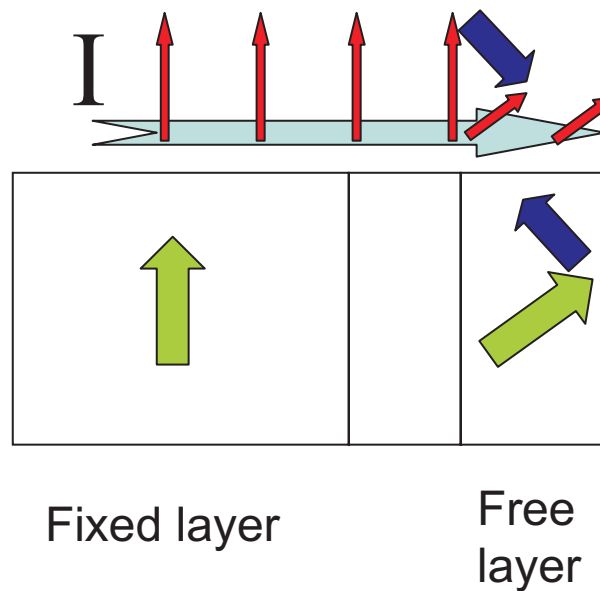


Figure 1.3: Current I is sent through the spin valve. Due to interaction with the magnetization of a free layer the transverse spin polarization of the spin current is absorbed at the interface. By conservation of angular momentum, the spin current exerts an equal and opposite torque on the magnetization.

magnetic memories [19], and generation of high frequency radiation [17]. In state of art magnetic devices or media, externally generated magnetic fields are employed to reverse the moments [20–22]. A current pulse through perpendicular FINIF spin valves can reverse the free layer magnetization more effectively in small structures since one does not waste energy on generation of magnetic field outside of the sample, thus also improving possibilities for further miniaturization.

The macroscopic magnetization can also acquire torques from the lattice. These torques can be mediated by *e.g.* crystal or shape anisotropy fields. In fact, any magnetization dynamics, that is caused by interactions with the lattice, lead to torques acting on both the lattice and the magnetization. This transfer of torques can be seen as a result of the conservation law of angular momentum, that is to say: the torque received by the magnetization should be equal to the torque lost by the lattice. We call these kind of torques as *magnetomechanical torques*. Magnetomechanical torques generated by demagnetizing currents in samples with shape anisotropy [23] promise new functionalities for mechanical transducers (nanomotors). Predicted some time ago [24] and observed experimentally [25], magnetomechanical torques due to ferromagnetic resonance (FMR) open new possibilities for sensors and detectors. Magnetic resonance force microscopy (MRFM) employs similar principles and it has already proven to be a powerful imaging technique [26].

In the first part of this Introduction we deal with nanoelectromechanical systems that

can be used for detecting magnetomechanical torques. Then we proceed to magnetoelectronic circuit theory that is a very convenient tool for describing spin-transfer torques. We introduce the Landauer-Büttiker formalism, since spin-resolved scattering theory of transport is an important ingredient of magnetoelectronic circuit theory. Next, the spin-transfer torque effect is described. The Landau-Lifshitz-Gilbert equation is introduced in Section 1.5 allowing us to describe the magnetization dynamics as a result of magnetic fields and, in generalized form, spin-transfer torques. Finally we describe several examples in which magnetomechanical torques arise and show one of possible applications for magnetomechanical and spin-transfer torques - nanomotors. We show that at small scales the spin-transfer torque may dominate torques created by Larmor response in electro-magnetic motors.

1.1 Nanoelectromechanical systems (NEMS)

The study of nanoelectromechanical systems (NEMS) [27–29] is a newly developing branch of mesoscopic physics that appeared after recent advances in nanostructure technology. A typical NEMS device contains a nano-to-micron scale mechanical resonator, *e.g.* a cantilever - a suspended beam which is clamped at one end (Fig. 1.4). The mechanical resonator can then be coupled electrostatically [30] or via magnetomotive forces [31] to an electric circuit. A mechanical resonator holds a number of normal vibrational modes that is comparable to the number of atoms, but only the lowest flexural modes are usually excited. For small amplitudes, a mechanical resonator is described by a harmonic oscillator with different modes provided the quality factor is sufficiently large. The quality factor for a given oscillator is defined as $Q = \omega_e/\beta$, where ω_e is the frequency of the mode and β is a damping constant related to the time $1/\beta$ necessary for the energy stored in the oscillator to decay by a factor e from its initial value. Nano-to-micron scale mechanical resonators typically display quality factors for the lowest modes in the range $10^3 - 10^4$ [26].

According to the general theory of elasticity [32], the dynamics of a cantilever are described by the elastodynamical equations for the strain tensor. The general problem is three dimensional and it can become nonlinear. For a long beam the problem simplifies significantly when the bending or torsion is small. The beam should be thin compared to the radius of curvature in the case of bending. In case of torsion, compared to the length at which two points have difference in torsion by π . Under such conditions the elastodynamical equations can be integrated in the transverse direction leading to the equations of bending and torsional motions of a beam [32]:

$$\rho S \frac{\partial^2 X(y,t)}{\partial t^2} - EI_z \frac{\partial^4 X(y,t)}{\partial y^4} - 2\beta_x \rho S \frac{\partial X(y,t)}{\partial t} = f_x, \quad (1.1)$$

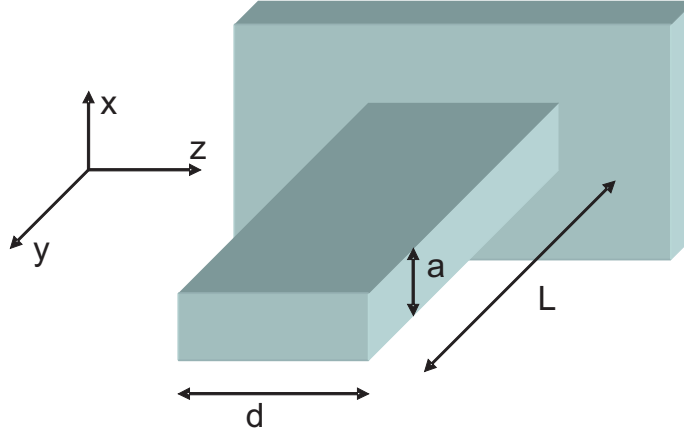


Figure 1.4: A suspended beam (cantilever) clamped at one end.

$$\rho S \frac{\partial^2 Z(y,t)}{\partial t^2} - EI_x \frac{\partial^4 Z(y,t)}{\partial y^4} - 2\beta_z \rho S \frac{\partial Z(y,t)}{\partial t} = f_z, \quad (1.2)$$

$$\rho I \frac{\partial^2 \varphi(y,t)}{\partial t^2} - C \frac{\partial^2 \varphi(y,t)}{\partial y^2} - 2\beta_\varphi \rho I \frac{\partial \varphi}{\partial t} = f_\varphi, \quad (1.3)$$

where $X(y,t)$ and $Z(y,t)$ are the displacements of the cantilever from its equilibrium position, $\varphi(y,t)$ is the angle of torsion, $I = I_x + I_z$ ($I_x = \int x^2 dz dx$, $I_z = \int z^2 dz dx$) is the moment of inertia of the cross-section about its center of mass, ρ is the mass density, E is Young's modulus, S is the cross section, C is an elastic constant defined by the shape and material of the cantilever ($C = \frac{1}{3}\mu da^3$ for a plate with thickness a much smaller than width d , $a \ll d$, μ is the Lamé constant), $f_{x(z)}$ is an external force per unit length and f_φ is an external torque in the y direction per unit length.

Let us first analyze one of the bending modes. In case of small damping and no external force applied, the solution can be found immediately by separating variables:

$$X(y,t) = e^{i\omega t} (b_1 \cosh(ky) + b_2 \sinh(ky) + b_3 \cos(ky) + b_4 \sin(ky))$$

where $k^2 = \sqrt{\rho S / (EI)} (\omega - i\beta)$ and the coefficients b_i are determined by the boundary conditions. For a cantilever clamped at one end, the resonant frequencies can be found as

$$v_b = \frac{\alpha_n^2}{2\pi L^2} \sqrt{\frac{EI_z}{\rho S}}$$

with $\alpha_n = k_n L$ and k_n being a solution of the equation $1 + \cosh(kL) \cos(kL) = 0$. For example, a cantilever with length $L = 1 \mu\text{m}$ and thickness $a = 0.03 \mu\text{m}$ has the lowest mode frequency $v_b = 0.56 \frac{a}{L^2} \sqrt{\frac{E}{12\rho}} \approx 40 \text{MHz}$ assuming the bulk material values for silicon (Si): $E = 1.5 \times 10^{11} \text{Nm}^{-2}$ [33] and $\rho = 2.33 \times 10^3 \text{kgm}^{-3}$.

Let us repeat the same analysis for the torsional mode that has the form:

$$\varphi(y,t) = e^{i\omega t} (b_1 \cos(ky) + b_2 \sin(ky)),$$

where $k = (\omega - i\beta)/c$ is the wave number, $c = \sqrt{C/(\rho I)}$ and the coefficients b_i are again determined by the boundary conditions. For a cantilever clamped at one end, the resonant frequencies can be found as

$$v_t = \frac{c(1/2 + n)}{2L}$$

with $n = 0, 1, 2, 3, \dots$. For the same cantilever as above and with $a \ll d$ the lowest mode frequency is $v_t = c/(4L) \approx 1\text{GHz}$ ($\mu \sim 100\text{GPa}$ [33], $d = 0.1\mu\text{m}$). NEMS oscillating at frequencies in the GHz range have already been observed [31].

1.2 Magneto-electronic circuit theory

Magneto-electronic circuit theory [34] provides a powerful tool for analyzing electron spin and charge transport in disordered or chaotic FIN heterostructures with static magnetic configurations in the CPP geometry. Since this approach is a convenient tool for describing the spin-transfer effect, we give here a brief account of the theory.

1.2.1 Landauer-Büttiker formalism

Consider several reservoirs $1..i..N$ at chemical potentials μ_i coupled by ideal leads (*i.e.* without back scattering) to some scattering region. The reservoirs serve both as a source and sink of carriers. Let us determine the currents in the leads that connect the reservoirs with the scattering region. For sufficiently small biases the potentials μ_i are within a narrow range at the Fermi energy so that the energy dependence of transmission and reflection probabilities can be disregarded. Let us introduce a special chemical potential μ_0 that is the smallest of the μ_i . Below μ_0 , all states with positive and negative velocities are filled and consequently, we can consider only potentials $\Delta\mu_i = \mu_i - \mu_0$. The reservoir i injects a current $e v_i (dn_i/dE) \Delta\mu_i$ into lead i . Here v_i is the velocity and $dn_i/dE = 1/(2\pi\hbar v_i)$ density of states for carriers at the Fermi energy. The current $(e/h) \Delta\mu_i$ provided by the reservoir i is combined with the reflected current $-R_{ii}(e/h) \Delta\mu_i$ and sum over all transmitted currents from other reservoirs $-\sum_{j \neq i} T_{ij}(e/h) \Delta\mu_j$ where T_{ij} and R_{ii} are elastic scattering probabilities for an incident carrier to be transmitted from a reservoir j into the reservoir i and to be reflected from reservoir i back into reservoir i , respectively.

The current in lead i thus becomes

$$I_i = \frac{e}{h} \left[\left(\sum_{j \neq i} T_{ij} \Delta \mu_j \right) - (M - R_{ii}) \Delta \mu_i \right] \quad (1.4)$$

where M is the number of channels in lead i . Elastic scattering probabilities can be expressed via the reflection matrix $(r_{ii})_{mn}$ for the reservoir i and the transmission matrix from reservoir i to reservoir j , $(t_{ji})_{mn}$ (m and n describe channels in leads):

$$R_{ii} = \text{Tr} \left[r_{ii} (r_{ii})^\dagger \right]$$

$$T_{ji} = \text{Tr} \left[t_{ji} (t_{ji})^\dagger \right]$$

1.2.2 Spin resolved version of Landauer-Büttiker formalism

Let us generalize the Landauer-Büttiker formalism to the case when reservoirs are replaced by chaotic normal nodes that can have quasiequilibrium spin accumulations. The transport through the leads can be expressed in terms of the energy-dependent isotropic distribution functions $\hat{f}_i(\varepsilon)$ in each node, that are 2×2 energy-dependent matrices in spin space of spin-1/2 electrons. The distribution functions are related to local electrochemical potentials μ_c^i and spin accumulations μ_s^i in the nodes:

$$\mu_c^i = \frac{1}{2} \int_{\varepsilon_0}^{\infty} d\varepsilon \text{Tr} [\hat{f}_i(\varepsilon)] \quad (1.5)$$

$$\mu_s^i = \frac{1}{2} \int_{\varepsilon_0}^{\infty} d\varepsilon \text{Tr} [\hat{\sigma} \hat{f}_i(\varepsilon)] \quad (1.6)$$

where a reference energy ε_0 lies below the Fermi energy by much more than the thermal energy and potential voltage biases and $\hat{\sigma} = (\sigma_x, \sigma_y, \sigma_z)$ is a vector of the Pauli matrices.

Intuitively or by formal derivation, one can generalize Eq. (1.4) to the case of spin-dependent transport [34]:

$$\hat{I}_i = \frac{e}{h} \left\{ \sum_{j \neq i} \left[\sum_{mn} \hat{t}_{ij}^{mn} \hat{f}_j (\hat{t}_{ij}^{mn})^\dagger \right] - (M \hat{f}_i - \sum_{mn} \hat{r}_{ii}^{mn} \hat{f}_i (\hat{r}_{ii}^{mn})^\dagger) \right\} \quad (1.7)$$

where mn index designates summation over all incident and outgoing channels, ij designates the nodes and \hat{I} is the 2×2 tensor current related to spin \mathbf{I}_s and charge I_0 currents as $\hat{I} = (\hat{1} I_0 + \hat{\sigma} \cdot \mathbf{I}_s) / 2$, where $\hat{1}$ is the 2×2 unit matrix.

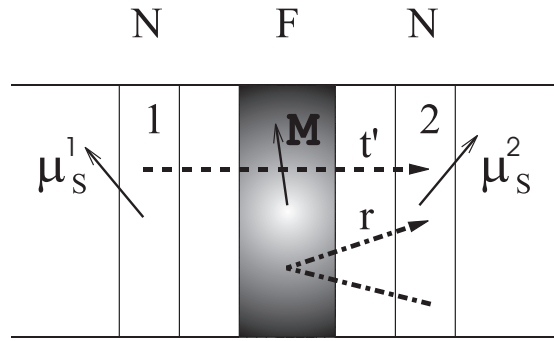


Figure 1.5: NI|F|N2 circuit element of an arbitrary multilayered spin valve structure (μ_s^i describes spin accumulation in normal metals).

1.2.3 Charge and spin currents in F|N multilayer structures

An arbitrary multilayered spin valve structure (or a multiterminal device) can be divided into smaller elements; the same way as electronic circuit can be divided into resistive elements allowing formulation of Kirchoff's rules. For convenience, we chose an N|F|N composite to be a generalized resistive element in our spin valve and we connect the resistive elements by ideal leads and nodes taken in normal metals (*e.g.* setup in Fig. 1.3 consists of two N|F|N elements). The charge current is conserved in each node and, provided spin flip in the nodes is small, the same is true for the spin current. Here we disregard spin flip processes since they are usually small and can be disregarded. However, in some cases they have to be taken into account [35] (Section 1.4).

Let us apply Eq. (1.7) to a N1|F|N2 circuit element, choosing the normal metals as nodes (Fig. 1.5). Non-collinear spin accumulation in the nodes are created by currents from other non-specified regions of the device. The entire F layer including the interfaces is considered as a magnetic scatterer. On the normal metal side in the region 2

$$\hat{I} = \frac{e}{h} \left\{ \sum_{mn} [\hat{t}'^{mn} \hat{f}^{N1} (\hat{r}^{mn})^\dagger - (\delta_{mn} \hat{f}^{N2} - \hat{r}^{mn} \hat{f}^{N2} (\hat{r}^{mn})^\dagger)] \right\} \quad (1.8)$$

where \hat{r}^{mn} is the spin-dependent reflection coefficient for electrons reflected from channel n into channel m in the node 2, \hat{t}'^{mn} is the spin dependent transmission coefficient for electrons transmitted from channel n in the node 1 into channel m in the node 2.

In the absence of spin-flip processes, the matrices \hat{r}^{mn} and \hat{t}'^{mn} should be diagonal in spin space provided the axis z is parallel to the magnetization of the ferromagnet (we are free to chose this reference frame). Expanding the spin-dependent distribution matrices in nodes 1 and 2 into 2×2 Pauli and unit matrices; $\hat{f}^N = \hat{1} f_0^N + \hat{\sigma} \mathbf{f}_s^N$ and the unit vector \mathbf{m}_z parallel to the axis z , we obtain for spin and charge currents in the node 2:

$$I_0 = (G_\uparrow + G_\downarrow) \Delta f_0^N + (G_\uparrow - G_\downarrow) \Delta \mathbf{f}_s^N \cdot \mathbf{m}_z \quad (1.9)$$

$$\begin{aligned}
\mathbf{I}_s = & \mathbf{m}_z [(G_\uparrow - G_\downarrow)\Delta f_0^N + (G_\uparrow + G_\downarrow)\Delta \mathbf{f}_s^N] \\
& - 2(\mathbf{m}_z \times \mathbf{f}_s^{N2} \times \mathbf{m}_z) \text{Re} G_{\uparrow\downarrow}^r + 2(\mathbf{f}_s^{N2} \times \mathbf{m}_z) \text{Im} G_{\uparrow\downarrow}^r \\
& + 2(\mathbf{m}_z \times \mathbf{f}_s^{N1} \times \mathbf{m}_z) \text{Re} G_{\uparrow\downarrow}^t - 2(\mathbf{f}_s^{N1} \times \mathbf{m}_z) \text{Im} G_{\uparrow\downarrow}^t
\end{aligned} \tag{1.10}$$

where $\Delta f_0^N = f_0^{N1} - f_0^{N2}$ and $\Delta \mathbf{f}_s^N = \mathbf{f}_s^{N1} - \mathbf{f}_s^{N2}$. We introduced spin up(down) conductances $G_{\uparrow(\downarrow)} = \frac{e^2}{h} \sum_{nm} t_{nm}^{\uparrow(\downarrow)} (t_{nm}^{\uparrow(\downarrow)})^*$, and mixing conductance and transmission $G_{\uparrow\downarrow}^r = \frac{e^2}{h} \sum_{nm} [\delta_{nm} - (r_{nm}^\uparrow)^* r_{nm}^\downarrow]$ and $G_{\uparrow\downarrow}^t = \frac{e^2}{h} \sum_{nm} t_{nm}^{\uparrow} (t_{nm}^{\downarrow})^*$, respectively.

1.3 Spin-transfer effect

The spin-transfer effect arises when one sends charge currents through spin valves with noncollinear magnetizations (Fig. 1.3). The transverse spin-current in the normal metal spacer is absorbed by the free layer magnetization. The cause of the absorption is band-structure mismatch between majority and minority conductance bands in the ferromagnet (Fig. 1.1) and conductance band in the normal metal [9]. This mismatch leads to absorption of the transverse component via two mechanisms: the spin-dependent scattering at the interface and the destructive interference of transverse components of electron spins entering the ferromagnet [34]. The interference appears since electron states from the normal metal are not eigenstates in the ferromagnet and have to be represented as a linear combinations of two states with k_\uparrow^F and k_\downarrow^F wave vectors. In ferromagnets with a large cross-section area, a large number of transverse modes exists and up and down states follow paths of different lengths before arriving to some arbitrary chosen point in the ferromagnet. The difference in wave vectors for two states propagating in the ferromagnet is equivalent to a spin precession around the exchange field. The phase acquired during the precession is proportional to the path length and thus averaging over all such paths eliminates the transverse component of the spins provided the exchange magnetic field is strong enough and the point is far enough from the interface. The distance at which the transverse component of the spin current disappears is called the ferromagnetic coherence length (λ_c). An electron spin, travelling a distance Δ in the ferromagnet, acquires rotation by a phase $\Delta(k_\uparrow^F - k_\downarrow^F)$. The coherence length, λ_c can then be estimated as $\lambda_c = \pi/|k_\uparrow^F - k_\downarrow^F|$. In transition metals the coherence length is much smaller than all other length scales such as spin-diffusion length or mean free path which is confirmed by band structure calculations [9].

One can obtain the same result from the magnetoelectronic circuit theory Eq. (1.10). This theory is also applicable when the node 2 in Fig. 1.5 is a ferromagnet and the scattering element is the interface of the ferromagnet with the normal metal. This allows us to describe the absorption of the transverse spin current in a ferromagnet. Since spin-up and -down states are eigen states in the ferromagnet, the distribution function in the ferromag-

netic node, \hat{f}^F , does not have transverse spin-components. According to Eq. (1.10), the transverse spin current is then proportional to the transverse component of \hat{f}^N and to the mixing transmission $G_{\uparrow\downarrow}^t = \frac{e^2}{h} \sum_{nm} t_{nm}^{\uparrow} (t_{nm}^{\downarrow})^*$. Due to the exchange field, the product of the transmission coefficients acquire rapidly oscillating phase factor as a function of the length of the trajectory. Consequently, after averaging over all channels, the transverse spin current quickly decays in the ferromagnet. According to band structure calculations for transition metals, the mixing transmission decays at length of $\lesssim 1$ nm [36] (becoming even smaller with disorder). Since the coherence length is the smallest length scale even smaller than the mean free path, the spin transfer effectively happens at the interface. The situation is different for weak ferromagnets in which λ_c may be larger.

1.4 Spin-flip in diffusive systems

The torques, due to the spin-transfer effect can be modified by spin-orbit interactions, interactions with magnetic impurities or nonuniform magnetizations at interfaces, leading to a partial angular momentum transfer to the lattice. Such effects are a source of small mechanical torques that may even affect the motion of small mechanical structures [37]. The spin-orbit (SO) interaction is a relativistic correction to the motion of electrons in an electric field. The Hamiltonian for the spin-orbit interaction is

$$H_{SO} = \frac{\alpha}{\hbar k_F^2} [\hat{\boldsymbol{\sigma}} \times \nabla V] \cdot \hat{\mathbf{p}} \quad (1.11)$$

where $\hat{\mathbf{p}}$ and $\hat{\boldsymbol{\sigma}}$ are the operators for momentum and electron spin respectively, α is the dimensionless spin-orbit coupling constant and ∇V is the gradient of the electrostatic potential due to non-magnetic impurities. The spin-orbit interaction becomes important for heavy (large atomic number Z) elements. Interactions with magnetic impurities can be introduced by

$$H_{sm} = V_{sm}(\mathbf{r}) \hat{\boldsymbol{\sigma}} \cdot \mathbf{S}(\mathbf{r}) \quad (1.12)$$

where $V_{sm}(\mathbf{r})$ is the strength of the coupling of the itinerant electron spin to the spin of the magnetic impurity $\mathbf{S}(\mathbf{r})$. The general problem of spin-transfer in the presence of the above effects is complicated. In case of isotropic diffusive system, the mentioned effects can be included in the spin-diffusion equation for both ferromagnets and normal metals [34]. The diffusion equations for charge and spin can be obtained after substitution of currents in equation:

$$\partial_x j_0 = 0, \quad \frac{\partial}{\partial x} \mathbf{j}_s = \mathbf{f}_s / \tau_{sf}, \quad (1.13)$$

where the spin-flip relaxation time $1/\tau_{sf} = 1/\tau_{so} + 1/\tau_{sm}$ is a material dependent parameter that includes the spin-flip due to magnetic and non-magnetic impurities. The

charge and spin currents in the normal metal are $j^N = D\partial_x f_0^N$ and $\mathbf{j}_s^N = D\partial_x \mathbf{f}_s^N$ respectively, where f_0^N and \mathbf{f}_s^N are the local charge and spin distribution functions defined as $\widehat{f}^N = \widehat{1}f_0^N + \widehat{\sigma} \cdot \mathbf{f}_s^N$, and D is the diffusion constant. In the ferromagnet, the particle and spin currents are $j^F = (D_\uparrow \partial_x f_\uparrow + D_\downarrow \partial_x f_\downarrow)/2$ and $\mathbf{j}_s^F = \mathbf{m}\partial_x (D_\uparrow f_\uparrow - D_\downarrow f_\downarrow)/2$, where D_\uparrow and D_\downarrow are the diffusion constants for spin-up and spin-down electrons. The diffusion equation in the normal metal:

$$\partial_x^2 D f_0^N = 0, \quad \frac{\partial^2}{\partial x^2} D \mathbf{f}_s^N = \mathbf{f}_s / \tau_{sf}^N,$$

and in the ferromagnet:

$$\partial_x^2 (D_\uparrow f_\uparrow + D_\downarrow f_\downarrow) = 0, \quad \frac{\partial^2}{\partial x^2} (D_\uparrow f_\uparrow - D_\downarrow f_\downarrow) = (f_\uparrow - f_\downarrow) / \tau_{sf}^F.$$

1.5 Magnetization dynamics

The dynamics of the order parameter of small magnetic clusters and films is a basic problem of condensed matter physics with considerable potential for technological applications [38, 39]. Here we describe a phenomenological approach that is usually used to describe the magnetization dynamics.

We would like to consider temperatures well below the ferromagnetic critical temperature T_c , so that the equilibrium magnetization density saturates to some material-specific value M_s/V where V is the volume of the ferromagnet. Since we are interested in the low energy excitations in the ferromagnet, only slow motions of the magnetization density with a fixed magnitude are relevant, however, the magnetization direction can still vary with coordinate. Thus equation for the magnetization density must be written as follows

$$\frac{\partial \mathbf{M}(\mathbf{r}, t)}{\partial t} = \boldsymbol{\Omega} \times \mathbf{M}(\mathbf{r}, t) \quad (1.14)$$

where $\boldsymbol{\Omega}$ is some angular velocity that in principle can vary during the dynamics (we are not considering second derivative since we are interested in slow dynamics). The equilibrium state of the ferromagnet can be found by minimizing the Gibbs free energy when temperature T , volume V and external magnetic field \mathbf{H} are constant. Let us introduce an effective field \mathbf{H}_{eff} :

$$\delta \widetilde{F} = - \int \mathbf{H}_{\text{eff}} \delta \mathbf{M} dV,$$

where $\delta \widetilde{F}$ is a variation of the Gibbs free energy as a result of $\delta \mathbf{M}$. The energy dissipated

by the magnet as the magnetization moves

$$Q = T \left(\frac{\partial S}{\partial t} \right)_{TVH} = -\frac{\partial \tilde{F}}{\partial t},$$

where Q is the rate of energy dissipation and S is the entropy (for solids with $T \ll T_c$ we can consider zero temperature limit, thus temperature does not appear in formulas any further). Using Eq. (1.14) we have

$$Q = \int \mathbf{H}_{\text{eff}} \frac{\partial \mathbf{M}}{\partial t} dV = \int \mathbf{H}_{\text{eff}} [\boldsymbol{\Omega} \times \mathbf{M}(\mathbf{r}, t)] dV.$$

We can conclude that the dynamics is dissipationless when $\boldsymbol{\Omega} = \text{const} \cdot \mathbf{H}_{\text{eff}}$. To lowest order in magnetizations the magnetic part of the Gibbs free energy is of the form:

$$E_{mg} = \int \sum_{ij} \left(\frac{1}{2} A_{ij} \frac{\partial \mathbf{M}}{\partial x_i} \frac{\partial \mathbf{M}}{\partial x_j} + \frac{1}{2} D_{ij} M_i M_j - \mathbf{M} \mathbf{H} \right) dV, \quad (1.15)$$

where symmetric tensors A_{ij} and D_{ij} describe the exchange stiffness and anisotropies of the ferromagnet respectively. The effective field is a functional derivative of the magnetic Gibbs free energy:

$$\mathbf{H}_{\text{eff}} = \sum_{ij} \left(A_{ij} \frac{\partial^2 \mathbf{M}}{\partial x_i \partial x_j} - D_{ij} M_i \mathbf{x}_j \right) + \mathbf{H} \quad (1.16)$$

We can now find the constant by considering a ferromagnet with uniform magnetization and without anisotropies, which according to Eq. (1.16) means $\mathbf{H}_{\text{eff}} = \mathbf{H}$. The behavior of a moment in an external magnetic field \mathbf{H} is well known

$$\frac{d\mathbf{M}}{dt} = -\gamma \mathbf{M} \times \mathbf{H},$$

and we arrive at the conclusion $\text{const} = \gamma$.

In reality, the magnetization dynamics leads to some small dissipation due to interactions with conduction electrons and generation of spin-waves (magnons). Landau and Lifshitz introduced dissipation in a phenomenological way, arriving at what is known as Landau-Lifshitz (LL) equation:

$$\frac{d\mathbf{M}}{dt} = -\gamma \mathbf{M} \times \mathbf{H}_{\text{eff}} + \frac{\lambda}{M_s} \mathbf{M} \times (\mathbf{M} \times \mathbf{H}_{\text{eff}}), \quad (1.17)$$

where λ is a material constant describing damping. In 1955 Gilbert developed a Lagrangian formulation of the magnetization dynamics where the role of the generalized coordinates is played by the components of the magnetization M_x , M_y and M_z . In this

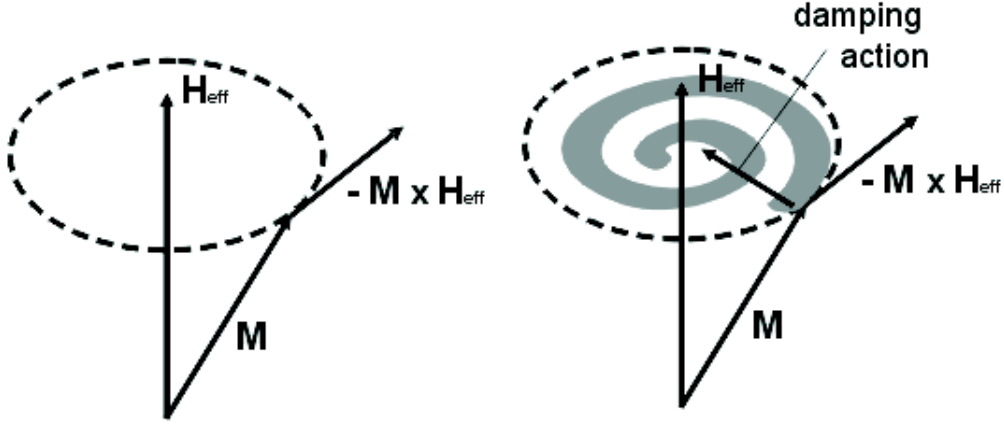


Figure 1.6: (left) Undamped magnetization precession. (right) Damped magnetization precession (\mathbf{H}_{eff} describes the effective magnetic field).

framework, the phenomenological dissipation is introduced quite naturally as a 'viscous' force, whose components are proportional to the time derivatives of the generalized coordinates. The resulting Landau-Lifshitz-Gilbert (LLG) equation has the form [40, 41]:

$$\frac{d\mathbf{M}}{dt} = -\gamma\mathbf{M} \times \mathbf{H}_{\text{eff}} + \frac{\alpha}{M_s}\mathbf{M} \times \frac{d\mathbf{M}}{dt}, \quad (1.18)$$

where the phenomenological Gilbert constant is typically $\alpha \leq 0.01$. Note that for small damping (which is usually the case) both LL and LLG equations are equivalent and therefore it does not matter which equation to use.

The dynamics due to LL or LLG equation is represented schematically in Fig. 1.6. The first term is responsible for the rotation around the effective field as shown in the left figure. The damping term creates a torque that pushes the magnetization in the direction of the effective field as it is shown on the right in Fig. 1.6.

In Section 1.3 we concluded that in ferromagnets thicker than the ferromagnetic coherence length the transverse component of spin-current is absorbed by the magnetization. The torque transferred to the magnetization can be easily expressed as $\tau = -\frac{\hbar}{2e}\mathbf{m} \times (\mathbf{I}_s \times \mathbf{m})$ where \mathbf{m} is a unit vector along the magnetization. The normal metal can receive angular momentum as a result of the adiabatic response (spin pumping) of the electrons in the normal metal to the time-dependent magnetization dynamics, leading to dynamical torques on the magnetization [42]. For uniform magnetization densities, we generalize LLG equation by accounting for the extra torques (spin-transfer torques and

dynamical torques respectively):

$$\frac{d\mathbf{M}}{dt} = -\gamma\mathbf{M} \times \mathbf{H}_{\text{eff}} + \frac{\alpha}{M_s}\mathbf{M} \times \frac{d\mathbf{M}}{dt} - \gamma\frac{\hbar}{V2e}\mathbf{m} \times (\mathbf{I}_s \times \mathbf{m}) \quad (1.19)$$

$$- \gamma\frac{\hbar^2}{V2e^2} \left(\text{Re}(G_{\uparrow\downarrow}^r - G_{\uparrow\downarrow}^t)\mathbf{m} \times \frac{d\mathbf{m}}{dt} + \text{Im}(G_{\uparrow\downarrow}^r - G_{\uparrow\downarrow}^t)\frac{d\mathbf{m}}{dt} \right). \quad (1.20)$$

$$(1.21)$$

Current-induced magnetization dynamics can be realized in perpendicular spin valves with one hard (fixed) ferromagnet that acts as a polarizer and a second soft (free layer) ferromagnet that reacts on the spin-transfer torque. A recent beautiful experiment allowed time domain measurement of macrospin magnetization dynamics driven by the spin-transfer torque [17].

The knowledge of the magnetization dynamics is very important for magnetization reversal applications, such as random-access memories (MRAM) [19]. Ultra-fast mechanisms of magnetization reversal, like the so-called precessional switching (Fig. 1.7) in which the magnetization vector traces straight paths on the unit sphere, attract a lot of attention [20–22]. Techniques of magnetization reversal by the spin-transfer torque in magnetic layers [5, 6, 15–17] as well as in magnetic wires with domain walls [43, 44] may be employed in applications soon. Completely different switching strategies, *e.g.* using antiferromagnets [45], capture interest as well.

1.6 Magnetomechanical torques

Magnetomechanical torques (forces) provide the coupling between a mechanical resonator and spins. The principle of the Magnetic Resonance Force Microscopy (MRFM) is based on such a coupling [26]. A sample is placed on a force microscope cantilever (Fig. 1.8) and a permanent magnet generates a magnetic field gradient which exerts a force on the cantilever. The force originates either from unpaired electron spins in the sample or from nuclear magnetic moments. The sample magnetization is then modulated by a radio-frequency coil at the resonant frequency of the cantilever resulting in its excitation that is measured by optical-fiber interferometry.

The MRFM technique can be used for detection of the ferromagnetic resonance (FMR). In one of realizations, one directly measures the magnetomechanical torques acting on the lattice [25]. The torsional mode of the cantilever is employed (Fig. 1.9) and the magnetomechanical torques can be understood from the LLG Eq. (1.18). When rf fields are constantly pumping the magnetization motion, the magnetization precesses around the equilibrium direction for each cycle, losing some part of its momentum due to the Gilbert

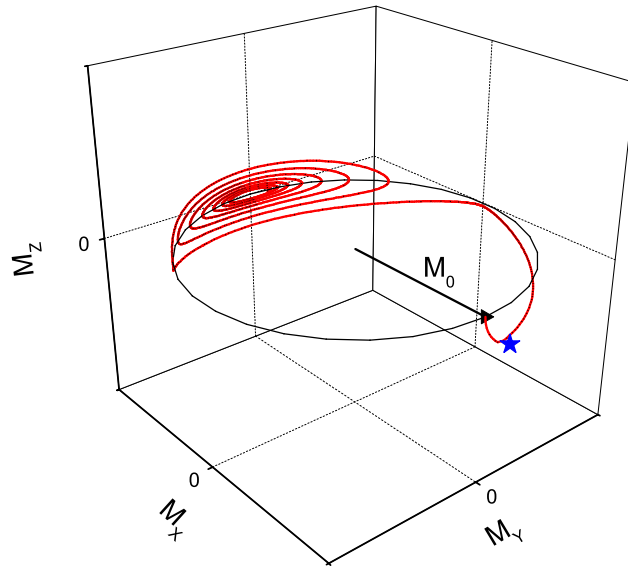


Figure 1.7: Precessional switching. A short magnetic pulse is applied until the moment designated by star, after that the magnetization evolves due to demagnetizing field along z -direction for a thin film in $x - y$ plane.

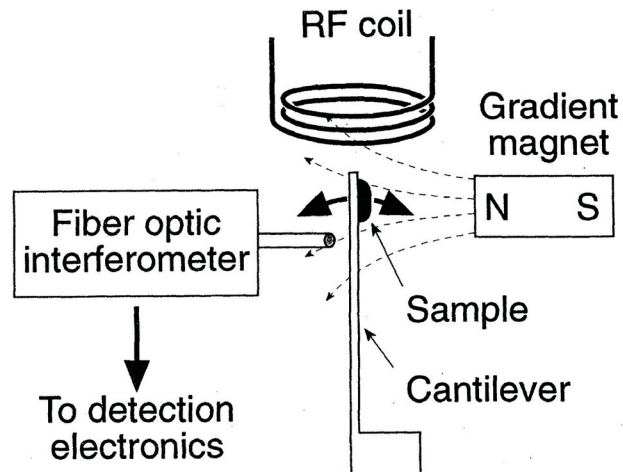


Figure 1.8: Typical Magnetic Resonance Force Microscopy setup [26].

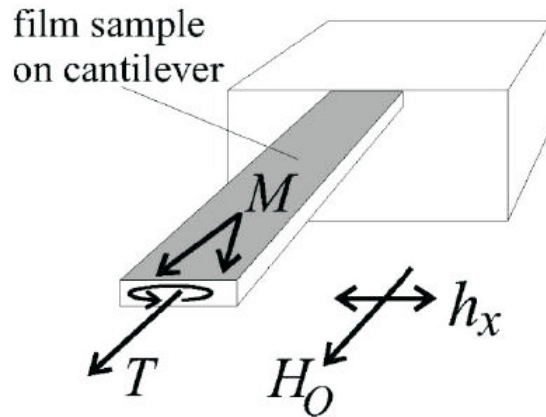


Figure 1.9: Mechanical detection of FMR (\mathbf{H}_0 is an external magnetic field and \mathbf{h}_x is an oscillating rf magnetic field) [25].

damping. The momentum that is thereby transferred to the lattice causes a torsion of the cantilever that can be observed.

1.7 Electro-magnetic and spin-transfer motors

Using a broad definition of "motor" as apparatus that converts electrical energy into motion, most sources cite Faraday as developing the demonstration devices in 1821. Most people nowadays wouldn't recognize them as anything resembling a modern electric motor.

The classic motor has a rotating armature in the form of an electromagnet with two poles. A rotary switch called a commutator reverses the direction of the electric current twice every cycle, to flow through the armature so that the poles of the electromagnet push and pull against the permanent magnets on the outside of the motor. As the poles of the armature electromagnet pass the poles of the permanent magnets, the commutator reverses the polarity of the armature electromagnet. During that instant of switching polarity, inertia keeps the classical motor going in the proper direction (See Fig. 1.10).

A maximum torque generated by the structure in Fig. 1.10 is

$$\tau_{DC} = BSI$$

where B is the magnetic flux density (usually ferromagnetic materials can not exceed 1.5T before they saturate, for these reasons, 1 T will be taken as the maximum flux density), S is the cross-section of the armature and I is the charge current flowing in the structure.

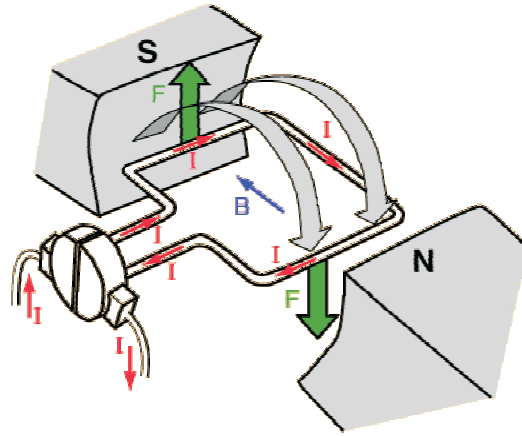


Figure 1.10: An electro-magnetic motor operated by DC currents (current I is sent through the armature, \mathbf{B} is the magnetic flux generated by permanent magnets).

One can see that as the motor becomes N times smaller the ratio torque/current becomes N^2 smaller. A maximal spin-transfer torque can be estimated as (see Section 1.5)

$$\tau_{ST} = I\hbar/(2e)$$

where the torque is equal to the angular momentum transferred by spins of the current I . By comparing these two torques we conclude that in structures smaller than 10 – 100 nm the spin-transfer torques are dominant. The spin-transfer motor does not require generation of magnetic fields which is advantageous for small structures.

In a realization of a motor that is based on spin-transfer torques, one needs to employ magnetomechanical torques in order to transfer the spin-transfer torques to the mechanical motion. One of the possible realizations of the spin-transfer motor is presented in Fig. 1.11. In this multilayer structure one of the magnetizations is rigidly fixed (*e.g.* by a strong crystal anisotropy) and the other is free (due to strong shape anisotropy it only moves in the plane of the film). The middle normal metal has no spin-flip. Let us first suppose that the whole structure can not move. Then due to spin-transfer torques the magnetizations align parallel for one direction of the current, while for the other direction of the current antiparallel [4] (see Fig. 1.11 and Chapter 2 of this thesis). Suppose for a while that the magnetization has inertia (a small external magnetic field along the rotor can provide the effect of inertia, forcing the magnetization to keep rotation at parallel or antiparallel instants when no other torque acts on the magnetizations) and we reverse the direction of the current every time the magnetizations are parallel or antiparallel. In this case, the magnetization in the free layer starts to rotate as a propeller. However, a torque in the direction of the propeller rotation acts on the fixed layer as well and consequently on the whole rotor. The rotor starts to rotate when released. In order to transfer the charge current to the rotor, one may use a conducting liquid which may be preferable for

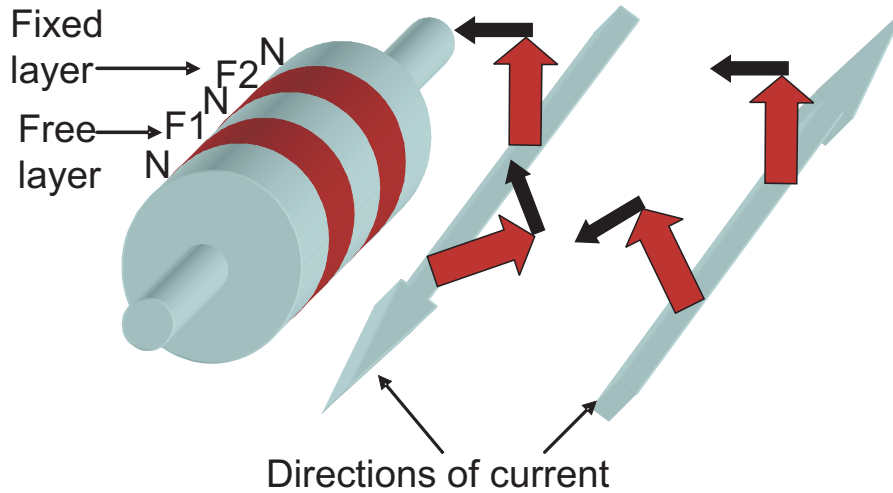


Figure 1.11: A realization of the spin-transfer motor. A rotor consists of two ferromagnetic layers, one of which is fixed. The spin-transfer torques are shown by smaller arrows.

small scales. For simplicity, we suppose that all spin-flip happens in reservoirs and in the conducting liquid.

Another realization of the spin-transfer motor contains two ferromagnetic layers that have fixed by anisotropies magnetizations (see Fig. 1.11). The maximal torques are generated when the angle between the magnetizations is 90 degrees. For this realization we do not need to reverse the current, and the rotor rotates due to the spin-transfer torque when a DC current is sent through the structure (see Fig. 1.11). The quantitative analysis of the spin-transfer motor is presented in an upcoming publication (to be published in Applied Physics Letters).

1.8 This thesis

In the second chapter of the thesis, we consider the spin-transfer effect in metallic FINIF multilayer structures. By applying the diffusion equation, we calculate the angular magnetoresistance and torques for asymmetric structures.

Spin-flip is taken into account at the end of the second chapter and further in the third chapter. The latter chapter also deals with electron interference effects in ferromagnetic layers with thickness of the order of the ferromagnetic coherence length. In this case, the transverse component of the spin-current is not completely absorbed due to the destructive interference, therefore, part of it can transmit through the ferromagnet. This has an effect on the spin-transfer torque and transport equations.

In the last chapter, we consider the *magnetomechanical* torques in the regime of the resonant magnetovibrational coupling. The transfer of energy from the magnetization motion into the mechanical motion and *vice versa* is optimal in this regime. We propose

a transducer of mechanical motion that is based on the spin-transfer torque effect and on resonant magnetovibrational coupling. Finally, in the same chapter, we consider the full magnetization reversal induced by magnetovibrational coupling.

References

- [1] J. Bass and W. Pratt, Jr., *J. Magn. Magn. Mater.* **200**, 274 (1999).
- [2] M. Baibich, J. M. Broto, A. Fert, F. N. V. Dau, F. Petroff, P. Eitenne, G. Creuzet, A. Friederich, and J. Chazelas, *Phys. Rev. Lett.* **61**, 2472 (1988).
- [3] L. Berger, *Phys. Rev. B* **54**, 9353 (1996).
- [4] J. C. Slonczewski, *J. Magn. Magn. Mater.* **159**, L1 (1996).
- [5] E. B. Myers, D. C. Ralph, J. A. Katine, R. N. Louie, and R. A. Buhrman, *Science* **285**, 867 (1999).
- [6] M. Tsoi, A. Jansen, J. Bass, W. Chiang, M. Seck, V. Tsoi, and P. Wyder, *Phys. Rev. Lett.* **80**, 4281 (1998).
- [7] Y. B. Bazaliy, B. A. Jones, and S.-C. Zhang, *Phys. Rev. B* **57**, R3213 (1998).
- [8] A. Brataas, Y. V. Nazarov, and G. E. W. Bauer, *Phys. Rev. Lett.* **84**, 2481 (2000).
- [9] M. D. Stiles and A. Zangwill, *Phys. Rev. B* **66**, 014407 (2002).
- [10] X. Waintal, E. B. Myers, P. W. Brouwer, and D. C. Ralph, *Phys. Rev. B* **62**, 12317 (2000).
- [11] K. Xia, P. J. Kelly, G. E. W. Bauer, A. Brataas, and I. Turek, *Phys. Rev. B* **65**, 220401(R) (2002).
- [12] J. Grollier, V. Cros, A. Hamzic, J. M. George, H. Jaffres, A. Fret, G. Faini, J. B. Youssef, and H. Legall, *Appl. Phys. Lett.* **78**, 3663 (2001).
- [13] J. A. Katine, F. J. Albert, R. A. Buhrman, E. B. Myers, and D. C. Ralph, *Phys. Rev. Lett.* **84**, 3149 (2000).
- [14] J.-E. Wegrowe, X. Hoffer, P. Guittienne, A. Fabian, L. Gravier, and T. Wade, *J. Appl. Phys.* **91**, 6806 (2002).
- [15] J. Wegrowe, D. Kelly, Y. Jaccard, P. Guittienne, and J. Ansermet, *Europhys. Lett.* **45**, 626 (1999).

-
- [16] S. I. Kiselev, J. C. Sankey, I. N. Krivorotov, N. C. Emley, R. J. Schoelkopf, R. A. Buhrman, and D. C. Ralph, *Nature* **425**, 380 (2003).
- [17] I. N. Krivorotov, N. C. Emley, J. C. Sankey, S. I. Kiselev, D. C. Ralph, and R. A. Buhrman, *Science* **307**, 228 (2005).
- [18] S. Kaka, M. R. Pufall, W. H. Rippard, T. J. Silva, S. E. Russek, and J. A. Katine, *Nature* **437**, 389 (2005).
- [19] S. S. P. Parkin, *Applications of Magnetic Nanostructures* (Taylor and Francis, New York, U.S.A, 2002), p. 237.
- [20] C. H. Back, D. Weller, J. Heidmann, D. Mauri, D. Guarisco, E. L. Garwin, and H. C. Siegmann, *Phys. Rev. Lett.* **81**, 3251 (1998).
- [21] T. Gerrits, H. van den Berg, J. Hohlfeld, L. Bär, and T. Rasing, *Nature* **418**, 509 (2002).
- [22] H. W. Schumacher, C. Chappert, P. Crozat, R. C. Sousa, P. P. Freitas, J. Miltat, J. Fassbender, and B. Hillebrands, *Phys. Rev. Lett.* **90**, 0117201 (2003).
- [23] A. Kovalev, G.E.W.Bauer, and A. Brataas, *Appl. Phys. Lett.* **83**(8), 1584 (2003).
- [24] O. Benda, *IEEE Trans. Mag.* **5**, 921 (1969).
- [25] A. Jander, J. Moreland, and P. Kabos, *Appl. Phys. Lett.* **78**, 2348 (2001).
- [26] J. A. Sidles, J. L. Garbini, K. J. Bruland, D. Rugar, O. Zuger, S. Hoen, and C. S. Yannoni, *Rev. Mod. Phys.* **67**, 249 (1995).
- [27] M. L. Roukes, *Physics World* **14** (2), 25 (2001), cond-mat/0008187.
- [28] M. Blencowe, *Phys. Rep.* **395**, 159 (2004).
- [29] K. C. Schwab and M. L. Roukes, *Phys. Today* (2005).
- [30] M. D. LaHaye, O. Buu, B. Camarota, and K. C. Schwab, *Science* **304**, 74 (2004).
- [31] X. M. H. Huang, C. A. Zorman, M. Mehregany, and M. Roukes, *Nature* **421**, 496 (2003).
- [32] L. D. Landau and E. M. Lifshitz, *Theory of elasticity* (Pergamon, Oxford, 1959), 2nd ed.
- [33] M. G. Simmons and H. Wang, *Single crystal elastic constants and calculated aggregate properties* (MIT Press, 1975).

-
- [34] A. Brataas, Y. V. Nazarov, and G. E. W. Bauer, *Eur. Phys. J. B* **22**, 99 (2001).
- [35] W. Park, D. V. Baxter, S. Steenwyk, I. Moraru, W. Pratt, Jr., and J. Bass, *Phys. Rev. B* **62**, 1178 (2000).
- [36] M. Zwierzycki, Y. Tserkovnyak, P. Kelly, A. Brataas, and G. Bauer, *Phys. Rev. B* (2005).
- [37] P. Mohanty, G. Zolfagharkhani, S. Kettemann, and P. Fulde, *Phys. Rev. B* **70**, 195301 (2004).
- [38] B. Hillebrands and K. O. (Eds.), *Spin Dynamics in Confined Magnetic Structures* (Springer, Berlin, 2003).
- [39] S. Maekawa and T. S. (Eds.), *Applications of Magnetic Nanostructures* (Taylor and Francis, New York, 2002).
- [40] T. L. Gilbert, *Phys. Rev.* **100**, 1243 (1955).
- [41] T. L. Gilbert, *IEEE Trans. Mag.* **40**, 3443 (2004).
- [42] Y. Tserkovnyak, A. Brataas, and G. E. W. Bauer, *Phys. Rev. Lett.* **88**, 117601 (2002).
- [43] G. Tatara and H. Kohno, *Phys. Rev. Lett.* **92**, 086601 (2004).
- [44] T. O. A. Yamaguchi, S. Nasu, K. Miyake, K. Mibu, and T. Shinjo, *Phys. Rev. Lett.* **92**, 077205 (2004).
- [45] A. V. Kimel, A. Kirilyuk, P. A. Usachev, R. V. Pisarev, A. M. Balbashov, and T. Rasing, *Nature* **435**, 655 (2004).

Chapter 2

Spin transfer in diffusive ferromagnet-normal metal systems with spin-flip scattering

The spin transfer in biased disordered ferromagnet (F) - normal metal (N) systems is calculated by the diffusion equation. For F1-N2-F2 and N1-F1-N2-F2-N3 spin valves, the effect of spin-flip processes in the normal metal and ferromagnet parts are obtained analytically. Spin-flip in the center metal N2 reduces the spin-transfer, whereas spin-flip in the outer normal metals N1 and N3 can increase it by effectively enhancing the spin polarization of the device.

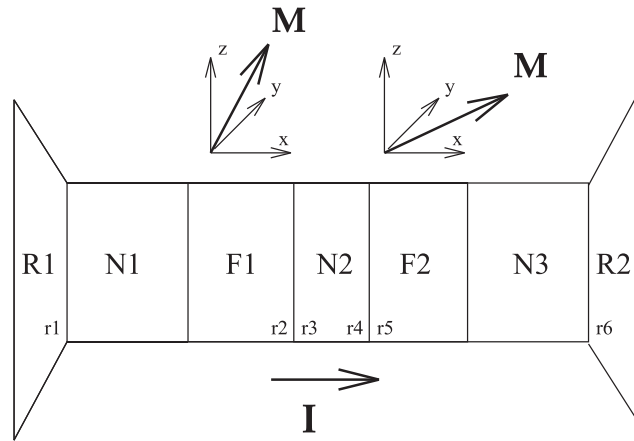


Figure 2.1: *N1-F1-N2-F2-N3 multilayer system with noncollinear magnetizations.*

2.1 Introduction

A spin-polarized electric current flowing through magnetic multilayers with canted magnetizations produces torques on the magnetic moments of the ferromagnets [1, 2]. The effect is inverse to the giant magnetoresistance, in which a current is affected by the relative orientation of the magnetization directions. The spin-current-induced magnetization torque arises from an interaction between conduction electron spins and the magnetic order parameter, transferring angular momentum between ferromagnetic layers, hence the name “spin transfer”. The observed asymmetry of the switching with respect to the direction of current flow in the magnetization switching in cobalt layers [3–6] is strong evidence that spin transfer dominates charge current-induced Oersted magnetic fields in mesoscopic small structures. Spin-transfer devices are promising for applications by the ability to excite and probe the dynamics of magnetic moments at small length scales. Reversing magnetizations with little power consumption can be utilized in current-controlled magnetic memory elements. As a result the spin-transfer effect has already been the subject of several theoretical studies [7–15].

The torque can be formulated by scattering theory in terms of the spin dependence of the reflection coefficients of the interface and the incoherence of spin-up and -down states inside the ferromagnet. This leads to a destructive interference of the component of the spin current perpendicular to the magnetization over the ferromagnetic decoherence length, which is smaller than the mean free path for not too weak ferromagnets [7–11, 14, 15]. In this paper we solve the spin-dependent diffusion equation for a multilayer system consisting of two reservoirs, three normal metal layers, and two ferromagnetic layers, (see Fig. 2.1), generalizing the approach of Valet and Fert [16] to noncollinear systems.

Here we present an approach based on a diffusion equation that reveals the main physical effects of spin-flip scattering in different parts of the multilayer on the spin transfer:

Spin-flip scattering in the middle normal metal N2 reduces the spin transfer, whereas spin-flip scattering in the outer normal metals N1 and N3 can enhance the spin transfer. Spin-flip at interfaces is not considered analytically, although in Appendix 2.B we include it into our approach. Since interface spin-flip is again a smaller correction to most (but not all [17]) interfaces, the present analytic results are therefore quite generally valid. We mainly focus on relatively large systems in which the bulk resistance dominates. Interfaces play an essential role in transferring the torques, but are assumed to not significantly increase the total as well as the mixing resistance (the inverse mixing conductance) in the limit of large systems. The inverse mixing conductance of a bulk (normal metal) layer with an interface is simply the sum of the inverse interface mixing conductance and the conventional bulk layer resistance [18]. When the layer is sufficiently thick, the former can be disregarded. Physically this means that potential and spin-accumulation drops at the interfaces are so small that their contribution can be disregarded. A typical interface resistance for, *e.g.*, Co/Cu is $AR_{\text{surface}} \sim \text{f}\Omega\text{m}^2$. The corresponding typical bulk resistance for clean and dirty Co/Cu layer varies between $AR_{\text{bulk}} = 0.01L[\text{nm}] \text{ f}\Omega\text{m}^2$ and $0.1L[\text{nm}] \text{ f}\Omega\text{m}^2$ (see, for example, [19] and [20]) where L is the length of the layers expressed in nm. In the presence of spin-flip the analytic expressions derived below are valid when the layers are thicker than 100 nm for pure samples and 10 nm for alloys, which is reasonable for experimental fabrication, and furthermore reveal qualitative effects of spin-flip relaxation process on the spin torques for thinner layers. In the absence of spin-flip scattering our analytic results also hold for general structures (Appendix 2.B). Related calculations of the torque and the magnetoresistance for submicron Co/Cu multilayers using the Boltzmann equation was presented in [15].

The paper is organized as follows: in Section 2.2 we explain the averaging mechanisms of spin transfer and the boundary conditions for the diffusion equation. The latter are formulated for a N1-F1-N2-F2-N3 multilayer system and solved analytically in the presence of spin-flip processes in the bulk layers in Sections 2.3 and 2.4. In Section 2.5 we summarize our conclusion. In Appendix 2.A, magnetoelectronic circuit theory [8, 10] is shown to be consistent with the results from the diffusion equation in the absence of spin-flip scattering. Interfaces are considered in Appendix 2.B, where we also discuss the possibility to take into account spin-flip at interfaces.

2.2 Diffusive approach to multilayer systems

Electron states with spins that are not collinear to the magnetization direction are not eigenstates of a ferromagnet, but precess around the magnetization vector. In three dimensions, a noncollinear spin current is composed of many states with different Larmor frequencies which average out quickly in a ferromagnet as a function of penetration depth. The efficient relaxation of the nondiagonal terms in the spin-density matrix is equivalent

to the suppression of spin accumulation noncollinear to the magnetization in the ferromagnet [8–10, 15]. This spin-dephasing mechanism does not exist in normal metals, in which the spin-wave functions remain coherent on the length scale of the spin-diffusion length, which can be of the order of microns. In ballistic systems, the spin transfer occurs over the ferromagnetic decoherence length $\lambda_c = 1/|k_F^\uparrow - k_F^\downarrow|$. In conventional ferromagnets the exchange energy is of the same order of magnitude as the Fermi energy, and λ_c is of the order of the lattice constant. The strongly localized regime in which the mean free path is smaller than the inverse Fermi wavevector, $\ell < 1/k_F$, is not relevant for elemental metals. In conventional metallic ferromagnets $\ell \gg 1/k_F$, and the length scale of the spin transfer λ_c is necessarily smaller than the mean free path ℓ , and therefore is not affected by disorder. This argument does not hold for gradual interfaces and domain walls. The opposite limit was considered in [21] (although the authors intend to address the opposite limit in a forthcoming publication), where $\lambda_c = \sqrt{2\hbar D_0/J}$ (λ_J in [21]), or with $D_0 \sim \ell^2/\tau$, $\lambda_c \sim \ell\sqrt{2\hbar/J\tau}$. The limit considered in [21] implies $2\hbar/J\tau > 1$ or $\lambda_c > \ell$ and therefore does not hold for ferromagnetic conductors like Fe, Co, Ni and its alloys.

Semiclassical methods cannot describe processes on length scales smaller than the mean free path, and thus cannot properly describe abrupt interfaces. It is possible, however, to express boundary conditions in terms of transmission and reflection probabilities which connect the distribution functions on both sides of an interface, and have to be computed quantum mechanically [22]. For transport, these boundary conditions translate into interface resistances, which arise from discontinuities in the electronic structure and disorder at the interface. This phenomenon was also extensively studied in the quasi-classical theory of superconductivity [23], where a generalized diffusion approach can be used in the bulk of the superconductor, but proper boundary conditions must be used at the interfaces between a superconductor and another normal or superconducting metal.

These effects can be taken into account by first-principles band-structure calculations [22]. In collinear systems it is possible to circumvent the problem by replacing the interfaces by regions of a fictitious bulk material, the resistances of which can be fitted to experiments. This is no longer possible when the magnetizations are noncollinear, because potential steps are essential for a description of the dephasing of the noncollinear spin current and the torque. However, in the case of a small imaginary part of the mixing interface conductance (which holds for intermetallic interfaces) this again becomes the correct procedure, as shown in Appendix 2.B.

We wish to model the multilayer system (Fig. 2.1) by the diffusion equation and interface boundary conditions. Let $\hat{f}(\varepsilon)$ be the 2×2 distribution matrix at a given energy ε and \hat{I} the 2×2 current matrix in spin space. It is convenient to expand these matrices into a scalar particle and a vector spin contribution $\hat{f} = \hat{1}f_0 + \hat{\sigma} \cdot \mathbf{f}_s$, $\hat{I} = (\hat{1}I_0 + \hat{\sigma} \cdot \mathbf{I}_s)/2$. For normal metals $\hat{f}^N = \hat{1}f_0^N + \hat{\sigma} \cdot \mathbf{s}$, where f_0^N is the local charge-related chemical potential and the spin distribution function has magnitude f_s^N and direction \mathbf{s} . In the ferromagnet

$\widehat{f}^F = \widehat{1}f_0^F + \widehat{\sigma} \cdot \mathbf{m}f_s^F = \widehat{1}(f_\uparrow + f_\downarrow)/2 + \widehat{\sigma} \cdot \mathbf{m}(f_\uparrow - f_\downarrow)/2$, where f_\uparrow and f_\downarrow are the diagonal elements of the distribution matrix when the spin-quantization axis is parallel to the magnetization in the ferromagnet \mathbf{m} .

The diffusion equation describes transport in both the normal metal and the ferromagnet. We first consider a single interface and disregard spin-flip scattering. The particle and spin currents in the normal metal with diffusion constant D are $j = D\partial_x f_0^N$ and $\mathbf{j}_s^N = D\partial_x \mathbf{f}_s^N$, respectively. The particle and spin currents are conserved:

$$D\partial_x^2 f_0^N = 0, \quad D\frac{\partial^2}{\partial x^2} \mathbf{f}_s^N = 0. \quad (2.1)$$

In the ferromagnet the particle and spin currents are $j = D_\uparrow \partial_x f_\uparrow + D_\downarrow \partial_x f_\downarrow$ and $\mathbf{j}_s^F = \mathbf{m}\partial_x(D_\uparrow f_\uparrow - D_\downarrow f_\downarrow)$ (see [8], Eqs. (38)-(39)), where D_\uparrow and D_\downarrow are the diffusion constants for spin-up and -down electrons. Current conservation of the spin components parallel and antiparallel to the magnetization direction in the ferromagnet read:

$$D_\uparrow \partial_x^2 f_\uparrow = 0, \quad D_\downarrow \partial_x^2 f_\downarrow = 0. \quad (2.2)$$

Eqs. (2.1) and (2.2) are applicable only inside the bulk layers. The boundary conditions at the interface arise from the continuity of the particle and spin distribution functions on the normal and the ferromagnetic metal sides [8, 10]:

$$f_0^N|_{\text{N-surface}} = (f_\uparrow + f_\downarrow)/2|_{\text{F-surface}}, \quad (2.3)$$

$$\mathbf{f}_s^N|_{\text{N-surface}} = \mathbf{m}(f_\uparrow - f_\downarrow)/2|_{\text{F-surface}}. \quad (2.4)$$

Furthermore, particle current is conserved [8, 10]:

$$[D\partial_x f_0^N]|_{\text{N-surface}} = \partial_x(D_\uparrow f_\uparrow + D_\downarrow f_\downarrow)|_{\text{F-surface}}. \quad (2.5)$$

We have discussed above why the noncollinear component of the spin-accumulation decays on the length scale of the order of the lattice spacing. This leads to the third boundary condition at the F-N interface, namely, that the spin current is conserved only for the spin component parallel to the magnetization direction [8, 10]:

$$[D\partial_x \mathbf{f}_s^N]|_{\text{N-surface}} = \mathbf{m}\partial_x(D_\uparrow f_\uparrow - D_\downarrow f_\downarrow)|_{\text{F-surface}} + \vec{\tau}, \quad (2.6)$$

where $\vec{\tau}$ is the nonconserved part of the spin current leading to torques acting on the magnetization in the ferromagnet. One should keep in mind here that in Eq. (2.6) the collinear to the magnetization part of the left side has to be equal to the first term of the right side, and the transverse part of the left side has to be equal to $\vec{\tau}$.

Solving these equations, we recover Eq. (2.29) with the mixing conductance, as found

by the magnetoelectric circuit theory (Appendix 2.A) [8, 10]. The magnetoelectronic circuit theory is thus equivalent to the diffusion approach when the system size is larger than the mean free path. However, the magnetoelectronic circuit theory is a more general approach that can also be used for circuits or parts of circuits that are smaller than the mean free path. Note that the boundary conditions above do not contain explicit reference to interface conductance parameters and are therefore valid only for bulk resistances which are sufficiently larger than the interface resistances. The gain by using the diffusion equation is, that we can now easily derive simple analytical results, also in the presence of spin-flip relaxation. In normal as well as ferromagnetic metals, spin-flip scattering leads to

$$\partial_x j_0 = 0, \quad \frac{\partial}{\partial x} \mathbf{j}_s = \mathbf{f}_s / \tau_{sf}, \quad (2.7)$$

where the spin-flip relaxation time τ_{sf} is a material dependent parameter.

2.3 Results for systems without spin-flip

Let us now apply this method to the spin transfer in a N1-F1-N2-F2-N3 system (Fig. 2.1) to obtain explicit results for the figure of merit, *viz.* the ratio of the spin torque to the charge current through (or voltage bias across) the system. The layers are characterized by the lengths L_{N1} , L_{F1} , L_{N2} , L_{F2} and L_{N3} and by diffusion constants D_{N1} , $D_{F1,\uparrow(\downarrow)}$, D_{N2} , $D_{F2,\uparrow(\downarrow)}$ and D_{N3} for each normal and ferromagnetic metal layer, respectively. The resistances of the system are R_{N1} , $R_{F1,\uparrow}$, $R_{F1,\downarrow}$, R_{N2} , $R_{F2,\uparrow}$, $R_{F2,\downarrow}$ and R_{N3} with, for example, $R_{N1} = L_{N1}/(A_{N1}D_{N1})$ and $R_{F1,\uparrow} = L_{F1}/(A_{F1}D_{F1,\uparrow})$ (L and A are the length and cross section of a layer respectively). The assymetry between the ferromagnetic layers can be achieved by using different materials or by varying thicknesses of layers. Let us initially disregard spin-flip scattering.

The continuity of the spin-current at the interface N1-F1 can easily be shown from Eqs. (2.1), (2.4) and (2.6). As a result the two layers N1-F1 behave effectively like a single ferromagnetic layer with renormalized resistance:

$$\tilde{R}_{F1,\uparrow} = R_{F1,\uparrow} + 2R_{N1}, \quad (2.8a)$$

$$\tilde{R}_{F1,\downarrow} = R_{F1,\downarrow} + 2R_{N1}. \quad (2.8b)$$

The same is true for the interface F2-N3. As a result it is sufficient to treat only the F1-N-F2 system. In general, there are spin-current discontinuities at the interfaces F1-N and N-F2 which, due to momentum conservation, lead to torques acting on the magnetic moments in the ferromagnetic layers. Taking into account all diffusion equations (2.1) and (2.2) and boundary conditions (2.3)-(2.6), and also introducing the parameters $R = R_{N2}$, $R_{i\pm} = (\tilde{R}_{Fi,\uparrow} \pm \tilde{R}_{Fi,\downarrow})/4$, where $i = 1, 2$, the torques can be written as

$$\vec{\tau}_1 = I_0 R_{2-} \frac{(R + R_{1+} - \alpha R_{1-} R_{2+} / R_{2-})}{(R + R_{2+})(R + R_{1+}) - \alpha^2 R_{1+} R_{2+}} (\alpha \mathbf{m}_1 - \mathbf{m}_2), \quad (2.9a)$$

$$\vec{\tau}_2 = I_0 R_{1-} \frac{R + R_{2+} - \alpha R_{2-} R_{1+} / R_{1-}}{(R + R_{2+})(R + R_{1+}) - \alpha^2 R_{1+} R_{2+}} (\mathbf{m}_1 - \alpha \mathbf{m}_2), \quad (2.9b)$$

where τ_1 and τ_2 are torques acting on the magnetizations of the first and second ferromagnet respectively, $\alpha = (\mathbf{m}_1 \cdot \mathbf{m}_2) = \cos \theta$, θ being the angle between the magnetizations. The resistance can also be calculated:

$$\mathfrak{R}(\theta) = R + R_{1+} + R_{2+} - \frac{R_{1-}^2 + 2\alpha R_{1-} R_{2-} + R_{2-}^2 + (1 - \alpha^2)(R_{1-}^2 R_{2+} + R_{2-}^2 R_{1+})/R}{R + R_{1+} + R_{2+} + R_{1+} R_{2+} (1 - \alpha^2)/R} \quad (2.10)$$

It is worthwhile to rewrite the above Eq. (2.9) using the effective polarization $P = R_- / R_+$ (which is the polarization of a current flowing through F or N-F layers connected to reservoirs) and the ferromagnet charge current resistance $R_i = R_{i+}$. The (absolute values of the) torques are then

$$|\tau_1| = \frac{|1 + R/R_1 - \alpha P_1/P_2|}{(1 + R/R_2)(1 + R/R_1) - \alpha^2} I_0 P_2 |\sin \theta|, \quad (2.11a)$$

$$|\tau_2| = \frac{|1 + R/R_2 - \alpha P_2/P_1|}{(1 + R/R_1)(1 + R/R_2) - \alpha^2} I_0 P_1 |\sin \theta|. \quad (2.11b)$$

As one can see from Eqs. (2.9) and (2.11) there is an asymmetry with respect to current inversion. For example, if only one polarization can rotate (one ferromagnet is much wider than the other or exchange biased), domains in the two magnetic layers can be aligned antiparallel by currents flowing in one direction, and reoriented parallel by reversing the current flow. This happens because only one state (parallel or antiparallel) is at equilibrium for a fixed direction of the current. If the currents are large enough (depending on other sources of torques such as external fields, magnetocrystalline anisotropy and damping) the magnetization will flip, which can be monitored by a change in the total resistance of

$$\frac{R(\uparrow\downarrow) - R(\uparrow\uparrow)}{R(\uparrow\downarrow)} = \frac{4R_{1-} R_{2-}}{R^2 + (R_{1+} + R_{2+})^2 - (R_{1-} + R_{2-})^2}. \quad (2.12)$$

In the case of unit polarization and $R \approx 0$ the relative resistance change Eq. (2.12) can be 100%. This asymmetry was predicted by spin-transfer theory [2], and was observed experimentally [3–5]. Note, however, that in these experiments the mean free path is comparable to the size of the systems, and the present theory cannot be directly applied.

From Eq. (2.11) follows that the torques are equal to zero for parallel and antiparallel alignments. When the numerator of Eq. (2.11) $1 + R/R_{1(2)} - \alpha P_{1(2)}/P_{2(1)}$ never vanishes, the torque increases with θ from zero to a maximal value which corresponds to an angle

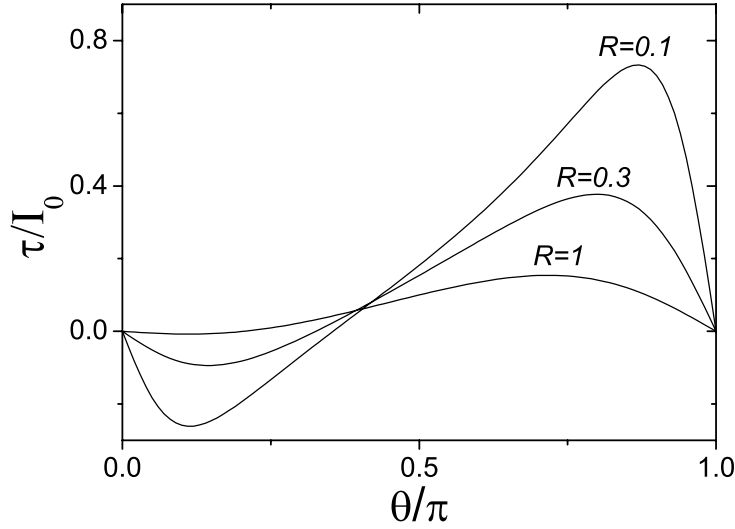


Figure 2.2: Torque acting on the first ferromagnet as a function of the relative angle between the two magnetizations for different normal metal resistances (the resistances are expressed in units $R_1 = R_2$, $P_1 = 0.5$, $P_2 = 0.2$).

larger than $\pi/2$ and vanishes again when configurations become antiparallel. When the nominator of Eq. (2.9) does vanish for some angle θ_0 , the absolute value of torque has a local maximum before θ_0 (see Fig. 2.2). In principle, it is possible to have an equilibrium magnetization angle $\theta = \theta_0$ for one current direction while equilibrium magnetization angle $\theta = 0$ or π for the opposite current direction (this can lead to asymmetry for the transition from the antialigned state to the aligned state in comparison with the transition from aligned to antialigned observed experimentally [6]).

We propose a setup in which only one magnetization can rotate (usually it is achieved by taking one ferromagnetic layer much wider than the other or by exchange biasing). If one ferromagnetic layer (for example the first one) has a resistance $R_1 \ll R$ and the other $R_2 > R$, the torque τ_2 vanishes whereas the other torque can be simplified to

$$\tau_1 = I_0 P_2 |\sin \theta| \quad (2.13)$$

The maximal torque in this setup occurs when the magnetizations of ferromagnet F1 and ferromagnet F2 are perpendicular.

In general, the spin torque is maximal when the resistance R of the normal metal vanishes, as could have been expected since this also gives the maximum magnetoresistance effect. In Eqs. (2.9) and (2.11) the size of the magnets does not play a dominant role for small normal metal resistances. In this case the torques depend mainly on the

polarizations.

2.4 Results for systems with spin-flip

So far, we have disregarded spin-flip scattering, which can be included readily, however. Here the system N1-F1-N2-F2-N3 is analyzed, and spin-flip in each normal metal part is considered separately. Introducing spin-flip in N1 and N3 leads to a simple result: Eq. (2.8) without spin-flip remains valid, but with modified spin resistances,

$$R_{N1(N3)}^{sf} = R_{N1(N3)} \frac{\tanh(L_{N1(N3)}/\ell_{sd})}{(L_{N1(N3)}/\ell_{sd})}, \quad (2.14)$$

where ℓ_{sd} is the normal metal spin-flip diffusion length. When $L \gg \ell_{sd}$, the resistance is governed by the spin-flip diffusion length ℓ_{sd} , which means that only part of the metal takes part in the spin transfer whereas the rest plays the role of the reservoir. This reduction of the active thickness of the device can lead to an effective polarization increase by decreasing the effect of R_N in Eq. (2.8). Spin-flips in the middle normal metal have a larger impact. The torques in the presence of spin-flips in N2 read

$$|\tau_1| = \frac{\beta + R^{sf}/R_1 - \alpha P_1/P_2}{(\beta + R^{sf}/R_2)(\beta + R^{sf}/R_1) - \alpha^2} I_0 P_2 |\sin \theta|, \quad (2.15a)$$

$$|\tau_2| = \frac{\beta + R^{sf}/R_2 - \alpha P_2/P_1}{(\beta + R^{sf}/R_1)(\beta + R^{sf}/R_2) - \alpha^2} I_0 P_1 |\sin \theta|, \quad (2.15b)$$

where $\beta = \cosh(L/\ell_{sd})$ and $P_{1(2)}$ and $R_{1(2)}$ are given by Eqs. (2.8) and (2.14). R^{sf} is an effective normal metal resistance:

$$R^{sf} = R \frac{\sinh(L/\ell_{sd})}{L/\ell_{sd}}. \quad (2.16)$$

For $L \geq \ell_{sd}$ the torque is significantly reduced by spin-flips, becoming exponentially small for longer samples.

Let us now consider spin-flips in the ferromagnet. The treatment of the N1-F1-N2-F2-N3 system is cumbersome, so let us concentrate on the simple case of a F-N-F system. In that case formulas remain unchanged, provided R_+ and R_- are renormalized as

$$R_{1(2)-}^{sf} = R_{1(2)-} \frac{\tanh(L_{F1(F2)}/\ell_{sd}^F)}{L_{F1(F2)}/\ell_{sd}^F}, \quad (2.17a)$$

$$R_{1(2)+}^{sf} = R_{1(2)+} \frac{\tanh(L_{F1(F2)}/\ell_{sd}^F)}{L_{F1(F2)}/\ell_{sd}^F}. \quad (2.17b)$$

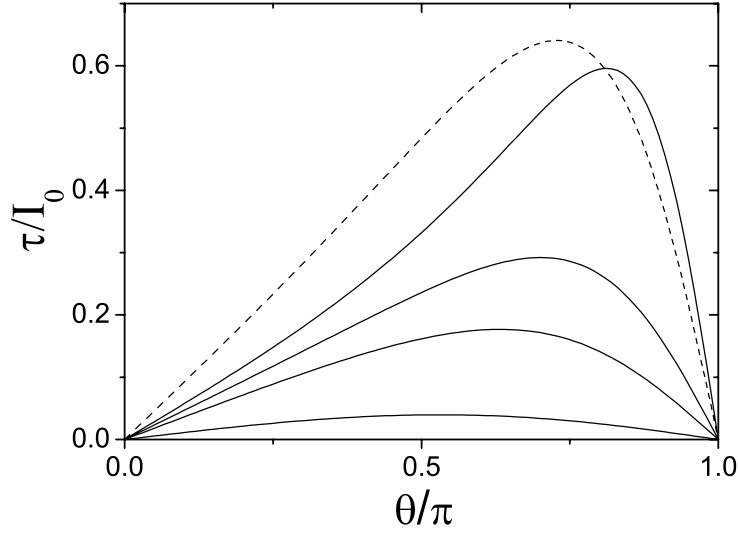


Figure 2.3: Torque on each ferromagnet as a function of the relative angle between the two magnetizations for different spin-flip diffusion lengths in the normal metal (the resistance $R = 0.2$ is expressed in units $R_1 = R_2$, $P_1 = P_2 = 0.4$, and $L/\ell_{sd} = 0, 1, 1.5$, and 3 , and the lower plot corresponds to the higher ratio). With dashed line we plot Slonczewski's result [2] for the same polarization.

where ℓ_{sd}^F is the ferromagnet spin-flip diffusion length. These resistances should be used in Eqs. (2.9) for the torques in F-N-F systems. If spin-flip in the normal metal exists, then formulas (2.15) should be used. Eqs. (2.17) imply that there is no polarization change (as defined below Eqs. (2.9)) and only the ferromagnet resistances $R_{1(2)}$ are affected. For $L \gg \ell_{sd}^F$ the bulk of the ferromagnet behaves like a reservoir (just like for the normal metal in the same limit) and only a slice with thickness ℓ_{sd}^F is active. In general, spin-flip in the ferromagnet leads to reduced torques as $R_{1(2)}$ becomes smaller. The effect may be quite small as long as the resistance of the ferromagnet is sufficiently larger than that of the normal metal (this can also be seen from Eqs. (2.8) and (2.11)), so that the polarization of the current is maintained.

Finally we would like to discuss magnetoresistance and torque for the symmetric $R_{1+} = R_{2+}$ and $R_{1-} = R_{2-}$. For the angular magnetoresistance we extract from (2.10) the formula observed by Pratt [24] and also shown to be universal for any disordered F-N-F perpendicular spin valves in [18],

$$\frac{R(\theta) - R(0)}{R(\pi) - R(0)} = \frac{1 - \cos \theta}{\chi(1 + \cos \theta) + 2}, \quad (2.18)$$

with one parameter χ that is given by circuit theory,

$$\chi = \frac{1}{1 - p^2} \frac{|\eta|^2}{\text{Re}\eta} - 1, \quad (2.19)$$

in terms of the normalized mixing conductance $\eta = 2g_{\uparrow\downarrow}/g$, the polarization $p = (g_{\uparrow} - g_{\downarrow})/g$, and the average conductance $g = g_{\uparrow} + g_{\downarrow}$. As we do not take interface resistances into account, in our case the parameters can be expressed only via bulk resistances: $g = 1/(R_{\uparrow} + R) + 1/(R_{\downarrow} + R)$, $\eta = 2/(Rg)$, $p = 2R_{-}/(2R_{+} + R)$. From Eqs. (2.11) and (2.10) the analytical expressions of the spin torque on either ferromagnet for current and voltage biased systems read

$$|\tau| = \frac{p(\chi + 1)|\sin\theta|}{\chi(\cos\theta + 1) + 2} I_0, \quad (2.20)$$

$$|\tau| = \frac{pg}{2} \frac{\eta|\sin\theta|}{(\eta - 1)\cos\theta + 1 + \eta} \frac{\mu_l - \mu_r}{2\pi}, \quad (2.21)$$

where $\mu_{l(r)}$ is the chemical potential in the left (right) ferromagnet. In the presence of spin-flip for the angular magnetoresistance we can write (restricting ourself to F-N-F case again)

$$\frac{R(\theta) - R(0)}{R(\pi) - R(0)} = \frac{(1 + \chi(\beta - 1)/2)(1 - \cos\theta)}{\chi(\beta + \cos\theta) + 2}, \quad (2.22)$$

where all parameters should be calculated according to Eqs. (2.16) and (2.17). The dependences of the torque on angle now read

$$|\tau| = \frac{p(\chi + 1)|\sin\theta|}{(\chi(\cos\theta + \beta) + 2)} I_0, \quad (2.23)$$

$$|\tau| = \frac{pg}{2} \frac{\eta|\sin\theta|}{A_1 \cos\theta + A_2} \frac{\mu_l - \mu_r}{2\pi}, \quad (2.24)$$

where we introduced two parameters

$$A_1 = -\frac{p^2}{1 + \frac{\chi\beta - 1}{2\chi + 1}} \left(1 + \frac{\chi\beta + \chi}{2}\right) + \chi \left(1 + \frac{(\kappa_1 + \chi\kappa_2)}{\chi + 1} - \kappa_2 p\right), \quad (2.25)$$

$$A_2 = \frac{p^2}{1 + \frac{\chi\beta - 1}{2\chi + 1}} \left(1 - \frac{\chi\beta + 2}{2}(\beta + 1)\right) + \left(1 + \frac{(\kappa_1 + \chi\kappa_2)}{\chi + 1} - \kappa_2 p\right)(\chi\beta + 2), \quad (2.26)$$

$$\text{and } \kappa_1 = \frac{L_N/\ell_{N,sd}}{\sinh(L_N/\ell_{N,sd})} - 1, \quad \kappa_2 = \frac{L_F/\ell_{F,sd}}{\tanh(L_F/\ell_{F,sd})} - 1.$$

An interesting result can be drawn from Eqs. (2.22) and (2.23) by comparison with the Eqs. (2.18) and (2.20). In order to fit the torque and the magnetoresistance in the presence of spin-flip we need an additional parameter β (β was defined in Eqs. (2.15)), which depends only on the spin-flip diffusion length in the normal metal spacer. The general form of Eqs. (2.22) and (2.23) with only two important parameters seems to be valid even in the presence of interfaces, but this has to be confirmed by future studies. Eq. (2.24) is cumbersome depending explicitly on the diffusion length in the ferromagnets. In Fig. 2.3 we plot results of Eq. (2.23) for different spin-diffusion lengths in the normal metal. The smaller diffusion length corresponds to smaller torques. The curves only qualitatively resemble Slonczewski's result for ballistic systems, but it should be pointed out that for the cases $p = 1$ and $\eta = 2$, both approaches result in the same formula.

2.5 Conclusion

We investigated transport in multilayer systems in the diffusive limit with arbitrary magnetizations in the ferromagnetic layers. The boundary conditions for diffusion equations including spin transfer were discussed, and analytic expressions for the magnetization torques and the angular magnetoresistance were obtained. The torque can be engineered not so much via the geometry of the samples (such as the layer thicknesses), but rather via the materials, the ferromagnetic polarization being an important parameter. The asymmetry with respect to the current flow direction has been addressed and the resistance change under magnetization reversal was calculated for different current directions. The effect of spin-flip in the normal metal and ferromagnet was studied analytically. Spin-flip in the center normal metal suppresses the spin-transfer, whereas spin-flip in the outer normal metals can effectively increase the polarization and spin transfer. The spin-flip processes in the ferromagnet also diminish the spin transfer, but not as drastically as long as the resistance of the ferromagnet is larger than the normal metal resistance. Finally we show in Appendix 2.A that the diffusive approach with carefully chosen boundary conditions leads to results which coincide with those from circuit theory.

We are grateful to Yuli Nazarov, Yaroslav Tserkovnyak and Daniel Huertas-Hernando for stimulating discussions. This work was supported in part by the NEDO International Joint Research Grant Program "Nano-magneto-electronics", NSF grant DMR 99-81283 and DARPA award No. MDA 972-01-1-0024.

2.A Appendix: Circuit theory approach to the diffusive systems

Here we show that the diffusion approach is equivalent to circuit theory and that the mixing conductance is also a valid concept in systems which are dominated by bulk transport [25]. We consider an F1-N2-F2 system Fig. 2.1 (N1 and N3 can also be included) connected to two reservoirs R1 and R2 with negligible interface resistances. Note that this does not mean that the interface is neglected, because it plays an essential role in the boundary conditions as mentioned in the main text. Since the system is diffusive, a thin slice of a ferromagnet or a normal metal can be considered as a node. The mixing conductance can be written in terms of the reflection and transmission coefficients, and incorporates any kind of details of the contacts, *e.g.*, tunnel, diffusive, and ballistic contacts. We are free to define interface resistors via the location of the nodes. Here it is chosen such that the interface width is larger than the ferromagnetic decoherence length but smaller than the mean free path. We introduce six nodes: r1 is in R1 just before the interface, r2 and r3 are before and after the F1-N2 interface, r4 and r5 are before and after the N2-F3 interface, and r6 is in R2 just after the interface (Fig. 2.1).

Let us first find the charge and the spin current in F1 (F2) at the interface where the spin transfer takes place. The currents read

$$I_0 = (G^\downarrow + G^\uparrow)(f_0^F - f_0^N) + (G^\downarrow - G^\uparrow)f_s^F, \quad (2.27a)$$

$$\mathbf{I}_s = \mathbf{m} \left[(G^\downarrow - G^\uparrow)(f_0^F - f_0^N) + (G^\downarrow + G^\uparrow)f_s^F \right], \quad (2.27b)$$

where f_0^N is the particle distribution function in r1 (r6) and f_0^F is the spin distribution function in r2 (r5). The distribution function at r2 and r3 (r4 and r5) is identical due to the continuity boundary condition. The spin-current between the ferromagnet reservoir r2 (r5) and the normal metal reservoir r4 (r3) driven by the nonequilibrium distributions can be found by using circuit theory,

$$\mathbf{I}_{1(2)} = \mathbf{m}2G_N(f_s^F - \mathbf{s} \cdot \mathbf{m}f_s^N) - 2\text{Re}G^{\uparrow\downarrow}f_s^N(\mathbf{s} - (\mathbf{s} \cdot \mathbf{m})\mathbf{m}) + (\mathbf{s} \times \mathbf{m})2\text{Im}G^{\uparrow\downarrow}f_s^N, \quad (2.28)$$

where the spin accumulation in the normal metal reservoir r4 (r3) is given by the unit vector \mathbf{s} and the spin distribution function f_s^N . Use was made of $G^\downarrow = G^\uparrow = G_N$ because r2 (r5) is close to the interface. The component of the current perpendicular to the magnetization \mathbf{m} is transferred to the magnetization at the interface whereas the parallel component is conserved. The torque acting on the magnetization in F1 (F2) therefore becomes

$$\vec{\tau}_{1(2)} = -2\text{Re}G^{\uparrow\downarrow}f_s^N(\mathbf{s}^N - (\mathbf{s}^N \cdot \mathbf{m})\mathbf{m}) + (\mathbf{s}^N \times \mathbf{m})2\text{Im}G^{\uparrow\downarrow}f_s^N. \quad (2.29)$$

The mixing conductance is related to the reflection coefficients of an electron from the normal metal to the ferromagnet:

$$G_{\uparrow\downarrow} = \sum_{nm} [\delta_{nm} - (r_{nm}^{\uparrow})^* r_{nm}^{\downarrow}]. \quad (2.30)$$

Let us now evaluate the mixing conductance for a disordered system. We assume that the junction consists of two connected parts. The normal metal section is described by a single scattering matrix for both spin- \uparrow and spin- \downarrow electrons. The ferromagnetic section requires two independent scattering matrices, one for spin- \uparrow and one for spin- \downarrow electrons. Scattering at the F-N boundary is disregarded here since it is assumed that the total resistance is dominated by the diffuse normal metal and ferromagnetic metal parts of the junction. The total reflection matrix r^α for spin- α electrons can then be found by concatenating the normal metal and ferromagnetic parts as

$$r^\alpha = r_N + t_N' r_F^\alpha \sum_{n=0}^{\infty} (r_N' r_F^\alpha)^n t_N \equiv r_N + \chi^\alpha. \quad (2.31)$$

By inserting Eq. (2.31) into the definition for the mixing conductance we find that the mixing conductance can be expressed as $G_{\uparrow\downarrow} = G_N + \delta G_{\uparrow\downarrow}$, where

$$\delta G_{\uparrow\downarrow} = \sum_{nm} [(r_N)_{nm}^* \chi_{nm}^{\downarrow}] + (\chi_{nm}^{\uparrow} (r_N)_{nm})^* + (\chi_{nm}^{\uparrow})^* \chi_{nm}^{\downarrow}. \quad (2.32)$$

Eq. (2.32) depends on the phase difference between the scattering paths of spin-up and -down electrons. It is assumed that there are no correlations between the scattering matrices of the spin- \uparrow and spin- \downarrow electrons in the ferromagnetic part, which is consistent with the a small coherence length. Consequently, in a diffusive systems $\delta G_{\uparrow\downarrow} = 0$. However, the up- and down-spin parts of the total scattering matrix of the combined normal metal and ferromagnetic system *are* correlated since both spin directions see the same scattering centers in the normal metal part. This leads to the conclusion that, for a diffusive hybrid system,

$$G_{\uparrow\downarrow}^D = G_N. \quad (2.33)$$

From Eqs. (2.27,2.28 and 2.29) and taking into account Eq. (2.33), and noting that $2G_N = 1/R$ and $G_{\downarrow} = 1/R_{\downarrow}$, $G_{\uparrow} = 1/R_{\uparrow}$ one can easily find Eq. (2.11).

2.B Appendix: Treatment of interfaces

We show in this Appendix how interfaces can be included into our approach. The general forms of the boundary conditions at an FIN interface can be written

$$f_s^N|_{N\text{-interface}} = (f_\uparrow + f_\downarrow)|_{F\text{-interface}} + \Delta f, \quad (2.34)$$

$$\mathbf{f}_s^N|_{N\text{-interface}} = \mathbf{m}(f_\uparrow + f_\downarrow)|_{F\text{-interface}} + \Delta \mathbf{f}_s. \quad (2.35)$$

In the absence of spin-flip scattering at the interface the potential Δf and spin-accumulation $\Delta \mathbf{f}_s$ drops can be found from the magnetoelectronic circuit theory as follows:

$$I_0 = (G^\uparrow + G^\downarrow)\Delta f + (G^\uparrow - G^\downarrow)(\Delta \mathbf{f}_s \cdot \mathbf{m}), \quad (2.36)$$

$$\mathbf{I}_s = \mathbf{m}[(G^\uparrow - G^\downarrow)\Delta f + (G^\uparrow + G^\downarrow)(\Delta \mathbf{f}_s \cdot \mathbf{m})] + 2\text{Re}G^{\uparrow\downarrow}\mathbf{f}_s^N + 2\text{Im}G^{\uparrow\downarrow}(\mathbf{f}_s^N \times \mathbf{m}). \quad (2.37)$$

When the imaginary part of the mixing conductance is small, the interface can be replaced by a fictitious bulk material. Suppose we add a slice of ferromagnet as well as a slice of normal metal with parameters $R_\pm = (R_\uparrow \pm R_\downarrow)/4$ and R_N respectively, the potential and spin-accumulation drops read

$$\Delta f = IR_N + (\mathbf{m} \cdot \mathbf{I}_s)R_- + I_0R_+, \quad (2.38)$$

$$\Delta \mathbf{f}_s = \mathbf{I}_sR_N + \mathbf{m}(\mathbf{m} \cdot \mathbf{I}_s)R_+ + \mathbf{m}I_0R_-. \quad (2.39)$$

In general, Eqs. (2.38) and (2.39) have some R_N and R_\pm as a solution.

Taking into account results from the previous Appendix and Eq. (2.36,2.37,2.38,2.39) one can immediately derive that the fictitious bulk layers should obey

$$R_N = 1/G^{\uparrow\downarrow}, R_\uparrow = 1/G_\uparrow - 1/G^{\uparrow\downarrow}, R_\downarrow = 1/G_\downarrow - 1/G^{\uparrow\downarrow}. \quad (2.40)$$

When interface and bulk spin-flip may be disregarded and $\text{Im}G^{\uparrow\downarrow} = 0$, the interface thus leads to the following renormalized up, down and normal metal resistances of the layers adjacent to it, R_N^f , R_\uparrow^f and R_\downarrow^f :

$$R_N^f = R_N + 1/G^{\uparrow\downarrow}, R_\uparrow^f = R_\uparrow + 1/G_\uparrow - 1/G^{\uparrow\downarrow}, R_\downarrow^f = R_\downarrow + 1/G_\downarrow - 1/G^{\uparrow\downarrow}. \quad (2.41)$$

Recent experiments indicate that interface spin-flip scattering may not be neglected in many systems [26]. It is straightforward to introduce spin-flip diffusion into the fictitious layers, although difficulties arise from the necessity to link the analytical solutions between regions with different spin-flip rates, ℓ/ℓ_{sd} . Only when the N(F) fictitious layer has the same spin-flip rate as the adjacent N(F) layer can we carry out analytic calculations. In this case the total system is equivalent to a bulk system with resistances given

by Eqs. (2.41) (these resistances should be used in Eqs. (2.14,2.16,2.17)). Otherwise, the problem becomes too cumbersome for an analytic treatment and has to be studied numerically.

References

- [1] L. Berger, *Phys. Rev. B* **54**, 9353 (1996).
- [2] J. C. Slonczewski, *J. Magn. Magn. Mater.* **159**, L1 (1996).
- [3] E. B. Myers, D. C. Ralph, J. A. Katine, R. N. Louie, and R. A. Buhrman, *Science* **285**, 867 (1999).
- [4] J. A. Katine, F. J. Albert, R. A. Buhrman, E. B. Myers, and D. C. Ralph, *Phys. Rev. Lett.* **84**, 3149 (2000).
- [5] J. Grollier, V. Cros, A. Hamzic, J. M. George, H. Jaffres, A. Fret, G. Faini, J. B. Youssef, and H. Legall, *Appl. Phys. Lett.* **78**, 3663 (2001).
- [6] J.-E. Wegrowe, X. Hoffer, P. Guittienne, A. Fabian, L. Gravier, and T. Wade, *J. Appl. Phys.* **91**, 6806 (2002).
- [7] X. Waintal, E. B. Myers, P. W. Brouwer, and D. C. Ralph, *Phys. Rev. B* **62**, 12317 (2000).
- [8] A. Brataas, Y. V. Nazarov, and G. E. W. Bauer, *Eur. Phys. J. B* **22**, 99 (2001).
- [9] M. D. Stiles and A. Zangwill, *Phys. Rev. B* **66**, 014407 (2002).
- [10] A. Brataas, Y. V. Nazarov, and G. E. W. Bauer, *Phys. Rev. Lett.* **84**, 2481 (2000).
- [11] K. Xia, P. J. Kelly, G. E. W. Bauer, A. Brataas, and I. Turek, *Phys. Rev. B* **65**, 220401(R) (2002).
- [12] D. Huertas-Hernando, Y. V. Nazarov, A. Brataas, and G. E. W. Bauer, *Phys. Rev. B* **62**, 5700 (2000).
- [13] Y. B. Bazaliy, B. A. Jones, and S.-C. Zhang, *Phys. Rev. B* **57**, R3213 (1998).
- [14] K. Xia, P. J. Kelly, G. E. W. Bauer, I. Turek, J. Kudrnovsky, and V. Drchal, *Phys. Rev. B* **63**, 064407 (2001).
- [15] M. D. Stiles and A. Zangwill, *J. Appl. Phys.* **91**, 6812 (2002).
- [16] T. Valet and A. Fert, *Phys. Rev. B* **48**, 7099 (1993).

- [17] W. Park, D. V. Baxter, S. Steenwyk, I. Moraru, W. Pratt, Jr., and J. Bass, *Phys. Rev. B* **62**, 1178 (2000).
- [18] G. E. W. Bauer, Y. Tserkovnyak, D. Huertas-Hernando, and A. Brataas, *Phys. Rev. B* **67**, 094421 (2003).
- [19] J. Bass and W. Pratt, Jr., *J. Magn. Magn. Mater.* **200**, 274 (1999).
- [20] K. Eid, D. Portner, R. Loloee, W. Pratt, Jr., and J. Bass, *J. Magn. Magn. Mater.* **224**, L205 (2001).
- [21] S. Zhang, P. M. Levy, and A. Fert, *Phys. Rev. Lett.* **88**, 236601 (2002).
- [22] K. M. Schep, J. B. A. N. van Hoof, P. J. Kelly, G. E. W. Bauer, and J. E. Inglesfield, *Phys. Rev. B* **56**, 10805 (1997).
- [23] C. J. Lambert and R. Raimondi, *J. Phys.: Condens. Matter.* **10**, 901 (1998).
- [24] L. Giacomoni, B. Dieny, W. Pratt, Jr., R. Loloee, and M. Tsoi (unpublished).
- [25] Y. Tserkovnyak and A. Brataas, *Phys. Rev. B* **64**, 214402 (2001).
- [26] H. Kurt, W.-C. Chiang, C. Ritz, K. Eid, W. Pratt, Jr., and J. Bass (to be published).

Chapter 3

Perpendicular spin *valves* with ultra-thin ferromagnetic layers

We address two finite size effects in perpendicular transport through magnetic multilayers. When the magnetic layer thickness in spin valves becomes of the order or smaller than the spin-flip diffusion length, structural asymmetries affect the transport properties. A magnetic layer with thickness approaching the magnetic coherence length becomes transparent for spin currents polarized perpendicular to the magnetization. We use the generalized magnetoelectronic circuit theory to investigate both effects on the angular magnetoresistance (aMR) and spin transfer torque. We analyze recent aMR experiments to determine the spin-flip diffusion length in the ferromagnet as well as the interface spin-mixing conductance and propose a method to measure the ferromagnetic coherence length.

3.1 Introduction

Since the discovery of the giant magnetoresistance (GMR) [1] electron transport in magnetic metallic heterostructures has been studied intensively and with considerable progress. The field developed from studies of large area multilayers of ferromagnetic (F) and normal metals (N) in which the current flows in the plane of the interfaces (CIP) to nanostructures with current perpendicular to the planes (CPP) [2]. Current-induced magnetization excitation has been predicted for perpendicular F|N|F spin valves [3, 4] and subsequently observed [5–8]. In these experiments applied currents excite a spin accumulation in the normal metal spacer that exerts a torque on the ferromagnets. When this torque overcomes the damping, the magnetization starts to precess coherently, possibly leading to a complete magnetization reversal [9]. By fits of the parameters of the diffusion equation [10] to a wealth of experimental data of the GMR in CPP structure, the spin-dependent interface and bulk material resistances of the most important transition metal combinations are well known by now [2, 11]. First-principles calculations in general agree well with the experimental values [12]. Also in view of possible applications for switching purposes in magnetic random access memories, a comparably accurate modeling of the spin torque as a function of material combinations and applied bias is desirable.

Physically, the spin-transfer torque is a consequence of angular momentum conservation when a spin current polarized transverse to the magnetization direction is absorbed at the magnetic interface [13]. The transverse spin current can penetrate the ferromagnet up to a skin depth equal to the ferromagnetic coherence length $\lambda_c = \pi / |k_{\uparrow}^F - k_{\downarrow}^F|$. In transition metals λ_c is much smaller than all other length scales such as spin-diffusion length or mean-free path [14–16]. When the ferromagnetic layer thickness $d_F \gg \lambda_c$ the spin-transfer torque is a pure interface property governed by the so-called spin-mixing conductance, [17] which is accessible to first principles calculations [18].

An excellent method to measure the torque and mixing conductance is the normalized angular magnetoresistance (aMR) of perpendicular F|N|F spin valves [19, 22, 23]

$$\text{aMR}(\theta) = \frac{R(\theta) - R(0)}{R(\pi) - R(0)}, \quad (3.1)$$

where $R(\theta)$ is electric resistance when the two magnetizations are rotated by an angle θ with respect to each other. Deviations of the aMR as a function of $\cos \theta$ from a straight line are proof of a finite mixing conductance [20]. Systematic new measurements of the aMR have been carried out recently by Urazhdin *et al.* [21] on Permalloy(Py)|Cu spin valves as a function of the Py thicknesses.

Interesting effects such as non-monotonic aMR, change of sign of the spin-transfer torque and strongly reduced critical currents for magnetization reversal have been pre-

dicted for asymmetric spin valves [24–26]. Asymmetry here means that the two ferromagnets in the spin valve are not equivalent for spin transport. This can be achieved by different thicknesses of the magnetically active regions of otherwise identical ferromagnetic contacts, but only when the spin-flip diffusion length in the ferromagnet l_{sd}^F is of the order or larger than one of the magnetic layer thicknesses. The magnetically soft Py is the material of choice, but its spin-flip diffusion length is only $l_{sd}^F \cong 5$ nm [11]. Urazhdin *et al.* [21] investigated spin valves with ultrathin $d_F \lesssim l_{sd}^F$, which means that the analysis of these experiments requires solution of the spin and charge diffusion equation in the ferromagnet.

Detailed calculations for transition metals [16, 30] confirm that a transverse spin current can penetrate the ferromagnet over distances $\lesssim 1$ nm as a consequence of incomplete destructive quantum interference. Urazhdin *et al.* investigated spin valves with Py layers of such thicknesses, claiming to observe an effect of this transverse component on the aMR. In weak ferromagnets like CuNi or PdNi alloys in which λ_c may become larger than the scattering mean-free path, the transverse component of spin current and accumulation can be treated semiclassically [27]. It is shown below that an effective conductance parameter (“mixing transmission”) can be introduced to parametrize transport in both regimes.

In this paper we treat the size effects related to $d_F \lesssim l_{sd}^F$ (Section 3.2) and $d_F \lesssim \lambda_c$ (Section 3.3) (but λ_c much smaller than the spin diffusion length). In Section 3.2 we apply magnetoelectronic circuit theory [17] combined with the diffusion equation to the F|N|F|N spin valves studied by Urazhdin *et al.*. We demonstrate that the angular magnetoresistance provides a direct measure for the mixing conductance [20] and find that the non-monotonicity in the aMR is indeed caused by the asymmetry as predicted. For F|N|F|N structures, that are also of interest because of their increased spin torque, [31, 32] we obtain several analytical results. The approach from Section 3.2 is generalized in Section 3.3 allowing us to treat ultrathin ferromagnetic layers or weak ferromagnets [28–30]. We find that there should be no measurable effects of λ_c on the aMR in F|N|F|N structures, but predict that the torque acting on the thin layer is modified. We proceed to conclude that the coherence length should be observable in the aMR of F|N|F|N|F structures. Finally, we propose a set-up to measure the ferromagnetic coherence length in a three-terminal device.

3.2 Magnetoelectronic circuit theory and diffusion equation for spin valves

In this Section we assume that $\lambda_c \ll d_F$. In Part 3.2.1 we recapitulate some old results: the magnetoelectronic circuit theory for spin valves, with emphasis on the inclusion of the

spin-flip diffusion in the ferromagnetic layers when the ferromagnetic layer thickness d_F is of the same order as the spin-flip diffusion length in the ferromagnet l_{sd}^F . In Part 3.2.2 we apply these results to recent experiments by Urazhdin *et al.* in which we can disregard spin-flip in the Cu spacers. In Part 3.2.3 we present new results for symmetric F|N|F|N|F structures.

3.2.1 Magneto-electronic circuit theory and diffusion equation

Magneto-electronic circuit theory [14] has been designed to describe charge and spin transport in disordered or chaotic multi-terminal ferromagnet-normal metal hybrid systems with non-collinear magnetizations. The material parameters of the theory are the bulk and interface spin-dependent conductances, as well as the so-called interface spin-mixing conductance $G_{\uparrow\downarrow}$. For spin valves, circuit theory can be shown to be equivalent to a diffusion equation when $\text{Im} G_{\uparrow\downarrow} \approx 0$, which is usually the case for intermetallic interfaces [24]. When the thickness of the ferromagnetic metal layer $d \gg l_{sd}^F$, the layer bulk resistance can be effectively replaced by that of a magnetically active region close to the interface of thickness l_{sd}^F . When connected to a reservoir or other type of spin sink, the effective thickness becomes $l_{sd}^F \tanh(d_F/l_{sd}^F)$ [24].

The aMR for general N|F|N|F|N structures with $\text{Im} G_{\uparrow\downarrow} = 0$ as derived previously [24] reads

$$\mathfrak{R}(\theta) = R_{\uparrow\downarrow} + R_1 + R_2 - \frac{R_{\uparrow\downarrow}(R_{1-} + \alpha R_{2-})^2 + (1 - \alpha^2)(R_{1-}^2 R_2 + R_{2-}^2 (R_1 + R_{\uparrow\downarrow}))}{(R_{\uparrow\downarrow} + R_1)(R_{\uparrow\downarrow} + R_2) - \alpha^2 R_1 R_2}. \quad (3.2)$$

with $\alpha = \cos \theta$, $4R_{1(2)} = 1/G_{1(2)\uparrow} + 1/G_{1(2)\downarrow} - 2R_{\uparrow\downarrow}$, $4R_{1(2)-} = 1/G_{1(2)\uparrow} - 1/G_{1(2)\downarrow}$, $P_{1(2)} = R_{1(2)-}/R_{1(2)}$, and $2R_{\uparrow\downarrow} = 1/G_{1\uparrow\downarrow} + 1/G_{2\uparrow\downarrow}$, where $G_{1(2)\uparrow}$ and $G_{1(2)\downarrow}$ are conductances of the left (right) ferromagnet including the left (right) normal layer, $G_{1\uparrow\downarrow}$ and $G_{2\uparrow\downarrow}$ are mixing conductances of the middle normal metal with adjacent ferromagnet interfaces as shown in Fig. 3.1. The torques felt by first and second ferromagnetic layer become

$$\tau_1/I_0 = \frac{\hbar}{2e} \frac{1 + R_{\uparrow\downarrow}/R_1 - \alpha P_1/P_2}{(1 + R_{\uparrow\downarrow}/R_1)(1 + R_{\uparrow\downarrow}/R_2) - \alpha^2} \quad (3.3)$$

$$\tau_2/I_0 = \frac{\hbar}{2e} \frac{1 + R_{\uparrow\downarrow}/R_2 - \alpha P_2/P_1}{(1 + R_{\uparrow\downarrow}/R_1)(1 + R_{\uparrow\downarrow}/R_2) - \alpha^2} \quad (3.4)$$

When we approximate the mixing conductance $1/R_{\uparrow\downarrow}$ by the Sharvin conductance of the normal metal, Eqs. (3.3,3.4) coincide with the expressions in [34] for asymmetric N|F|N|F|N spin valves with $\Lambda_{L(R)}^2 \equiv 2R_{1(2)}/R_{\uparrow\downarrow} + 1$, $P_{L(R)}\Lambda_{L(R)}^2 = 2R_{1(2)-}/R_{\uparrow\downarrow}$.

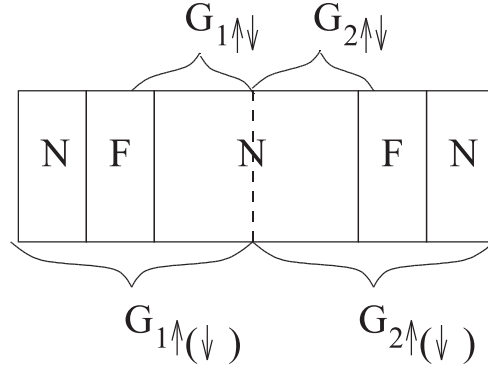


Figure 3.1: Definition of conductances $G_{1(2)\uparrow(\downarrow)}$ and mixing conductances $G_{1(2)\uparrow\downarrow}$ for N|F|N|F|N structure.

3.2.2 Extraction of the mixing conductance from experiment and asymmetric spin valves

Most material parameters in circuit theory are those of the two-channel resistor model. They can be determined for the collinear magnetic configurations, *i.e.* via the (binary) GMR. The only additional parameters for the non-collinear transport are the interface mixing conductances $G_{i\uparrow\downarrow}^r$, assumed here to be real. These can be found from a single parameter fit of the experimental aMR or from band structure calculations. A symmetric F|N|F structure is most suitable to carry out this program. The thus obtained $G_{i\uparrow\downarrow}^r$ should be transferable to other (asymmetric) structures grown by equivalent techniques. Urazhdin *et al.* fitted their experimental results for the normalized aMR by the simple formula [19] that follows from circuit theory [14]:

$$\text{aMR}(\theta) = \frac{1 - \cos \theta}{\chi(1 + \cos \theta) + 2}, \quad (3.5)$$

For symmetric junctions we identify $\chi = 2R/R_{\uparrow\downarrow}$ (see Eq. (18) in [24]).

Urazhdin *et al.* [21] used the structures Nb(150)Cu(20)FeMn(8)Py(d_1)Cu(10)Py(d_2)Cu(20)Nb(150), where the numbers in brackets are the thicknesses in nm. The exchange bias antiferromagnet FeMn is treated as a perfect spin sink, which means that the effective thickness of the left Py layer becomes $l_{sd}^F \tanh(d_1/l_{sd}^F) = 0.8l_{sd}$ ($d_1 = 6$ nm, $l_{sd}^F = 5.5$ nm). Note that this device is not exactly symmetric when $d_2 \gg l_{sd}^F$ as d_1 is not much larger than l_{sd}^F , but the calculated deviations from the fitted mixing resistances are smaller than the experimental error bars. When we replace d_1 by l_{sd}^F and $d_2 \gg l_{sd}^F$ the sample is symmetric and the aMR is well represented by Eq. (3.5) with $\chi = 1.96$ (see Fig. 3.2) [21].

We can use the measured value of χ to derive the mixing conductance $1/(AR_{\uparrow\downarrow})$ of an interface with area A by $R_{\uparrow\downarrow} = 2R/\chi$. For comparison with first principles calculations

for point contacts based on the scattering theory of transport, [18] the Sharvin resistance of the normal metal should be added [20]

$$R_{\uparrow\downarrow}^{pc} = R_{\uparrow\downarrow} + R_{sh}$$

Using the notation:

$$\begin{aligned} AR &= l_{sd}\rho_{Py}^* + AR_{PyCu}^* - AR_{\uparrow\downarrow}/2 \\ AR_- &= l_{sd}\rho_{Py}^*\beta_{Py} + AR_{PyCu}^*\gamma \end{aligned}$$

we may substitute the well established material parameters for bulk and interface resistances of Cu|Py [35] $l_{sd}\rho_{Py}^* = 1.4 \text{ f}\Omega\text{m}^2$, $l_{sd} = 5.5 \text{ nm}$, $AR_{PyCu}^* = 0.5 \text{ f}\Omega\text{m}^2$, $\beta_{Py} = 0.7$, $\gamma = 0.7$, disregarding the small bulk resistance of Cu which led us to $AR_{\uparrow\downarrow} = 1.3 \text{ f}\Omega\text{m}^2$ and $\eta = 1.49$. This value of the mixing resistance is larger than the Sharvin resistance $AR_{sh} = 1/G = 0.878 \text{ f}\Omega\text{m}^2$ of Cu used by Xiao *et al.* [34]. The point-contact mixing resistance of the Cu|Py interface that should be compared with band structure calculations is $AR_{\uparrow\downarrow}^{pc} = 2.2 \text{ f}\Omega\text{m}^2$, somewhat smaller than that found in [20] ($2.56 \text{ f}\Omega\text{m}^2$). Both results are close to the band structure calculations [18] of the point-contact mixing resistance for the disordered Cu|Co interface ($2.4 \text{ f}\Omega\text{m}^2$).

In Fig. 3.2 we compare plots of Eq. (3.2) with experimental aMR curves for symmetric and asymmetric F|N|F|N|S multilayers, [36] identifying the following relations between parameters:

$$\begin{aligned} AR_1 &= l_{sd}\rho_{Py}^* + AR_{PyCu}^* - AR_{\uparrow\downarrow}/2 \\ AR_2 &= d_2\rho_{Py}^* + AR_{PyCu}^* + AR_{PyNb} - AR_{\uparrow\downarrow}/2 \\ AR_{1-} &= l_{sd}\rho_{Py}^*\beta_{Py} + AR_{PyCu}^*\gamma \\ AR_{2-} &= d_2\rho_{Py}^*\beta_{Py} + 2AR_{PyCu}^*\gamma. \end{aligned}$$

We assume that the spin current into the superconductor vanishes. The resistance between the right ferromagnet and the right reservoir was taken to be $AR_{PyNb} = 5 \text{ f}\Omega\text{m}^2$. This is larger than the $AR_{PyNb} = 3 \text{ f}\Omega\text{m}^2$ reported in [35], but gives better agreement with the experiment. We observe good fits in Fig. 3.2 nicely reproducing the non-monotonic behavior around zero angle.

In Fig. 3.3 we plot the angular magnetoresistance for different thicknesses of the right Py layer, all relative to the parallel configuration, but not normalized to a relative scale as above. The lower curve was obtained from Eq. (3.2), the others were calculated numerically solving the bulk layer spin-diffusion equation in the ferromagnet. The non-monotonic angular magnetoresistance disappears when the right ferromagnetic layer becomes thicker and therefore the sample more symmetric. For the set of parameters in

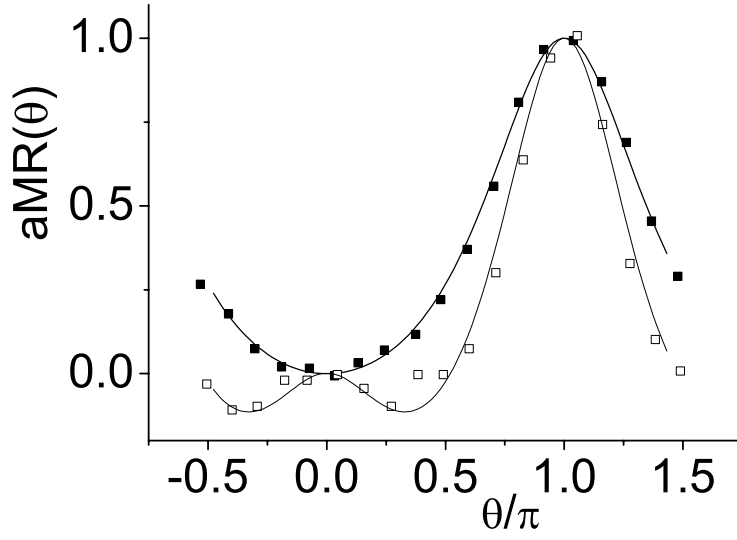


Figure 3.2: aMR of the $F|N|F|N$ structure for two thicknesses of the right ferromagnetic layer $d_2 = 0.27l_{sd}, 2.2l_{sd}$ ($d_1 > l_{sd}$). The filled (large d_2) and open (small d_2) squares are the experimental data [21].

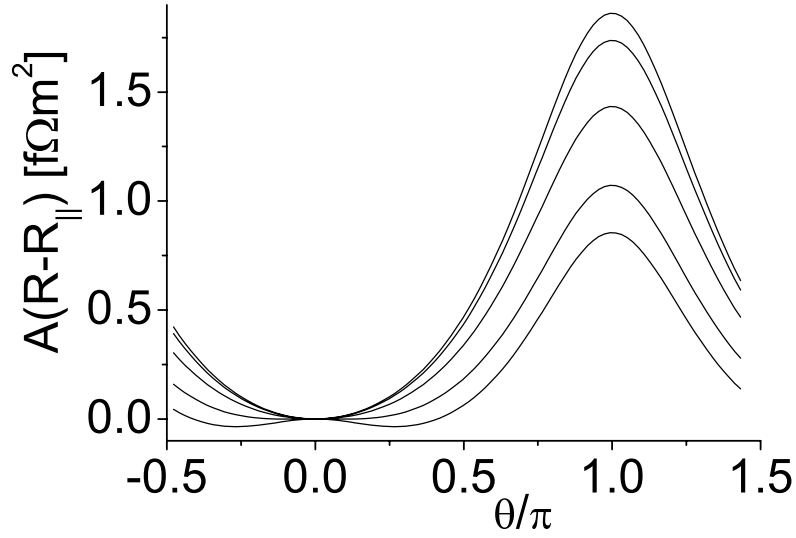


Figure 3.3: Angular magnetoresistance $\mathfrak{R}(\theta) - \mathfrak{R}(0)$ of the $F|N|F|N$ structure for different thicknesses of the right ferromagnetic layer $d_2 = 0.27l_{sd}, 0.5l_{sd}, 2l_{sd}, 2.5l_{sd}$ and ∞ (starting from the lower curve respectively ($d_1 \gg l_{sd}^F$, $AR_{PyNb} = 3 \text{ f}\Omega\text{m}^2$)).

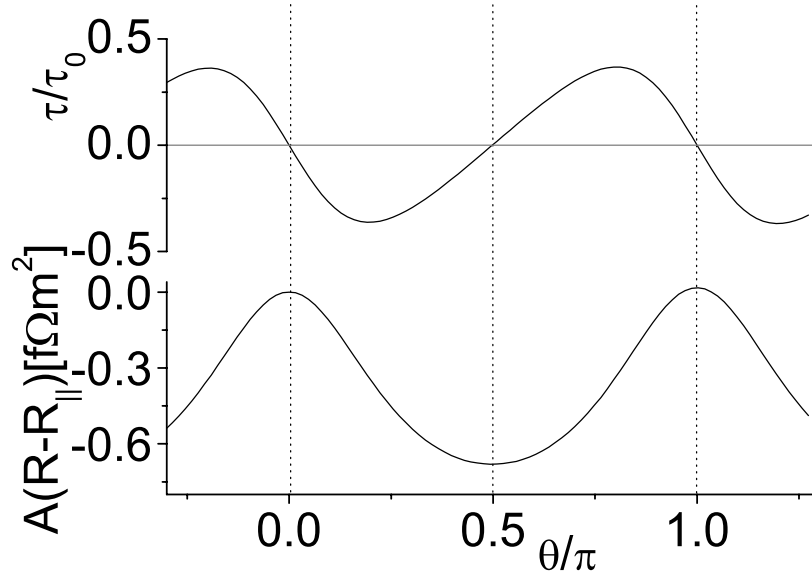


Figure 3.4: Angular magnetoresistance $\mathfrak{R}(\theta) - \mathfrak{R}(0)$ and spin-transfer torque on the left ferromagnet for the F|N|F|N structure with right F-layer thickness $d_2 = 0.27l_{sd}$ ($AR_{PyNb} \rightarrow \infty$, $\tau_0 = I_0\hbar/2e$).

Fig. 3.3 the non-monotonic behavior is rather weak but with circuit theory we can readily propose samples that maximize the effect. The minimum of the angular magnetoresistance Eq. (3.2) at finite θ_1 that coincides with a zero of the spin-transfer torque on the left ferromagnet [24, 25]:

$$\cos \theta_1 = \frac{(R_{\uparrow\downarrow} + R_1)R_{2-}}{R_1 - R_2}. \quad (3.6)$$

To observe the effect clearly, $\cos \theta_1$ should be small, which can be achieved by increasing R_2 , *e.g.* by the resistance of the right-most normal metal (within the spin-flip diffusion length). In Fig. 3.4 we plot the angular magnetoresistance Eq. (3.2) and the spin-transfer torque on the left ferromagnet Eqs. (3.3) when the resistance of the right contact is $AR_{PyNb} \rightarrow \infty$.

3.2.3 Analysis of symmetric F|N|F|N|F structures

Our approach offers analytic results for symmetric F|N|F|N|F structures when the outer layers are thicker than l_{sd}^F . In Fig. 3.5 we plot the angular magnetoresistance when the magnetizations of the outer layers are kept parallel for material parameters that are the same as above and close to set-up B from [21]. When the middle layer thickness $d_3 \gg l_{sd}^F$ the angular magnetoresistance is equal to that of two symmetric F|N|F structures in series. The analytical formula for the angular magnetoresistance in the regime $d_3 \ll l_{sd}^F$ is presented in Appendix 3.A. For $d_3 \gtrsim 0.3l_{sd}^F$ we cannot disregard spin flip in the middle

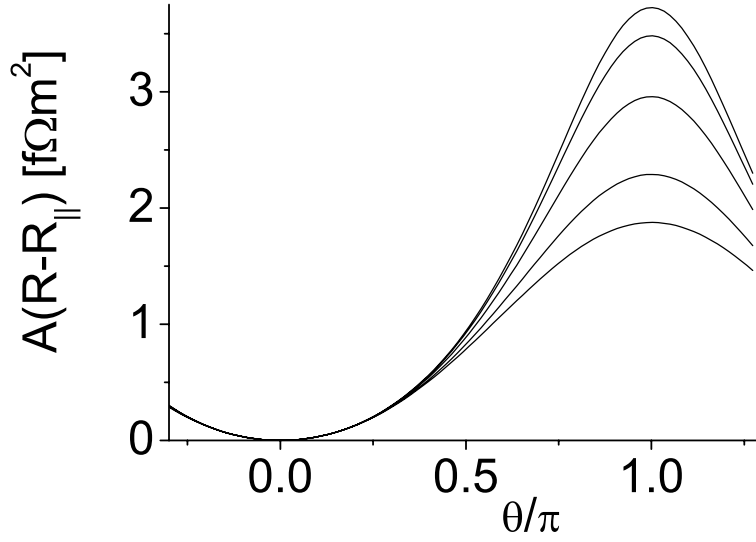


Figure 3.5: Angular magnetoresistance $\mathfrak{R}(\theta) - \mathfrak{R}(0)$ of the F|N|F|N|F structure for the middle F layer thicknesses $d = 0.27l_{sd}$, $0.5l_{sd}$, $2l_{sd}$, $2.5l_{sd}$ and ∞ (starting from the lower curve, respectively). The parallel resistance is subtracted.

layer and compute the resistances numerically.

A symmetric F|N|F|N|F setup with antiparallel outer layers can increase the torque [31]. Enhancement by a factor of 2 was reported by S. Nakamura *et al.* [32]. This result can be obtained from the magnetoelectronic circuit theory (see also S. Nakamura *et al.*, unpublished). With a current bias I_0 , assuming $d_3 \ll l_{sd}^F$, we derived a simple formula (note the similarity with the torque on the base contact of the three-terminal spin flip transistor[20]):

$$\tau/I_0 = \frac{\hbar}{2e} \frac{2R_- |\sin \theta|}{R_{\uparrow\downarrow} + R \sin^2 \theta}, \quad (3.7)$$

without invoking the parameters of the middle layer. When $d_3 \gg l_{sd}$ we can divide system into two F|N|F spin valves in series. Taking into account Eq. (3), the torque can be written down immediately:

$$\begin{aligned} \tau/I_0 &= \tau_{FNF}(\theta)/I_0 + \tau_{FNF}(\pi - \theta)/I_0 \\ &= \frac{\hbar}{2e} \frac{R_- |\sin \theta|}{R_{\uparrow\downarrow} + R(1 + \cos \theta)} + \frac{\hbar}{2e} \frac{R_- |\sin \theta|}{R_{\uparrow\downarrow} + R(1 - \cos \theta)} \end{aligned} \quad (3.8)$$

In Fig. 3.6 we plot results of these two analytic formulas as well as results of numeric calculations for the case $d = 0.8l_{sd}$. Note that these curves are symmetric with respect to $\theta = \pi/2$. By the dashed line we plot the torque for the corresponding symmetric F|N|F

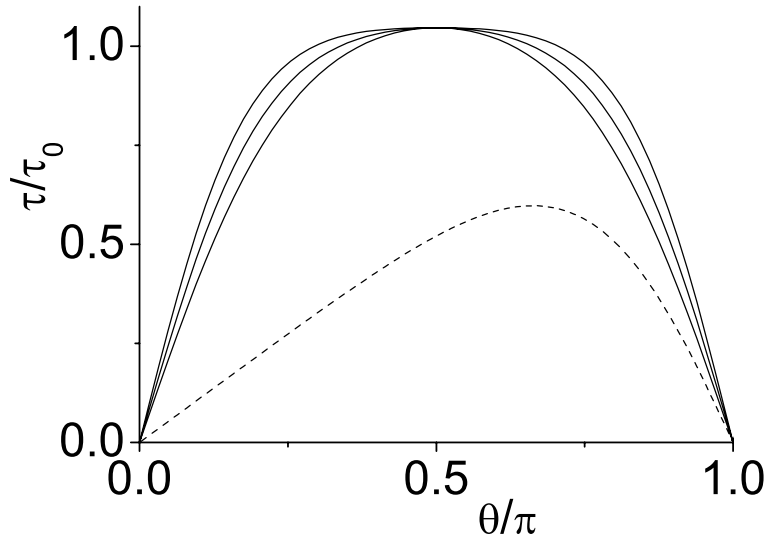


Figure 3.6: The spin-transfer torque on the middle ferromagnet for the $F|N|F|N|F$ structure for the thickness of the middle layer $d = 0.27l_{sd}$, $0.8l_{sd}$ and $10l_{sd}$ starting from the lower curve respectively (by bold line), the same for the corresponding symmetric $F|N|F$ structure (by dashed line), $\tau_0 = I_0\hbar/2e$.

structure.

3.3 Coherent regime

Urazhdin *et al.*'s [21] intentions to search for coherence effects in ultrathin magnetic layers encouraged us to study the regime $d_F \lesssim \lambda_c$. In this Section we formulate the magneto-electronic circuit theory that includes coherence effects in this regime in two and three terminal multilayer structures. Since λ_c is only a couple of monolayers, we are allowed to disregard spin-flip and diffuse scattering in the ferromagnetic material bulk layers.

3.3.1 Extended magnetoelectronic circuit theory

We consider an $N1|F|N2$ circuit element, choosing the normal metals as nodes with a possibly non-collinear spin accumulation and the entire F layer including the interfaces as resistive element (see Fig. 3.7). This allows us to treat the ferromagnet fully quantum mechanically by scattering theory. The current through the ferromagnet depends on the potential drop between and the spin accumulation in each of the normal metal nodes. Spin \mathbf{I}_s and charge I_0 currents can conveniently expressed as 2×2 -matrices in Pauli spin space

$\widehat{I} = (\widehat{1}I_0 + \widehat{\sigma} \cdot \mathbf{I}_s)/2$, where $\widehat{\sigma}$ is the vector or Pauli spin matrices and $\widehat{1}$ the 2×2 unit matrix. On the normal metal side [14] in the region 2

$$\widehat{I} = \frac{e}{h} \left\{ \sum_{nm} [\widehat{t}'^{nm} \widehat{f}^{N1} (\widehat{t}'^{nm})^\dagger - \delta_{nm} \widehat{f}^{N2} + \widehat{r}^{nm} \widehat{f}^{N2} (\widehat{r}^{nm})^\dagger] \right\} \quad (3.9)$$

where \widehat{r}^{mn} is the spin dependent reflection coefficient for electrons reflected from channel n into channel m in the node 2, \widehat{t}'^{mn} is the spin dependent transmission coefficient for electrons transmitted from channel n in the node 1 into channel m in the node 2 and δ_{nm} is the Kronecker delta symbol.

In the absence of spin flip processes the matrices \widehat{r}^{mn} and \widehat{t}'^{mn} should be diagonal in spin space provided the axis z is parallel to the magnetization of the ferromagnet (we are free to chose this frame reference as it is more convenient). Expressing the spin-dependent distribution matrices in nodes 1 and 2 via Pauli matrices; $\widehat{f}^N = \widehat{1}f_0^N + \widehat{\sigma} \mathbf{f}_s^N$ and the unit vector \mathbf{m}_z parallel to the axis z we obtain for spin and charge currents in the node N2:

$$I_0 = (G_\uparrow + G_\downarrow) \Delta f_0^N + (G_\uparrow - G_\downarrow) \Delta \mathbf{f}_s^N \cdot \mathbf{m}_z, \quad (3.10)$$

$$\begin{aligned} \mathbf{I}_s = & \mathbf{m}_z [(G_\uparrow - G_\downarrow) \Delta f_0^N + (G_\uparrow + G_\downarrow) \Delta \mathbf{f}_s^N] \\ & - 2(\mathbf{m}_z \times \mathbf{f}_s^{N2} \times \mathbf{m}_z) \text{Re} G_{\uparrow\downarrow}^{rN2|F} + 2(\mathbf{f}_s^{N2} \times \mathbf{m}_z) \text{Im} G_{\uparrow\downarrow}^{rN2|F} \\ & + 2(\mathbf{m}_z \times \mathbf{f}_s^{N1} \times \mathbf{m}_z) \text{Re} G_{\uparrow\downarrow}^{tN1|N2} - 2(\mathbf{f}_s^{N1} \times \mathbf{m}_z) \text{Im} G_{\uparrow\downarrow}^{tN1|N2}. \end{aligned} \quad (3.11)$$

where $\Delta f_0^N = f_0^{N1} - f_0^{N2}$ and $\Delta \mathbf{f}_s^N = \mathbf{f}_s^{N1} - \mathbf{f}_s^{N2}$. This agrees with the result of [14] except for the terms involving the mixing transmission [28–30]:

$$G_{\uparrow\downarrow}^{rN2|F} = \frac{e^2}{h} \sum_{nm} (\delta_{nm} - r_\uparrow^{nm} (r_\downarrow^{nm})^*); \quad G_{\uparrow\downarrow}^{tN1|N2} = \frac{e^2}{h} \sum_{nm} t_\uparrow^{nm} (t_\downarrow^{nm})^*.$$

The torque acting on the magnetization through the interface adjacent to N2 is the transverse component of the spin current flowing into the ferromagnet:

$$\begin{aligned} \vec{\tau}_2 = & -2(\mathbf{m}_z \times \mathbf{f}_s^{N2} \times \mathbf{m}_z) \text{Re} G_{\uparrow\downarrow}^{rN2|F} + 2(\mathbf{f}_s^{N2} \times \mathbf{m}_z) \text{Im} G_{\uparrow\downarrow}^{rN2|F} \\ & + 2(\mathbf{m}_z \times \mathbf{f}_s^{N1} \times \mathbf{m}_z) \text{Re} G_{\uparrow\downarrow}^{tN1|N2} - 2(\mathbf{f}_s^{N1} \times \mathbf{m}_z) \text{Im} G_{\uparrow\downarrow}^{tN1|N2}. \end{aligned} \quad (3.12)$$

When two opposite direction of the magnetization \mathbf{M} and $-\mathbf{M}$ are equivalent for the transport, we obtain $G_{\uparrow\downarrow}^{tN1|N2} = G_{\uparrow\downarrow}^{tN2|N1}$ as a consequence of time reversibility. This condition should hold in most cases (*e.g.* Stoner model is isotropic in spin space). The mixing transmission describes the part of the transverse spin current that is not absorbed by the ferromagnet and vanishes when the ferromagnetic layer is thicker than the ferromagnetic

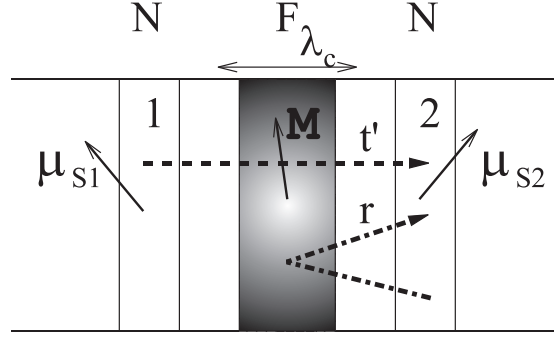


Figure 3.7: A contact through a thin ferromagnet between two normal metal nodes. The current is evaluated in the node 2.

coherence length λ_c [30]. It is complex, its modulus representing the transmission probability and the phase of the rotation of the transverse spin current by the ferromagnetic exchange field. First-principles calculations of $G_{\uparrow\downarrow}^r$ and $G_{\uparrow\downarrow}^t$ have been carried out by Zwierzycki *et al.* [30] showing small variation of the first and non-vanishing value of the second when the ferromagnetic layer becomes of the order of several monolayers.

3.3.2 Observation of ferromagnetic coherence in transport experiments

In this section we address coherence effects due to the transmission of transverse spin currents through ultrathin ferromagnetic layers or weak ferromagnets. These effects should be observable in Py structures when $d_F \lesssim 1.5$ nm. Band structure calculations show that in Cu|Co|Cu structures the mixing transmission can easily reach $G_{\uparrow\downarrow}^t \approx 0.1 (G_{\uparrow} + G_{\downarrow})$ for such thicknesses [30].

We may draw an important conclusion from the extended magnetoelectronic circuit theory applied to general (asymmetric) N1|F1|N2|F2|N3 structures: when the nodes are chosen in the middle normal metal and in the outer normal metals at the points that connect to the baths, a possibly finite mixing transmission completely drops out of the charge transport equations, *i.e.* the expressions remain exactly the same as those presented above for the N|F|N|F|N structure. For example, the charge and spin currents from N1 (and similarly from N3) into N2 read

$$I_0 = (G_{\uparrow}^{N1|N2} + G_{\downarrow}^{N1|N2})\Delta\mu_0^N + (G_{\uparrow}^{N1|N2} - G_{\downarrow}^{N1|N2})\Delta\mu_s^N \cdot \mathbf{m}_z \quad (3.13)$$

$$\begin{aligned}
\mathbf{I}_s = & \mathbf{m}_z \left[(G_{\uparrow}^{N1|N2} - G_{\downarrow}^{N1|N2}) \Delta\mu_0^N + (G_{\uparrow}^{N1|N2} + G_{\downarrow}^{N1|N2}) \Delta\mu_s^N \right] \\
& - 2(\mathbf{m}_z \times \mu_s^{N2} \times \mathbf{m}_z) \operatorname{Re} G_{\uparrow\downarrow}^{rN2|F1} + 2(\mu_s^{N2} \times \mathbf{m}_z) \operatorname{Im} G_{\uparrow\downarrow}^{rN2|F1} \\
& + 2(\mathbf{m}_z \times \mu_s^{N1} \times \mathbf{m}_z) \operatorname{Re} G_{\uparrow\downarrow}^{tN1|N2} - 2(\mu_s^{N1} \times \mathbf{m}_z) \operatorname{Im} G_{\uparrow\downarrow}^{tN1|N2}, \quad (3.14)
\end{aligned}$$

where $\Delta\mu_0^N = \mu_0^{N1} - \mu_0^{N2}$ and $\Delta\mu_s^N = \mu_s^{N1} - \mu_s^{N2}$ describe the potential and spin accumulation drops between the left and the middle nodes. By conservation of spin and charge currents in the center node, expression for aMR can be derived. However, the mixing transmission does not appear in Eqs. (3.13,3.14) since there is no spin accumulation in the outer nodes (reservoirs). Ferromagnets thin enough to allow transmission of a transverse spin current can therefore not be distinguished from conventional ones in the aMR. Our conclusions therefore disagree with the claims of ferromagnetic coherence effects in aMR experiments on N|F|N|F|N structures by Urazhdin *et al.* [21].

On the other hand, the *torque* on the thin ferromagnet F2 does change:

$$\vec{\tau}_2 = -2(\mathbf{m}_z \times \mu_s^{N2} \times \mathbf{m}_z) \operatorname{Re}(G_{\uparrow\downarrow}^{rN2|F2} - G_{\uparrow\downarrow}^{tN2|N3}) + 2(\mu_s^{N2} \times \mathbf{m}_z) \operatorname{Im}(G_{\uparrow\downarrow}^{rN2|F2} - G_{\uparrow\downarrow}^{tN2|N3}).$$

A parameterization of the torque via a combination $G_{\uparrow\downarrow}^{rN2|F2} - G_{\uparrow\downarrow}^{tN2|N3}$ was found in [13] by random matrix theory, which is equivalent with circuit theory when the number of transverse channels is large [20]. However these authors did not discuss their results in the limit of thin ferromagnetic layers. When $\operatorname{Im} G_{\uparrow\downarrow}^r \approx 0$ and $\operatorname{Im} G_{\uparrow\downarrow}^t \approx 0$, the torque τ_{coh} acting on the thin layer is modified from the incoherent expression τ as:

$$\tau_{\text{coh}} = \tau(G_{\uparrow\downarrow}^r - G_{\uparrow\downarrow}^t) / G_{\uparrow\downarrow}^r. \quad (3.15)$$

Naively one may expect that the reduced absorption of the transverse spin accumulation diminishes the torque, but this is not necessarily so (see Fig. 3.8). Since the mixing transmission may be negative, Eq. (3.15) shows that increased torques are possible. This can be understood as follows. A spin entering a ferromagnet will precess around an exchange field normal to its quantization axis. A negative mixing transmission $\operatorname{Re} G_{\uparrow\downarrow}^t < 0$ adds a phase factor corresponding to a rotation over an angle π during transmission. The outgoing spin then has a polarization opposite to the incoming one. The magnetization torque, *i.e.* the difference between in and outgoing spin currents, consequently increases compared to the situation in which the incoming transverse spin is absorbed as in thick ferromagnetic layers.

In contrast to N|F|N|F|N structures, we find that it *is* possible to observe $G_{\uparrow\downarrow}^t$ in the aMR of F|N|F|N|F devices. We study here the dependence of the aMR on the mixing transmission in a Py based multilayer. In Fig. 3.9 we present the aMR for different mixing transmissions in the middle layer of thickness $d_F = 0.27l_{sd}$. Unfortunately, it

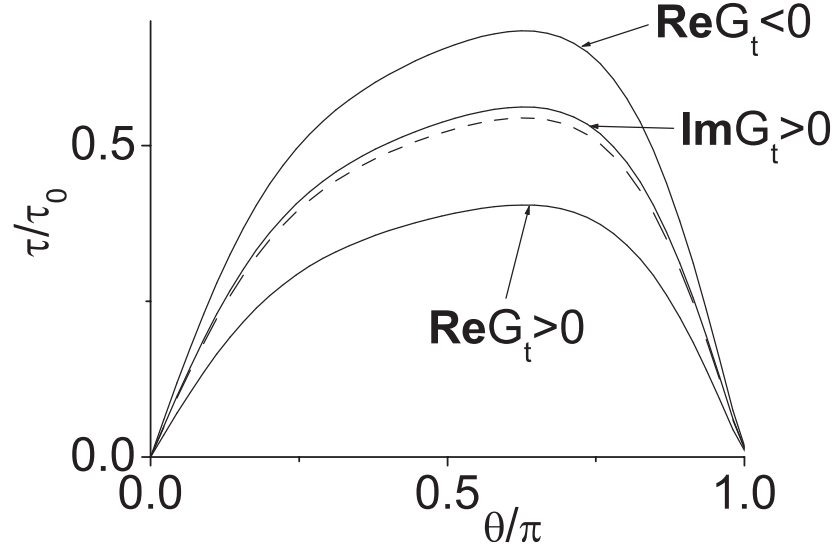


Figure 3.8: The torque on the thin right layer of thickness $d = 0.27l_{sd}$ for $F|N|F$ structure. The left layer has thickness $d \gg l_{sd}^F$. The curves starting from the lower one respectively, $Re(1/G_{\uparrow\downarrow}^t) = 5f\Omega m^2$, $Im(1/G_{\uparrow\downarrow}^t) = \infty$; $Re(1/G_{\uparrow\downarrow}^t) = \infty$, $Im(1/G_{\uparrow\downarrow}^t) = 5f\Omega m^2$; $Re(1/G_{\uparrow\downarrow}^t) = \infty$, $Im(1/G_{\uparrow\downarrow}^t) = \infty$; $Re(1/G_{\uparrow\downarrow}^t) = -5f\Omega m^2$, $Im(1/G_{\uparrow\downarrow}^t) = \infty$ ($\tau_0 = I_0\hbar/2e$).

seems difficult to obtain quantitative values for the mixing transmission from experiments since the dependence of the aMR on $G_{\uparrow\downarrow}^t$ is rather weak.

When the coherence length becomes larger than the scattering mean-free path, which can occur in weak ferromagnets like PdNi or CuNi, the transverse spin accumulation should be treated by a diffusion equation [37]. The result can be parametrized again in terms of a mixing transmission, which can subsequently be used in our circuit theory.

3.3.3 Three terminal device for observation of coherence effects

Finally, we propose an experiment that should be more sensitive to ferromagnetic coherence. We suggest the setup shown in Fig. 3.10 that is analogous to the spin-torque transistor [38] and the magnetoelectronic spin-echo [29] concepts. A current through the antiparallel ferromagnets F1 and F2 excites a spin accumulation in the normal metal N1. This spin accumulation can transmit F3 only when its thickness is less than λ_c . In that case a spin accumulation is induced in the upper normal metal N2 that can be detected as a voltage depending on the magnetization angle θ of the analyzing ferromagnet F4. We assume here that N1 is smaller than its spin-flip diffusion length (Cu is a good candidate with spin-diffusion lengths of up to a micron) such that the spin accumulation is constant under the contact to F3. Otherwise the signal at the ferromagnet F4 is diminished since part of the spin accumulation in N1 is lost due to spin-flip processes.

When the $G_{\uparrow\downarrow}^t$ of F3 is smaller than its $G_{\uparrow\downarrow}^r$ and ferromagnet F4 is not too leaky for

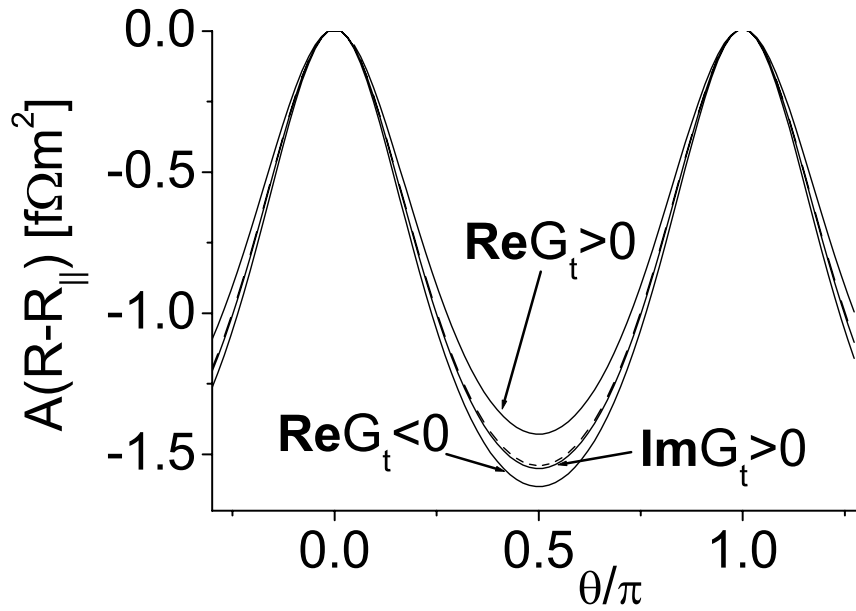


Figure 3.9: *aMR* of $F|N|F|N|F$ structure for the thickness of the middle layer $d = 0.27l_{sd}$. Outer layers are antiparallel with $d \gg l_{sd}^F$. The curves starting from the lower one respectively, $Re(1/G_{\uparrow\downarrow}^t) = -5f\Omega m^2$, $Im(1/G_{\uparrow\downarrow}^t) = \infty$; $Re(1/G_{\uparrow\downarrow}^t) = \infty$, $Im(1/G_{\uparrow\downarrow}^t) = 5f\Omega m^2$; $Re(1/G_{\uparrow\downarrow}^t) = \infty$, $Im(1/G_{\uparrow\downarrow}^t) = \infty$; $Re(1/G_{\uparrow\downarrow}^t) = 5f\Omega m^2$, $Im(1/G_{\uparrow\downarrow}^t) = \infty$.

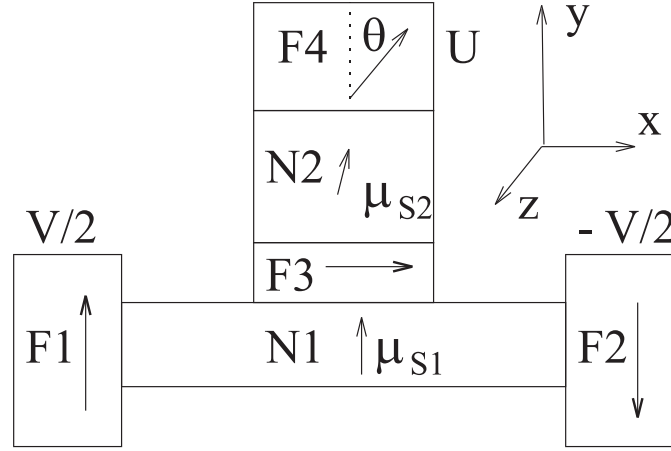


Figure 3.10: An experimental setup to observe the mixing transmission and measure the ferromagnetic coherence length in ferromagnet F3. The spin accumulation $\vec{\mu}_{S2}$ in the normal metal N2 is measured via the angular dependence of the potential $U(\theta)$ of the ferromagnet F4 that is weakly coupled to N2.

the spin current (e.g. connected via a tunnel junction) the spin accumulation in N2 can be found from Eqs. (3.10,3.11) in terms of the spin accumulation in N1:

$$\vec{\mu}_{S2} = \frac{|\mu_{S1}|}{(\text{Re } G_{\uparrow\downarrow}^r)^2 + (\text{Im } G_{\uparrow\downarrow}^r)^2} \begin{pmatrix} 0 \\ \text{Re } G_{\uparrow\downarrow}^r \text{Re } G_{\uparrow\downarrow}^t + \text{Im } G_{\uparrow\downarrow}^r \text{Im } G_{\uparrow\downarrow}^t \\ \text{Re } G_{\uparrow\downarrow}^r \text{Im } G_{\uparrow\downarrow}^t - \text{Im } G_{\uparrow\downarrow}^r \text{Re } G_{\uparrow\downarrow}^t \end{pmatrix} \quad (3.16)$$

$$\underset{\text{Im } G_{\uparrow\downarrow}^r \rightarrow 0}{\approx} \frac{|\mu_{S1}|}{\text{Re } G_{\uparrow\downarrow}^r} \begin{pmatrix} 0 \\ \text{Re } G_{\uparrow\downarrow}^t \\ \text{Im } G_{\uparrow\downarrow}^t \end{pmatrix} \quad (3.17)$$

where Eq. (3.17) holds to a good approximation when the layer F3 is metallic. The spin accumulation is indeed coherently rotated by the exchange field in F3. The angle dependence of the potential in F4 is $U(\theta) \approx \mu_{S1} P |G_{\uparrow\downarrow}^t| \cos \theta / (\text{Re } G_{\uparrow\downarrow}^r)$ with maximum along $\vec{\mu}_{S2}$, where P is the polarization of the contact N2|F4.

When the $G_{\uparrow\downarrow}^t$ of F3 is not smaller than $G_{\uparrow\downarrow}^r$ (or the spin current leak into F4 is significant), the spin accumulation μ_{S1} is affected by μ_{S2} and the final expressions are more complicated.

An angle dependence of $U(\theta)$ provides a direct proof of a finite mixing transmission. The ferromagnetic coherence length can be determined by repeating experiments for a number of layer thicknesses of F3. Such a direct experimental evidence should help to get a grip on this important parameter λ_c .

3.4 Conclusion

In this paper we extracted the spin-mixing conductance of a Py|Cu interface from the experimental data of Urazhdin *et al.* using material parameters measured independently by the MSU collaboration. We find good agreement with experiments on asymmetric F|N|F|N multilayers, reproducing quantitatively the non-monotonic aMR that we predicted earlier [24–26]. Magnetoelectronic circuit theory together with the diffusion equation is a convenient tool for the data analysis when the spin-flip diffusion length in the ferromagnet is of the same order as the layer thickness. We suggest carrying out current-induced magnetization reversal experiments on samples that display the non-monotonic aMR since we predict anomalous magnetization trajectories due to a vanishing torque at finite magnetization angle [24–26]. We also study the effects of the finite ferromagnetic coherence length in ultrathin ferromagnetic films or weak ferromagnets. For this purpose the magnetoelectronic circuit theory is extended to treat phase coherent transport in the ferromagnet. A coherence length that is larger than the ferromagnetic layer thickness does not modify the aMR of N|F|N|F|N structures, but a small effect should exist in F|N|F|N|F structures. In contrast, the spin-transfer torque is affected more strongly and may even be increased by the spin-coherence when the exchange field rotates the transverse spin current polarization by the angle π . Finally, we propose a three-terminal device that should allow experimental determination of the ferromagnetic coherence length.

3.A Appendix: Analytical results for F|N|F|N|F structure.

The aMR of a F(\uparrow)|N|F(θ)|N|F(\uparrow / \downarrow) CPP pillar can be described analytically when the thick outer layers are parallel or antiparallel, respectively.

$$R(\theta) = \frac{2(R_{\uparrow\downarrow} + R) + R_M}{\frac{R_{\uparrow\downarrow}(R_{M-}^2 + 4R_-(R_- + R_{M-}\alpha)) + (2R_MR_-^2 + R_{M-}^2R)(1 - \alpha^2)}{(R_{\uparrow\downarrow} + R)(2R_{\uparrow\downarrow} + R_M) - RR_M\alpha^2}}, \quad (3.18)$$

$$R(\theta) = 2(R_{\uparrow\downarrow} + R) + R_M - \frac{2R_-^2(1 - \alpha^2)}{R_{\uparrow\downarrow} + R(1 - \alpha^2)} - \frac{2R_{M-}^2(R_{\uparrow\downarrow} + R(1 - \alpha^2))}{(R_{\uparrow\downarrow} + R)(2R_{\uparrow\downarrow} + R_M) - RR_M\alpha^2}, \quad (3.19)$$

where $\alpha = \cos \theta$, $4R + 2R_{\uparrow\downarrow} = \frac{1}{G_{\uparrow}} + \frac{1}{G_{\downarrow}}$, $4R_{-} = \frac{1}{G_{\uparrow}} - \frac{1}{G_{\downarrow}}$ for the outer layers. The mixing resistance for two interfaces adjacent to any normal metal $R_{\uparrow\downarrow} = \frac{1}{G_{\uparrow\downarrow}}$ (we assume all interfaces identical). For the middle layer $4R_M = \frac{1}{G_{\uparrow}} + \frac{1}{G_{\downarrow}} - 4R_{\uparrow\downarrow}$, $4R_{M-} = \frac{1}{G_{\uparrow}} - \frac{1}{G_{\downarrow}}$.

References

- [1] M. Baibich, J. M. Broto, A. Fert, F. N. V. Dau, F. Petroff, P. Eitenne, G. Creuzet, A. Friederich, and J. Chazelas, *Phys. Rev. Lett.* **61**, 2472 (1988).
- [2] M. A. M. Gijs and G. E. W. Bauer, *Adv. Phys.* **46**, 285 (1997).
- [3] J. C. Slonczewski, *J. Magn. Magn. Mater.* **159**, L1 (1996).
- [4] L. Berger, *Phys. Rev. B* **54**, 9353 (1996).
- [5] M. Tsoi, A. Jansen, J. Bass, W. Chiang, M. Seck, V. Tsoi, and P. Wyder, *Phys. Rev. Lett.* **80**, 4281 (1998).
- [6] J. Wegrowe, D. Kelly, Y. Jaccard, P. Guittienne, and J. Ansermet, *Europhys. Lett.* **45**, 626 (1999).
- [7] E. B. Myers, D. C. Ralph, J. A. Katine, R. N. Louie, and R. A. Buhrman, *Science* **285**, 867 (1999).
- [8] M. Tsoi, A. Jansen, J. Bass, W. Chiang, M. Seck, V. Tsoi, and P. Wyder, *Phys. Rev. Lett.* **81**, 493 (1998).
- [9] I. N. Krivorotov, N. C. Emley, J. C. Sankey, S. I. Kiselev, D. C. Ralph, and R. A. Buhrman, *Science* **307**, 228 (2005).
- [10] T. Valet and A. Fert, *Phys. Rev. B* **48**, 7099 (1993).
- [11] J. Bass and W. Pratt, Jr., *J. Magn. Magn. Mater.* **200**, 274 (1999).
- [12] C. Galinon, K. Tewelde, R. Loloee, W.-C. Chiang, S. Olson, H. Kurt, W. Pratt, Jr., J. Bass, P. Xu, K. Xia, et al. (preprint).
- [13] X. Waintal, E. B. Myers, P. W. Brouwer, and D. C. Ralph, *Phys. Rev. B* **62**, 12317 (2000).
- [14] A. Brataas, Y. V. Nazarov, and G. E. W. Bauer, *Eur. Phys. J. B* **22**, 99 (2001).
- [15] J. C. Slonczewski, *J. Magn. Magn. Mater.* **247**, 324 (2002).

- [16] M. D. Stiles and A. Zangwill, *Phys. Rev. B* **66**, 014407 (2002).
- [17] A. Brataas, Y. V. Nazarov, and G. E. W. Bauer, *Phys. Rev. Lett.* **84**, 2481 (2000).
- [18] K. Xia, P. J. Kelly, G. E. W. Bauer, A. Brataas, and I. Turek, *Phys. Rev. B* **65**, 220401(R) (2002).
- [19] L. Giacomoni, B. Dieny, W. Pratt, Jr., R. Loloee, and M. Tsoi (unpublished).
- [20] G. E. W. Bauer, Y. Tserkovnyak, D. Huertas-Hernando, and A. Brataas, *Phys. Rev. B* **67**, 094421 (2003).
- [21] S. Urazhdin, R. Loloee, and W. Pratt, Jr., *Phys. Rev. B* **71**, 100401(R) (2004).
- [22] P. Dauguet, P. Gandit, J. Chaussy, S. Lee, A. Fert, and P. Holody, *Phys. Rev. B* **54**, 1083 (1996).
- [23] A. Vedyayev, N. Ryzhanova, B. Dieny, P. Dauguet, P. Gandit, and J. Chaussy, *Phys. Rev. B* **55**, 3728 (1997).
- [24] A. A. Kovalev, A. Brataas, and G. E. W. Bauer, *Phys. Rev. B* **66**, 224424 (2002).
- [25] J. Manschot, A. Brataas, and G. E. W. Bauer, *Phys. Rev. B* **69**, 092407 (2004).
- [26] J. Manschot, A. Brataas, and G. Bauer, *Appl. Phys. Lett.* **85**, 3250 (2004).
- [27] A. Shpiro, P. M. Levy, and S. Zhang, *Phys. Rev. B* **67**, 104430 (2003).
- [28] Y. Tserkovnyak, A. Brataas, and G. E. W. Bauer, *Phys. Rev. Lett.* **88**, 117601 (2002).
- [29] A. Brataas, G. Zarand, Y. Tserkovnyak, and G. E. W. Bauer, *Phys. Rev. Lett.* **91**, 166601 (2003).
- [30] M. Zwierzycki, Y. Tserkovnyak, P. Kelly, A. Brataas, and G. Bauer, *Phys. Rev. B* (2005).
- [31] L. Berger, *J. Appl. Phys.* **93**, 7693 (2003).
- [32] S. Nakamura, *Materia Japan* **43**, 498 (2004).
- [33] D. Huertas-Hernando, Y. V. Nazarov, A. Brataas, and G. E. W. Bauer, *Phys. Rev. B* **62**, 5700 (2000).
- [34] J. Xiao, A. Zangwill, and M. Stiles, *Phys. Rev. B* **70**, 172405 (2004).
- [35] W. Pratt, Jr. and et al, *IEEE Trans. Mag.* **33**, 3505 (1997).

- [36] S. Urazhdin, R. Loloee, and W. Pratt, Jr. (2004), cond-mat/0403441 v1.
- [37] S. Zhang, P. M. Levy, and A. Fert, Phys. Rev. Lett. **88**, 236601 (2002).
- [38] G. E. W. Bauer, A. Brataas, Y. Tserkovnyak, and B. J. van Wees, Appl. Phys. Lett. **82**, 3928 (2003).

Chapter 4

Magnetomechanical torques in small magnetic cantilevers

We study a small magnetic cantilever (e.g. a Si cantilever covered by a magnetic film or an entirely ferromagnetic cantilever). The magnetomechanical torques are found to cause line splittings in ferromagnetic resonance spectra and magnetization reversal facilitated by mechanical degree of freedom. We show that the magnetomechanical torques can extend the limits of detecting and exciting motion at the nanoscale. A "nanomotor" described here effectively transforms rf magnetic fields into mechanical oscillations. Furthermore we propose to integrate mechanical oscillators into magnetoelectronic devices that employ Slonczewski's torque. This opens new possibilities for electric transducers of nanomechanical motion.

4.1 Introduction

Micro- and nanoelectromechanical systems (NEMS) [1, 2] allow nanoscale control over as small sensors with spatial resolution on an atomic scale [3] operating at frequencies in the GHz range [4]. NEMS detection of extremely small forces corresponding to biomolecular interactions [5] and mass changes corresponding to single molecules [6] have been reported. Efforts have been made to merge the field of nanomechanics with that of nanoscale magnetism. The success in the detection of a single electron spin by magnetic resonance is a good example [7]. A nuclear spin sensor that is based on imposing a coherent motion on nuclear spins has been proposed [8]. Here we focus on the possibilities provided by the coupled motion of the strain field of a cantilever and the magnetization of a ferromagnet [9, 10]. Magnetization reversal in small magnetic clusters [11] is usually realized by external magnetic fields [12–15] or polarized spin currents employing spin-transfer torques [16–23]. Along alternative mechanisms to switch the magnetization such as employing antiferromagnets [24] and time-dependent magnetic fields [25], we suggest the effect of mechanically assisted magnetization reversal [10]. The fastest mechanical device reported in the literature is operated with the help of magnetomotive forces at GHz frequencies [4]. We propose to actuate such systems by demagnetizing currents that provide coupling between the mechanical and the magnetization motion most efficiently in the GHz range. Coupling of the magnetization motion to an electric circuit via spin-transfer torques and magnetoresistance then opens the possibility of high frequency transducers of nanomechanical motion. In this paper, we report consequences for the magnetovibrational coupling such as splitting of the ferromagnetic resonance (FMR) spectrum and magnetization reversal facilitated by the mechanical degrees of freedom. We argue that a predominantly ferromagnetic cantilever provides stronger coupling and, when integrated into a magnetoelectronic circuit, offers new functionalities for both mechanical and magnetic devices. Some preliminary results have been reported already [9, 10].

The paper is organized as follows. In Section 4.2, we describe our system, the magnetic cantilever, and derive a set of equations describing magnetomechanical motion. In Section 4.3, we solve these equations in the limit of small magnetization oscillations, finding a splitting of FMR spectra for the resonantly coupled mode. In Section 4.4, we propose a current-induced magnetic resonance technique in spin valves and demonstrate that magnetovibrational modes can be detected by this method. Finally, in Section 4.5, we analyze large magnetization oscillations in the presence of magnetovibrational couplings and demonstrate magnetization reversal assisted by the mechanical degrees of freedom.

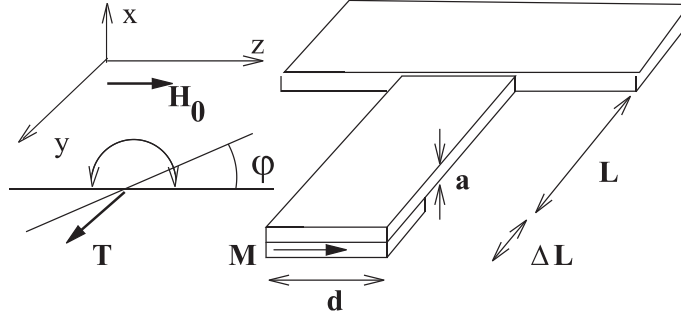


Figure 4.1: A magnetomechanical cantilever supporting magneto-vibrational modes. On a dielectric substrate (such as Si) a single-domain ferromagnetic film is deposited at the free end.

4.2 System

We consider first a small dielectric cantilever with a single-domain ferromagnetic layer deposited on its far end (see Fig. 4.1). A constant external field \mathbf{H}_0 is applied along the z axis. In Section 4.3 we also include an oscillating field H_y along the y axis to pump and probe the system. The effective field \mathbf{H}_{eff} felt by the magnetization consists of \mathbf{H}_0 as well as the crystal anisotropy and the demagnetizing fields. The strains are localized in the mechanical link of the cantilever between the ferromagnetic film at one end and the other end that is fixed. The lattice of the ferromagnet then oscillates without internal mechanical strains, but crystalline and form anisotropies couple the magnetic order parameter to the torsional mode of the cantilever.

Our setup consists of two weakly interacting subsystems - the magnetic and the mechanical. It is then useful to first study the two subsystems separately.

4.2.1 Magnetization motion in a single-domain ferromagnet

The magnetization \mathbf{M} of the ferromagnet precesses around an effective magnetic field \mathbf{H}_{eff} according to the Landau-Lifshitz-Gilbert equation [26]:

$$\frac{d\mathbf{M}}{dt} = -\gamma\mathbf{M} \times \mathbf{H}_{\text{eff}} + \frac{\alpha}{M_s}\mathbf{M} \times \frac{d\mathbf{M}}{dt}, \quad (4.1)$$

where γ denotes the gyromagnetic ratio. The phenomenological Gilbert constant is typically $\alpha \lesssim 0.01$ for metallic and $\alpha \lesssim 0.00001$ for insulating ferromagnets. The effective field is given by the functional derivative of the free energy of the system, that is of the form (in the lowest order in magnetizations in some specially chosen reference frame)

$$E_{mg} = \frac{1}{2}D_x M_x^2 + \frac{1}{2}D_y M_y^2 + \frac{1}{2}D_z M_z^2 - \mathbf{M}\mathbf{H}_0, \quad (4.2)$$

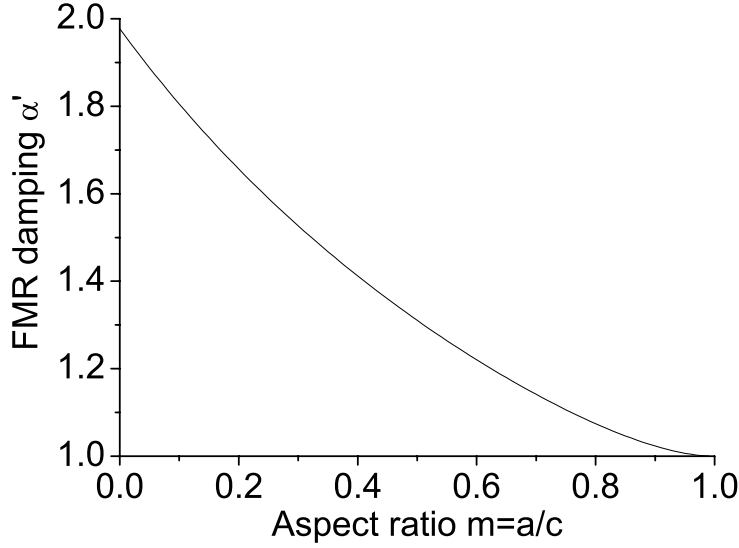


Figure 4.2: Dependence of FMR broadening on aspect ratio $m = a/c$ for ellipsoid with the semi-axes a and $b = c$ ($H_0 = M_s$).

where D_x , D_y and D_z describe the anisotropy of the magnetization along the Cartesian axes x , y and z , including demagnetizing effects and crystalline anisotropy. The associated effective field is given by $\mathbf{H}_{\text{eff}} = \mathbf{H}_0 - D_x M_x \mathbf{x} - D_y M_y \mathbf{y} - D_z M_z \mathbf{z}$.

4.2.2 Small magnetization oscillations and dependence of FMR broadening on shape and crystal anisotropies

To first order, the deviations from the equilibrium magnetization in the z -direction lie in the $x - y$ plane: $\mathbf{M} = m_x \mathbf{x} + m_y \mathbf{y} + M_s \mathbf{z}$, where M_s is the saturation magnetic moment. The magnetic susceptibilities $\chi_{yy}(\omega) = (m_y/H_y)_\omega$ and $\chi_{yx}(\omega) = (m_x/H_x)_\omega$ describe the linear response of the magnetization m_y to a (weak) rf magnetic field $H_y(H_x)$ at frequency ω and can be found after linearizing the LLG equation in frequency space:

$$\chi_{yy}(\omega) = \frac{\gamma^2 M_s (H_0 + (D_x - D_z) M_s)}{\omega^2 - (1 + \alpha^2) \omega_m^2 + i \alpha \omega (2H_0 + (D_x + D_y - 2D_z) M_s)}, \quad (4.3)$$

$$\chi_{yx}(\omega) = \frac{i \omega \gamma M_s}{\omega^2 - (1 + \alpha^2) \omega_m^2 + i \alpha \omega (2H_0 + (D_x + D_y - 2D_z) M_s)}, \quad (4.4)$$

where $\omega_m^2 = (H_0 + (D_x - D_z) M_s)(H_0 + (D_y - D_z) M_s)$ is the FMR resonant frequency. Note that the FMR damping has to be renormalized in the presence of anisotropies. The

broadening of the FMR lineshape is

$$\alpha' = \alpha \frac{(H_0/M_s + (D_x + D_y)/2 - D_z)}{\sqrt{(H_0/M_s + D_x - D_z)(H_0/M_s + D_y - D_z)}}$$

Let us consider an ellipsoid with the semi-axes a and $b = c$. For small crystalline anisotropies the anisotropy factors are defined by shape anisotropies

$$\begin{aligned} D_x &= \frac{4\pi}{m^2-1} \left[\frac{m}{2\sqrt{m^2-1}} \ln\left(\frac{m+\sqrt{m^2-1}}{m-\sqrt{m^2-1}}\right) - 1 \right] \stackrel{m \ll 1}{\approx} 4\pi - 2\pi m, \\ D_y = D_z &= \frac{2\pi m}{m^2-1} \left[m - \frac{1}{2\sqrt{m^2-1}} \ln\left(\frac{m+\sqrt{m^2-1}}{m-\sqrt{m^2-1}}\right) \right] \stackrel{m \ll 1}{\approx} \pi m, \end{aligned} \quad (4.5)$$

where $m = a/c$. The dependence of FMR broadening on the aspect ratio m is plotted in Fig. 4.2.

4.2.3 Nonlinear magnetization oscillations

Without Gilbert damping the dynamics of the magnetization can be analyzed analytically for different magnetic anisotropies [27]. We present here solutions for the “easy plane” anisotropy when $D_y = D_z = 0$ and $\mathbf{H}_0 = H_0 \mathbf{z}$ which is relevant for Section 4.4. Without the Gilbert damping but including the anisotropy factor D_x the LLG equations read

$$\begin{cases} \frac{dM_x}{dt} = -\gamma M_y H_0 \\ \frac{dM_y}{dt} = \gamma M_x H_0 + \gamma D_x M_z M_x \\ \frac{dM_z}{dt} = \gamma D_x M_y M_x \end{cases} \quad (4.6)$$

The x -component of the magnetization then obeys

$$\ddot{M}_x = -(H_0^2 - D_x E_{mg}) \gamma^2 M_x - \frac{\gamma^2}{2} D_x^2 M_x^3 \quad (4.7)$$

where the energy $E_{mg} = -H_0 M_z + D_x M_x^2/2$ is constant when there is no Gilbert damping.

This equation describes a so-called “Duffing oscillator”, one of the rare examples of a non-linear dynamic systems that can be solved analytically. The potential energy of the oscillator has two minima. As a result, one can observe effects like periodic motion centered at one of those minima that with increasing energy suddenly doubles its period. When a periodic external force is applied to such an oscillator, the system may carry out jumps between minima leading to stochastic motion in time. Duffing’s equation

$$\ddot{x} - kx + 2\lambda x^3 = 0 \quad (4.8)$$

can be integrated at once to give the first integral:

$$\dot{x}^2 - kx^2 + \lambda x^4 = Z, \quad (4.9)$$

where Z is the energy of the Duffing oscillator. By comparing Eqs. (4.6,4.7) to Eqs. (4.8,4.9) we obtain that $Z = \gamma^2(M^2H_0^2 - E_{mg}^2)$, $k = \gamma^2(D_x E_{mg} - H_0^2)$ and $\lambda = \gamma^2 D_x^2/4$. The energy minima of the Duffing oscillator therefore correspond to the energy maxima in our system. The magnetization can jump between the regions of maximal energy when external torques are applied which is analogous to the behavior of the Duffing oscillator (see Fig. 4.3). One can distinguish three different types of solutions.

1. $Z < 0$. “Small amplitude” solutions when motion is at energies close to an energy minimum (in Fig. 4.3 it corresponds to two small circles and $E_{mg} > 1$, the magnetization oscillates close to the perpendicular to the film direction). We express the solutions in terms of Jacobi elliptic functions dn:

$$x = \sqrt{\frac{k}{\lambda(2-v^2)}} \operatorname{dn} \left(\sqrt{\frac{k}{\lambda(2-v^2)}} t, v \right) \quad (4.10)$$

where v can be found from $Z = -\frac{k^2(1-v^2)}{4\lambda(1-v^2/2)^2}$.

2. $Z = 0$ corresponds to the separatrix (in Fig. 4.3 it is the longest possible trajectory in a shape of a bent "8"). Here the Jacobi functions degenerate to hyperbolic function ch:

$$x = \pm \sqrt{\frac{k}{\lambda}} \frac{1}{\operatorname{ch}(kt)} \quad (4.11)$$

3. $Z > 0$ (in Fig. 4.3 it corresponds to bent elliptical trajectories and $E_{mg} < 1$, the magnetization trajectories are squeezed in the perpendicular to the film direction). “Large amplitude” solutions via the Jacobi functions cn:

$$x = \sqrt{\frac{k}{\lambda(2v^2-1)}} v \operatorname{cn} \left(\sqrt{\frac{k}{\lambda(2v^2-1)}} t, v \right) \quad (4.12)$$

where $Z = -\frac{k^2 v^2(1-v^2)}{\lambda(2v^2-1)^2}$.

The analytical solution in our case can be written for the entire parameter space with the exception of the separatrix by a single formula as follows:

$$M_x = \sqrt{-2p_-} \operatorname{dn} \left(t\gamma\sqrt{-p_-/2}, 1 - p_+/p_- \right) \stackrel{p_- \ll p_+}{\approx} \sqrt{-2p_-} \cos(t\sqrt{p_+/2}) \quad (4.13)$$

$$M_y = -\frac{\dot{M}_x}{\gamma H_0}, \quad M_z = \frac{D_x M_x^2 - 2E_{mg}}{2H_0}, \quad (4.14)$$

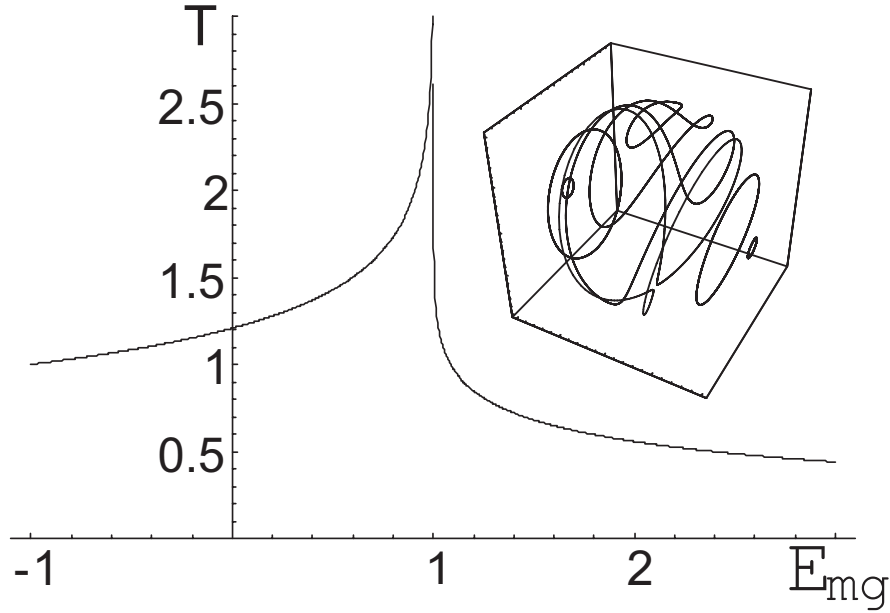


Figure 4.3: The period T_1 ($E_{mg} < 1$) and T_2 ($E_{mg} > 1$) of the magnetization dynamics in Eqs. (4.15) in units $2\pi / (\gamma\sqrt{(H_0 + D_x M)H_0})$ as a function of energy in units $H_0 M$. The inset shows a plot of typical trajectories at different energies on the unit sphere ($D_x M = 10H_0$).

where $p_{\pm} = H_0^2 - D_x E_{mg} \pm H_0 \sqrt{H_0^2 - 2D_x E_{mg} + D_x^2 M_s^2}$. When $D_x > 0$ this leads to the trajectories and oscillation periods depicted in Fig. 4.3. The motion is periodic with time periods that can be expressed by elliptic integrals K as

$$\begin{aligned} T_1 &= 4\sqrt{2}K(p_-/p_+) / (\gamma\sqrt{p_+}) \stackrel{p_- \ll p_+}{\approx} 2\pi\sqrt{2/p_+}; & E_{mg} < MH_0 \\ T_2 &= 2\sqrt{2}K(1 - p_+/p_-) / (\gamma\sqrt{-p_-}) \stackrel{|p_- - p_+| \ll |p_-|}{\approx} \pi\sqrt{-2/p_-}. & E_{mg} > MH_0 \end{aligned} \quad (4.15)$$

The variation of the periodicity has important consequence for the coupling to the lattice in the regime of large magnetization oscillations as explained below.

4.2.4 Cantilever oscillations and coupled magneto-mechanical equations

Throughout this paper, we assume that the torsional oscillations of the cantilever are small. The torsional motion of the part of the cantilever that is not covered by the ferromagnet

can be found by applying the variational principle to the total elastic energy [28]:

$$E_{el} = \frac{1}{2} \int_0^L C \tau^2 dy, \quad (4.16)$$

where $\tau = \partial\varphi/dy$ and C is an elastic constant defined by the shape and material of the cantilever ($C = \frac{1}{3}\mu da^3$ for a plate with thickness a much smaller than width d , $a \ll d$, μ is the Lamé constant). $T = C\tau(y)$ is the torque flowing through the cantilever at point y . The integration is taken from the clamping point $y = 0$ until the cantilever endpoint $y = L$. The equation of motion reads

$$C \frac{\partial^2 \varphi}{\partial y^2} = \rho I \frac{\partial^2 \varphi}{\partial t^2} + 2\beta \rho I \frac{\partial \varphi}{\partial t}, \quad (4.17)$$

where $I = \int (z^2 + x^2) dz dx \simeq ad^3/12$ is the moment of inertia of the cross-section about its center of mass, ρ the mass density, and β is a phenomenological damping constant related to the quality factor Q at the resonance frequency ω_e as $Q = \omega_e/(2\beta)$ (at 1 GHz $Q \sim 500$) [4]. Note that ω_e can be also a higher harmonic resonance frequency in what follows. The oscillating solution has the form $\varphi = \sin(ky)(A_1 \sin(\omega t) + A_2 \cos(\omega t))$, where $k = (\omega + i\beta)/c$ is the wave number, $c = c_t 2a/d = \sqrt{C/(\rho I)}$ and $c_t = \sqrt{\mu/\rho}$ is the transverse velocity of sound. The free constants A_1 and A_2 depend on the initial conditions. The boundary condition $\varphi|_{y=0} = 0$ at the clamping point is already fulfilled, and the boundary condition at the end $y = L$ is discussed in the following.

Combining Eqs. (4.2,4.16) and taking into account the smallness of the magnet $\Delta L \ll L$ we can write the free energy of the cantilever coupled to the magnetization:

$$F = V(-\mathbf{M}\mathbf{H}_0 + \frac{D_x}{2} [M_x + M_z \varphi(L)]^2 + \frac{D_z}{2} [M_z - M_x \varphi(L)]^2 + \frac{D_y M_y^2}{2}) + \frac{C}{2} \int_0^L \tau^2 dy. \quad (4.18)$$

Eq. (4.18) demonstrates that magneto-mechanical coupling is only possible when the factors D_x or D_z are non-zero (the anisotropy factor D_y does not contribute to the coupling since our mechanical motion is rotationally invariant with respect to the axis y and one needs anisotropies D_x and D_z to break the invariance). For small $\varphi = \varphi(L)$, where $\varphi(y)$ is the torsion angle at position y of the cantilever, the effective field $\mathbf{H}_{\text{eff}} = -\frac{\partial F}{\partial \mathbf{M}}$ is

$$\mathbf{H}_{\text{eff}} = (D_x M_z \varphi - D_x M_x) \mathbf{x} + D_x M_x \varphi \mathbf{z} - (D_z M_x \varphi + D_z M_z) \mathbf{z} - D_z M_z \varphi \mathbf{x} - D_y M_y + \mathbf{H}_0$$

where D_x , D_y and D_z describe the anisotropies ($D_x \simeq 4\pi$ for a thin film without crystal anisotropies). The equation of motion of the magnetization \mathbf{M} in the presence of the

mechanical degree of freedom then reads

$$\frac{d\mathbf{M}}{dt} = -\gamma\mathbf{M} \times \mathbf{H}_{\text{eff}} + \frac{\alpha}{M_s}\mathbf{M} \times \left(\frac{d\mathbf{M}}{dt} \right)_{\text{cant}}, \quad (4.19)$$

where the derivative $\left(\frac{d\mathbf{M}}{dt} \right)_{\text{cant}} = \frac{d\mathbf{M}}{dt} + \frac{d\phi}{dt}(-M_z\mathbf{x} + M_x\mathbf{z})$ is taken in the reference system of the cantilever since the magnetization damping is caused by interactions of the magnetization with the bulk of the cantilever.

By applying the variational principle to Eq. (4.18) we obtain Eq. (4.17) and the second boundary condition for its solutions. The magnetovibrational coupling can then be treated as a boundary condition to the mechanical problem, which is expressed as the torque $C\tau|_{y=L}$ exerted by the magnetization on the edge of the cantilever:

$$C\tau|_{y=L} = \frac{1}{\gamma} \left(\frac{d\mathbf{M}}{dt} + \gamma\mathbf{M} \times \mathbf{H}_0 \right) |_{y=L}, \quad (4.20)$$

This boundary condition is equivalent to the conservation law of the mechanical angular momentum written for the tip of the cantilever. Let us introduce an angular momentum $\mathbf{V}^{\text{el}}(y)$ for a thin slice at point $y \in \{0, L\}$ (without magnetic overlayer), then the conservation law is $d\mathbf{V}^{\text{el}}(y)/dt = \mathbf{T}(y)$, where $\mathbf{T}(y)$ is the torque flowing into the slice. This equation is modified by the coupling to the magnet in a region $y \in \{L, L + \Delta L\}$ (ΔL is the length of the cantilever covered by the magnetic layer) as:

$$\frac{d}{dt} \left(\mathbf{V}^{\text{el}}(L) + \left(-\frac{1}{\gamma}\right)\mathbf{M}(L)V \right) = \mathbf{T}(L) + \mathbf{T}_{\text{field}}. \quad (4.21)$$

where $\mathbf{T}_{\text{field}} = V\mathbf{M} \times \mathbf{H}_0$, V is the volume of the magnet and $\mathbf{T}(y)|_y = -C\tau(y)$. When $\Delta L \ll L$, internal strains in the magnetic section may be disregarded and the magnetization torque can be treated as a boundary condition Eq. (4.20).

The coupling of Eqs. (4.1) and (4.17) can be made explicit:

$$\begin{aligned} \partial\phi/dy|_{y=L} &= \frac{1}{C\gamma} \left(\frac{dM_y}{dt} + \gamma\mathbf{M} \times \mathbf{H}_0 \right) \\ \mathbf{H}_{\text{eff}} &= (D_x M_z \phi - D_x M_x) \mathbf{x} + D_x M_x \phi \mathbf{z} - (D_z M_x \phi + D_z M_z) \mathbf{z} - D_z M_z \phi \mathbf{x} - D_y M_y + \mathbf{H}_0 \end{aligned} \quad (4.22)$$

4.2.5 Entirely ferromagnetic cantilever

It is straightforward to generalize the free energy Eq. (4.18) to the case when the whole cantilever is covered by a ferromagnetic film or when the whole cantilever is ferromag-

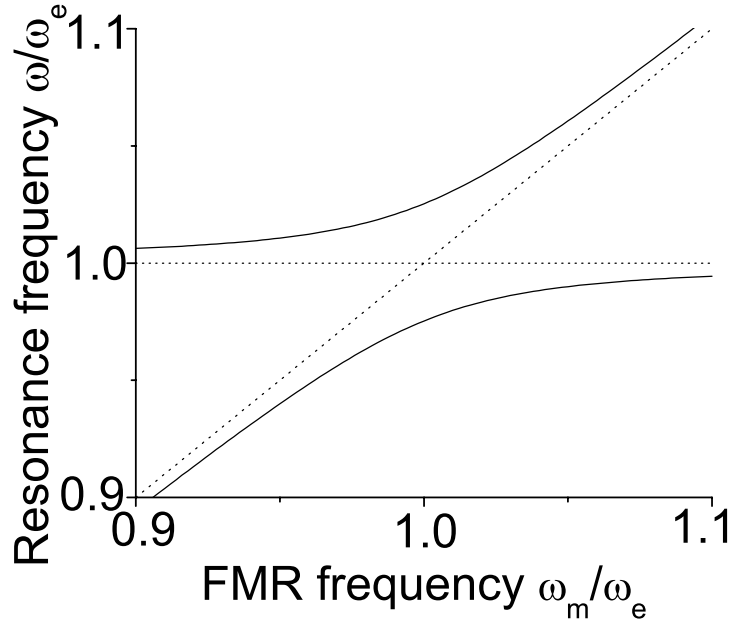


Figure 4.4: Dependence of the resonance frequency of the coupled motion on the FMR frequency ω_m of the uncoupled magnetization ($g \sim 0.001$).

netic. The free energy then has the form:

$$F = V(-\mathbf{M}\mathbf{H}_0 + \frac{D_x}{2}[M_x + M_z\bar{\varphi}]^2 + \frac{D_z}{2}[M_z - M_x\bar{\varphi}]^2 + \frac{D_y M_y^2}{2}) + \frac{C}{2} \int_0^L \tau^2 dy \quad (4.23)$$

where $\bar{\varphi} = \frac{1}{L} \int_0^L \varphi(y) dy$ is the average angle of torsion. In this case the system of the magnetomechanical equations becomes:

$$\begin{aligned} \frac{d\mathbf{M}}{dt} &= -\gamma \mathbf{M} \times \mathbf{H}_{\text{eff}} + \frac{\alpha}{M_s} \mathbf{M} \times \left(\frac{d\mathbf{M}}{dt} \right)_{\text{cant}} \\ C \frac{\partial^2 \varphi}{\partial y^2} &= \rho I \frac{\partial^2 \varphi}{\partial t^2} + \frac{S}{\gamma} \left(\frac{dM_y}{dt} + \gamma \mathbf{M} \times \mathbf{H}_0 \right) + 2\beta \rho I \frac{\partial \varphi}{\partial t} \\ C \partial \varphi / \partial x|_{x=L} &= 0 \end{aligned}$$

$$\mathbf{H}_{\text{eff}} = (D_x M_z \bar{\varphi} - D_x M_x) \mathbf{x} + D_x M_x \bar{\varphi} \mathbf{z} - (D_z M_x \bar{\varphi} + D_z M_z) \mathbf{z} - D_z M_z \bar{\varphi} \mathbf{x} - D_y M_y + \mathbf{H}_0 \quad (4.24)$$

The coupling can be much more efficient in the latter as compared to the former system since the volume of the magnet is larger. The disadvantage is that the form anisotropy wants to align the magnetization along the cantilever making the subsystems uncoupled. Another disadvantage, the possibility of spin wave excitations, is discussed in the next Section.

4.3 Small magnetization oscillations

4.3.1 Magnet at the tip of cantilever

To first order, the deviations from the equilibrium magnetization in the z -direction lie in the $x - y$ plane: $\mathbf{M} = m_x \mathbf{x} + m_y \mathbf{y} + M_s \mathbf{z}$, where M_s is the saturation magnetic moment (see Fig. 4.1). For small φ , the effective field oscillates in the $x - y$ plane: $\mathbf{H}_{\text{eff}} = (D_x M_s \varphi - D_x M_x) \mathbf{x} + D_x M_x \varphi \mathbf{z} - (D_z M_x \varphi + D_z M_s) \mathbf{z} - D_z M_s \varphi \mathbf{x} - D_y M_y + \mathbf{H}_0$, ($D_x \simeq 4\pi$ for a thin film without crystal anisotropy). Note that the coupling does not rely on a strong magnetocrystalline field, since the surface forces of demagnetizing currents also provide a restoring torque. For a thin ferromagnetic layer the latter dominates and the magnetization does not precess, but oscillates like a pendulum in the $y - z$ plane due to the oscillating field in the x -direction $\mathbf{H}_{\text{eff}} = D_x M_s \varphi \mathbf{x}$.

By using Eq. (4.20) with the substitution of φ in τ , $C\tau|_{y=L} = Ck \cos(kL)(A_1 \sin(\omega t) + A_2 \cos(\omega t)) = Ck\varphi \cot(kL)$, we obtain in frequency space and to first order in the magnetization oscillations:

$$Ck\varphi \cot(kL) = \frac{V}{\gamma}(-i\omega m_y - \gamma H_0 m_x) \quad (4.25)$$

$$\approx -C\varphi \frac{L}{2c^2}(\omega^2 + 2i\beta\omega - \omega_e^2), \quad (4.26)$$

where in the second line the \cot has been expanded close to the resonance frequency $\omega_e = c\pi(1/2 + s)/L$ (s is integer, here we concentrate mainly on coupling to the first harmonic and $s = 0$).

The magnetic susceptibilities $\chi_{yy}(\omega) = (m_y/H_y)_\omega$ and $\chi_{yx}(\omega) = (m_y/H_x)_\omega$ describe the linear response of the magnetization m_y to a (weak) rf magnetic field $H_y(H_x)$ at frequency ω . Generalization of Eqs (4.3,4.4) in the presence of magneto-vibrational coupling can be found after writing LLG equation in frequency space with use of Eq. (4.25), and taking into account smallness of the Gilbert damping α :

$$\chi_{yy}(\omega) = \frac{\gamma^2 M_s^2 (D_x - D_z + H_0(1 - g \tan(kL)))/M_s}{\omega^2 - \omega_m^2 + 2i\alpha'\omega\omega_m + [\omega^2 - H_0(H_0 + (D_y - D_z)M_s)]g \tan(kL)} \quad (4.27)$$

$$\chi_{yx}(\omega) = \frac{i\omega\gamma M_s}{\omega^2 - \omega_m^2 + 2i\alpha'\omega\omega_m + [\omega^2 - H_0(H_0 + (D_y - D_z)M_s)]g \tan(kL)} \quad (4.28)$$

where $g = M_s^2 V (D_x - D_z) c^2 / (CL\omega_e^2) = (2/\pi)^2 (D_x - D_z) (L/a)^2 (V/V_c) (M_s^2/\mu)$ is the magnetovibrational coupling constant (V and V_c are the volumes of the magnet and the cantilever respectively) and the unperturbed resonance frequency $\omega_m^2 = (H_0 + (D_x - D_z)M_s)(H_0 + (D_y - D_z)M_s)$. Note that the coupling constant is defined by the material parameters in the term M_s^2/μ , by the geometry in the term $(L/a)^2 (V/V_c)$ and by both

the geometry and the material parameters in the term $(D_x - D_z)$. The imaginary part of $\chi_{yy}(\omega)$ is proportional to the FMR absorption signal.

When the cantilever with the magnet is subjected to the rf magnetic field, the magneto-mechanical torques induce a mechanical motion. In effect we have then constructed a nano-scale motor that transforms the magnetic field oscillations into mechanical motion with amplitudes that are given by the susceptibility $\chi_{\varphi y}(\omega) = (\varphi/H_y)_\omega$. The latter follows from the LLG equation in frequency space using Eq. (4.25), and taking into account the smallness of the Gilbert damping α :

$$\chi_{\varphi y}(\omega) = \frac{i\omega g \tan(kL)}{\omega^2 - \omega_m^2 + 2i\alpha'\omega\omega_m + [\omega^2 - H_0(H_0 + (D_y - D_z)M_s)]g \tan(kL)} \quad (4.29)$$

In the absence of the external field H_0 the resonance frequencies in the vicinity of the resonance frequency ω_e can be found after expanding $\cot(kL)$ as in Eq. (4.26):

$$\omega_{1(2)} = \sqrt{\frac{1}{2} \left[\omega_e^2 + \omega_m^2 + g\omega_e^2 \pm \left((\omega_e + \omega_m)^2 + g\omega_e^2 \right) \left((\omega_e - \omega_m)^2 + g\omega_e^2 \right)^{1/2} \right]^{1/2}}. \quad (4.30)$$

When the external field H_0 is smaller than the demagnetizing field, Eq. (4.30) holds with $\omega_m^2 = (H_0 + (D_x - D_z)M_s)(H_0 + (D_y - D_z)M_s)$. This fact can be used to tune the FMR frequency in order to match the elastic frequency. In this limit of strong shape anisotropy (for example a thin ferromagnetic film with $D_x \sim 4\pi$) and when $H_0 G / (M_s \beta \omega_e^2) \ll 1$, Eqs. (4.27,4.29) simplify to

$$\chi_{yy}(\omega) \approx \frac{\gamma^2 M_s^2 (D_x - D_z)}{\omega^2 - \omega_m^2 + 2i\alpha'\omega\omega_m + \omega^2 g \tan(kL)}, \quad (4.31)$$

$$\chi_{\varphi y}(\omega) \approx \frac{i\omega g \tan(kL)}{\omega^2 - \omega_m^2 + 2i\alpha'\omega\omega_m + \omega^2 g \tan(kL)}. \quad (4.32)$$

Imaginary part of $\chi_{yy}(\omega)$ corresponding to the rf absorption is plotted in Fig. 4.5. We observe a typical anticrossing behavior between an optically active and non-active mode, with level repulsion and transfer of oscillator strength. The intrinsic damping of the mechanical system (for MEMS Q factors can reach 10^4 , which quickly deteriorate with decreasing size, however) imposes an extra damping on the magnetization dynamics, which close to the mode crossing may dominate the intrinsic damping due to a small Gilbert constant α . In case $\beta/\omega > \alpha'$ the damping growth when we move from purely magnetic motion into purely mechanical motion along one of the lines in Fig. 4.4. In case $\beta/\omega < \alpha'$ the damping diminishes along such line.

The amplitude of mechanical oscillations along one of the spectrum lines in Fig. 4.4 is plotted in Fig. 4.6. The efficiency of the nanomotor is maximal at resonance.

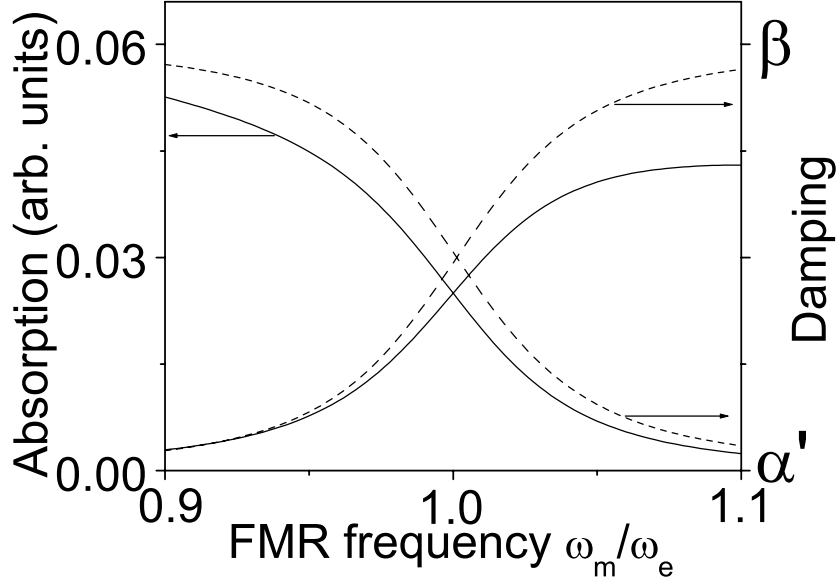


Figure 4.5: The oscillator strength corresponding to each resonance in Fig. 4.4 in arbitrary units plotted by full lines and their widths plotted by dashed lines ($g \sim 0.001$, $\beta/\omega > \alpha'$).

4.3.2 Ferromagnetic cantilever

Eq. (4.24) describes magnetomechanical dynamics for a ferromagnetic cantilever or a dielectric cantilever covered by a ferromagnet in the whole. The LLG equation is exactly the same as in case of previous subsections apart from the fact that the torsion angle should be averaged over the cantilever. Following Eq. (4.24) and for frequencies close to the mechanical resonance, the coupling can be written in Fourier space as follows

$$-C\bar{\varphi}\frac{L}{2c^2}(\omega^2 + 2i\beta\omega - \omega_e^2) = \frac{V_c}{2\gamma}(-i\omega m_y - \gamma H_0 m_x) \quad (4.33)$$

This result is identical to the expansion in Eqs. (4.25,4.26) after substituting $V_c/2$ by V . In the expression for the coupling constant g in Eqs (4.27,4.28) we have $V/V_c = 1/2$. The coupling constant is thus increased in comparison to the case of a small magnet at the tip of the cantilever in which $V/V_c \ll 1$.

The density of a metallic single crystal cantilever (Fe) is higher $\rho \sim 8000 \text{ kg/m}^3$ and the Lamé constant $\mu \sim 100 \text{ GPa}$ [29] is of the same order as for Si. Consequently, the metallic cantilever has to be smaller in order to have the same resonance frequency with the Si cantilever. Most importantly, we have to fulfill the condition $H_0 > D_z M_s$ that forces the equilibrium magnetization direction along the z -axis (alignment with the

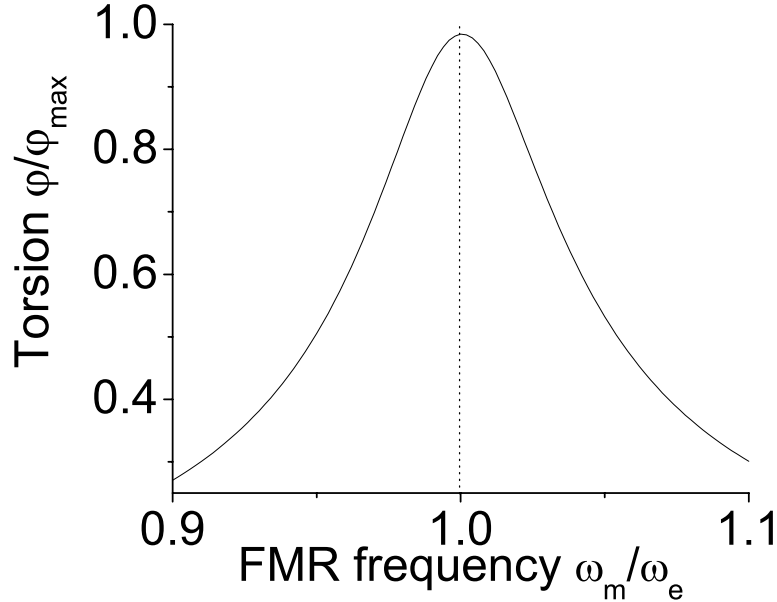


Figure 4.6: Amplitude of mechanical oscillations along one of the resonances in Fig. 4.4. The maximal efficiency of the “nanomotor” occurs when both subsystems are at resonance ($g \sim 0.001$).

y-axis would result in zero coupling). This condition can be easily fulfilled in our geometry by not too strong magnetic fields since the largest demagnetizing factor is D_x .

It follows from Eqs. (4.27,4.28) that a ferromagnetic cantilever is more suitable for observing the magneto-mechanically coupled modes since the coupling strength is larger by the factor $V_c/2V$ compared to the system with a small magnet at the tip of the cantilever. Close to the mechanical resonance frequency both systems will behave identically.

4.3.3 Observation

The magnetovibrational coupling in our cantilever is observable by sensitive local FMR techniques such as optical [30], magnetoresistive [39] or calorimetric [31]. It is also possible to detect the resonance by the static deflection of the same cantilever due to an additional constant magnetic field \mathbf{H}_T along the x -axis, as described by Lohndorf *et al.* [32]. In our approximation the field \mathbf{H}_T creates a torque $\gamma M_y H_T \vec{x}$, whose modulation at the FMR conditions should be detectable.

Since the vibrational frequencies of state-of-the-art artificial structures are relatively low, the use of soft ferromagnets (such as permalloy), is advantageous. The magnetic mode frequencies are then determined by shape anisotropies. The FMR frequency and

the mechanical resonance frequency should not differ by much more than $\Delta\omega \sim \omega\sqrt{g}$ for a pronounced effect. A Si cantilever with $a \times d \times L = (1 \times 5 \times 50) \mu\text{m}$ ($C = 10^{-13} \text{Nm}^2$) has a torsional resonance frequency of the order of $\omega_e = 10 \text{ MHz}$. Taking our ferromagnetic layer of dimensions $a_1 \times d \times \Delta L = 50 \text{ nm} \times 5 \mu\text{m} \times 5 \mu\text{m}$ (thickness, width and length), then $\omega\sqrt{g} \sim 100 \text{ KHz}$, meaning that we should tune the magnetic resonance to $\omega_e \pm 100 \text{ KHz}$ to observe the “polariton”. The necessary rf field H_x depends on the viscous dampings of mechanical and magnetization motion. At low frequencies additional sources of damping complicate measurements [33] and the coherent motion of the magnetization can be hindered by domain formation. Coupling to higher resonance modes [34] or structuring of the ferromagnet may help to carry out measurements. Use of weak ferromagnets to diminish the FMR frequency or scaling down the cantilever at expense of lower Q factors may help as well. However, it is extremely difficult to create mechanical devices that operate at microwave frequencies. Stiff silicon-carbide epilayers are used together with balanced, high-frequency displacement transducers in order to break the 1 GHz barrier [4].

An actual observation of the predicted splittings would give information about *e.g.* the magnetic moment of the film and the broadening would yield the quality factor of the elastic motion. From a technological point of view the tunable damping due to the magnetovibrational coupling might be interesting for optimizing switching speeds. A ferromagnet effectively absorbs microwaves and turns them into a precessing magnetization, which via the magnetovibrational coupling can be transformed into a coherent mechanical motion. On the other hand, the ferromagnet may interact with the mechanical motion, to cause a magnetization precession, which in turn emits polarized microwaves. The emission in the coupled regime is more energy efficient in comparison with a fixed magnetic dipole emission in the case of small Gilbert constant but relatively low mechanical quality factor. This might be interesting for *e.g.* on-chip communication applications.

In this Section we have calculated the magnetic susceptibility of a system with magnetovibrational coupling by magnetocrystalline fields or via surface forces of demagnetizing currents. A condition for effective energy transfer from an external rf magnetic field into mechanical motion and *vice versa* has been established. FMR spectra are predicted to split close to the resonance, and to strongly depend on the mechanical damping. The predicted effects should be observable with existing technology, but a further reduction of system size would strongly enhance them.

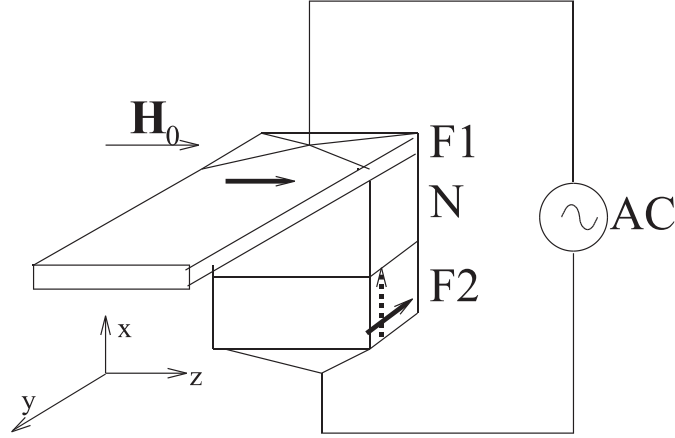


Figure 4.7: Electro-magneto-mechanical device. The free ferromagnetic layer in a spin valve is extended forming the cantilever. An AC current is sent through the base of the cantilever.

4.4 Probing magnetization dynamics by spin-transfer torques

All FMR observation techniques mentioned require the application of microwave fields to excite the magnetization dynamics. In this Section, we propose an alternative method to probe the magnetization dynamics in which the role of the microwave field is taken over by spin-transfer torques. By driving an AC current through F|N|F spin valve structures with fixed and free layer magnetizations that are canted with respect to each other, we can excite the free layer motion (Fig. 4.7) (excitation of the magnetization motion by DC currents has already been realized [39]). The magnetization dynamics should in turn influence the resistance of the device that can be measured. When the magnetic layer has a mechanically active extension, as in Fig. 4.7, we can also detect the magneto-vibrational mode.

4.4.1 Electrical detection of FMR

We consider here F1|N|F2 multilayer structures with perpendicular magnetizations \mathbf{m}_1 and \mathbf{m}_2 assuming \mathbf{m}_2 fixed by anisotropies or exchange biasing. An AC current exerts an oscillating torque τ_1 on the magnetization \mathbf{m}_1 [35]:

$$\frac{\tau_1}{I_0} = \frac{\hbar}{2e} \frac{1 + R_{\uparrow\downarrow}/R_1 - \beta P_1/P_2}{(1 + R_{\uparrow\downarrow}/R_1)(1 + R_{\uparrow\downarrow}/R_2) - \beta^2} \quad (4.34)$$

with $\beta = \cos \theta$, $4R_{1(2)} = 1/G_{1(2)\uparrow} + 1/G_{1(2)\downarrow} - 2R_{\uparrow\downarrow}$, $4R_{1(2)-} = 1/G_{1(2)\uparrow} - 1/G_{1(2)\downarrow}$, $P_{1(2)} = R_{1(2)-}/R_{1(2)}$, and $2R_{\uparrow\downarrow} = 1/G_{1\uparrow\downarrow}^r + 1/G_{2\uparrow\downarrow}^r$, where $G_{1(2)\uparrow}$ and $G_{1(2)\downarrow}$ are con-

ductances of the left (right) ferromagnet including the left (right) normal layer, $G_{1\uparrow\downarrow}^r$ and $G_{2\uparrow\downarrow}^r$ are mixing conductances of the middle normal metal with adjacent ferromagnet interfaces. The resulting magnetization dynamics causes oscillations of the resistance of the multilayer structure according to [35]

$$\Re(\theta) = R + R_1 + R_2 - \frac{R_{\uparrow\downarrow}(R_{1-} + \beta R_{2-})^2 + (1 - \beta^2)(R_{1-}^2 R_2 + R_{2-}^2 (R_1 + R_{\uparrow\downarrow}))}{(R_{\uparrow\downarrow} + R_1)(R_{\uparrow\downarrow} + R_2) - \beta^2 R_1 R_2}. \quad (4.35)$$

In the following, we consider only small deviations of \mathbf{m}_1 from the perpendicular to \mathbf{m}_2 direction. All the equations can then be rewritten keeping only the leading terms with respect to small β . The torque τ_1 is proportional to the current I_0 in this approximation:

$$\tau_1 = I_0 \frac{\hbar}{2e} \frac{1 + R_{\uparrow\downarrow}/R_1}{(1 + R_{\uparrow\downarrow}/R_1)(1 + R_{\uparrow\downarrow}/R_2)} = V |\mathbf{M} \times \mathbf{H}_x| \quad (4.36)$$

where we defined an effective rf field \mathbf{H}_x along the axis x that creates the same torque as the oscillating AC current. Thus the response function $(m_y/I_0)_\omega = K\chi_{yx}(\omega)$ with

$$KM_s V = \frac{\hbar}{2e} \frac{1 + R_{\uparrow\downarrow}/R_1}{(1 + R_{\uparrow\downarrow}/R_1)(1 + R_{\uparrow\downarrow}/R_2)}, \quad (4.37)$$

and the susceptibility can be found from Eq. (4.4). To the first order in the mechanical damping constant β we can write the dynamical impedance as:

$$Z(\omega) = R + R_1 + R_2 - \frac{R_{\uparrow\downarrow}(R_{1-}^2 + 2I_0 K\chi_{yx}(\omega)R_{2-}R_{1-}) + (R_{1-}^2 R_2 + R_{2-}^2 (R_1 + R_{\uparrow\downarrow}))}{(R_{\uparrow\downarrow} + R_1)(R_{\uparrow\downarrow} + R_2)}. \quad (4.38)$$

$|Z(\omega)|$ normalized by the resistance of the locked perpendicular magnetizations is plotted in Fig. 4.8. The parameters of the spin valve are the same with the symmetric setup of [35]. The current amplitude I_0 is chosen to correspond to magnetization oscillations of 15 degrees which appears to be readily experimentally accessible. In Fig. 4.8 the FMR resonance corresponds to the dip in the absolute value of the impedance that should be easily detectable.

4.4.2 Electrical detection of magnetovibrational mode

The method described in the previous chapter can also be used for detecting the magnetovibrational modes. The ferromagnet F1 is extended forming a ferromagnetic cantilever (Fig. 4.7). The magnetization \mathbf{m}_2 can have two directions (bold and dashed lines in Fig. 4.7) that are equally suitable for this purpose. In principle, the direction plotted by dashed line can cause a constant torsion of the cantilever when a constant current is sent through

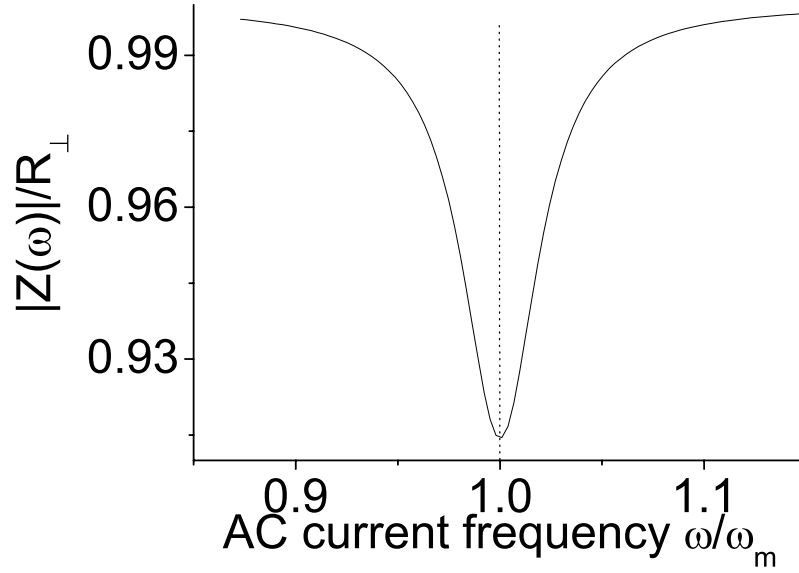


Figure 4.8: Dependence of the normalized impedance on the AC current frequency ($\alpha' = 0.02$).

the spin valve since in this case the spin-transfer torque is transferred to the mechanical torque via the shape anisotropy. We concentrate here on the direction of \mathbf{m}_2 indicated by the bold arrow which can be easier realized in experiment. When an AC current is sent through the system the oscillating torque causes oscillations of the magnetization \mathbf{m}_1 as explained in the previous Section. At resonance, we can observe the magnetovibrational mode as a splitting of the dip in the absolute value of the impedance plotted in Fig. 4.9. The width of the dips is a measure of the damping that is approximately half of the width in Fig. 4.8 for chosen parameters, which is consistent with the results of Section 4.3.1 .

In a long cantilever with a finite exchange stiffness, the macrospin magnetization motion can be complicated by spin waves. The effective field for the LLG Eq. (4.1) in the presence of nonuniform magnetization reads

$$\mathbf{H}_{\text{eff}} = -D_x M_x \mathbf{x} - D_y M_y \mathbf{y} - D_z M_z \mathbf{z} + \frac{2A}{M_s^2} \nabla^2 \mathbf{M} + \mathbf{H}_0 \quad (4.39)$$

where A is the exchange stiffness. The lowest-energy bulk spin wave mode is along the cantilever with the frequency that can be found from the LLG equation written in Fourier

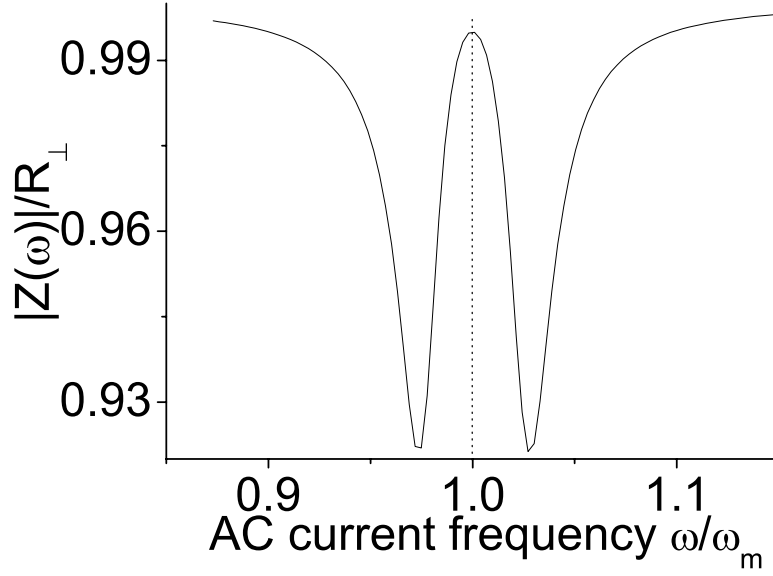


Figure 4.9: Dependence of the normalized impedance on the AC current frequency ($\omega_m = \omega_e$, $\alpha' = 0.02$, $\beta/\omega = 0.002$).

space:

$$\begin{bmatrix} -i\omega & \gamma\left(\frac{2A}{M_s}k^2 + (D_y - D_z)M_s + H_0\right) \\ -\gamma\left(\frac{2A}{M_s}k^2 + (D_x - D_z)M_s + H_0\right) & -i\omega \end{bmatrix} \begin{bmatrix} m_x/M_s \\ m_y/M_s \end{bmatrix} = 0 \quad (4.40)$$

where $\mathbf{M} = (m_x\mathbf{x} + m_y\mathbf{y})e^{i(\omega t + \mathbf{k}\cdot\mathbf{r})} + M_s\mathbf{z}$. The resonance frequency is $\omega_{sw} = \gamma\sqrt{\left(\frac{2A}{M_s}k^2 + (D_x - D_z)M_s + H_0\right)\left(\frac{2A}{M_s}k^2 + (D_y - D_z)M_s + H_0\right)}$. We estimate the difference between frequencies of the macrospin mode with $k = 0$ and the longest wavelength mode with $k = \pi/L$. For a thin film $\gamma\sqrt{4\pi M_s \frac{2A}{M_s} (\pi/L)^2} \approx 0.2$ GHz, where we adopted $A = 2 \times 10^{-11}$ J/m, $M_s = 1.4 \times 10^6$ A/m and $L = 1$ μ m. Since we excite the mechanical motion monochromatically by the AC currents, it is sufficient then to have the mode splitting larger than the broadening. This shows that in principle we can design the magnetic and mechanical subsystems to avoid bulk spin wave generation provided the mechanical damping as well as the Gilbert damping are relatively small. Note that by applying an antiferromagnetic layer on top of the cantilever we can strengthen exchange stiffness thus diminishing the possibility of spin waves even further.

It is also possible to include coupling of the mechanical motion to spin waves but this regime will not be considered here.

4.5 Large magnetization cones and magnetization reversal in the presence of coupling

In this Section, we extend the linearized magnetization motion to large angles relevant *e.g.* for the magnetization reversal.

4.5.1 Resonant magnetization oscillations and reversal

We consider resonant oscillations of the mechanical and magnetic degrees of freedom. We restrict ourself here to the case when only one anisotropy direction is present (*e.g.* $D_y = D_z = 0$) which is relevant for very thin ferromagnetic films with an easy plane anisotropy when $D_x \sim 4\pi$.

The coupling of Eqs. (4.1) and (4.17) is

$$\begin{aligned} \frac{\partial \varphi}{\partial y} \Big|_{y=L} &= \frac{1}{C\gamma} \left(\frac{dM_y}{dt} + \gamma \mathbf{M} \times \mathbf{H}_0 \Big|_y \right), \\ \mathbf{H}_{\text{eff}} &= (D_x M_z \varphi - D_x M_x) \mathbf{x} + D_x M_x \varphi \mathbf{z} + \mathbf{H}_0, \end{aligned} \quad (4.41)$$

We first address the maximal possible coupling strength of a system described by Eq. (4.41). Consider the two subsystems oscillating at a common frequency ω . The total mechanical energy is then $E_{me} = \rho IL \omega^2 \varphi_0^2$, where φ_0 is the maximal angle of the torsional motion. By equipartition this energy should be of the order of the magnetic energy $E_{mg} = M_s V H_0$. The maximal angle would correspond to the mechanical motion induced by full transfer of the magnetic energy to the lattice. By equalizing those energies, we find an estimate for the maximal angle of torsion $\varphi_0 = \sqrt{M_s V H_0 / (\rho IL \omega^2)}$. The coupling between the subsystems can be measured by the distribution of an applied external torque (*e.g.* applied by a magnetic field) over the two subsystems. The total angular momentum flow into the magnetic subsystem by the effective magnetic field is $(M_s V / \gamma) \omega$, whereas that corresponding to the mechanical subsystem at the same frequency is $(\rho IL \omega \varphi_0) \omega$. Their ratio is $\varphi_0 \omega / (\gamma H_0)$. The maximum angle φ_0 derived above is therefore also a measure of the coupling between the magnetic and mechanical subsystems. This estimate is consistent with the coupling strength of polariton modes at resonance of $g = \varphi_0^2 \omega^2 / (\gamma H_0)^2 \approx \varphi_0^2 D_x M_s / H_0$ in Eqs. (4.27, 4.28) (in this estimate we consider the case of not too strong external fields when $\omega \approx \gamma \sqrt{H_0 D_x M_s}$). An estimate for a cantilever with $\rho = 2330 \text{ kg/m}^3$ (Si) and $d = 100 \text{ nm}$ ($\omega \sim 1 \text{ GHz}$) leads to $g = \varphi_0^2 D_x M_s / H_0 \sim (L/a)^2 (M_s^2 / \mu) \sim 10^{-3}$. Increasing (L/a) and M_s or decreasing Lamé constant μ is beneficial for the coupling.

Magnetization reversal by a magnetic field in the coupling regime can be realized even without any damping by transferring magnetic energy into the mechanical system. Since we find that $\varphi_0 \ll 1$ for realistic parameters, the subsystems undergo many pre-

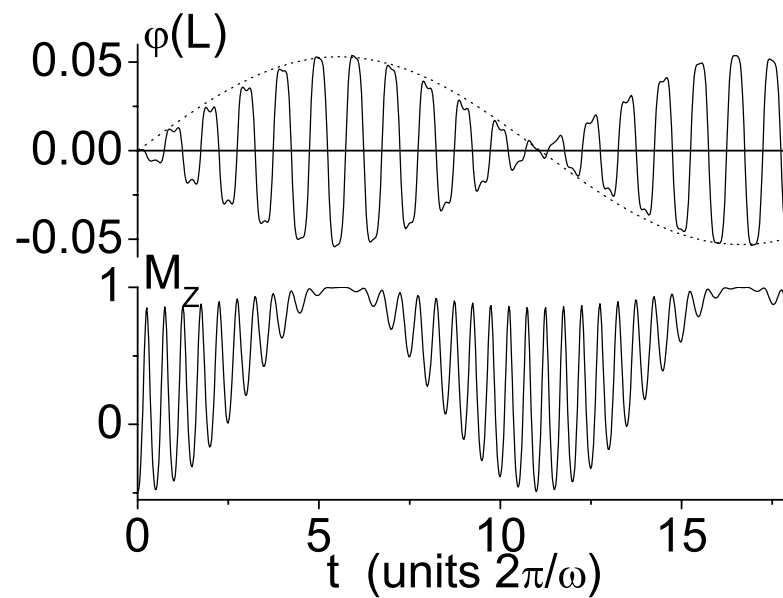


Figure 4.10: Time-dependent response of the magnetomechanical system to an external magnetic field switched on at $t = 0$ at an angle $2\pi/3$ with the initial magnetization, in the absence of dissipation. Plotted are the $\varphi(L)$ and z -components of the magnetization ($D_x M = 10H_0$).

cessions/oscillations before the switching is completed. The switching is then associated with a slow time scale corresponding to the global motion governed by the coupling or a weak damping relative to a fast time scale characterized by the Larmor frequency. The equation of motion for the slow dynamics (the envelope functions) can be derived by averaging over the rapid oscillations. To this end, we substitute LLG Eq. (4.19) and first of Eqs. (4.41), linearized in the small parameters α , β and φ_0 , into the equations for the mechanical and the magnetic energies:

$$\begin{aligned}\frac{d}{dt}E_{me} &= -2\beta E_{me} + C\tau|_{x=L}\frac{d\varphi}{dt}|_{x=L}, \\ \frac{d}{dt}E_{mg} &= -H_0\dot{M}_z + D_x M_x \dot{M}_x.\end{aligned}\quad (4.42)$$

We focus in the following on the regime $H_0 \ll D_x M_s$, which usually holds for thin films and not too strong fields, in which the magnetization motion is elliptical with long axis in the plane and small M_x even for larger precession cones. Disregarding terms containing higher powers of M_x and averaging over one period as indicated by $\langle \dots \rangle$

$$\begin{aligned}\left\langle \frac{dE_{me}}{dt} \right\rangle + \langle 2\beta E_{me} \rangle &= -VD_x \langle M_z M_x \dot{\varphi} \rangle, \\ \left\langle \frac{dE_{mg}}{dt} \right\rangle + \langle \alpha D_x^2 M_s M_x^2 \rangle &= D_x \langle M_z \dot{M}_x \varphi \rangle.\end{aligned}\quad (4.43)$$

By adiabatic shaping of time-dependent magnetic fields $H_0(t)$ we can keep the two subsystems at resonance at all times ($H_0(t)$ does not change much since we do not consider large angle cones that are very close to the antiparallel configuration). The slow dynamics $\varphi(L, t) \sim A(t)e^{i(\omega+\pi/2)t}$ and $M_x \sim W(t)e^{i\omega t}$ in time domain is then governed by the equation:

$$\begin{aligned}\dot{A} + \beta A &= -g\omega_m/M_s(-1 + \frac{D_x W^2}{4M_s H_0})W, \\ \dot{W} + \alpha' \omega W &= \omega M_s(-1 + \frac{D_x W^2}{4M_s H_0})A,\end{aligned}\quad (4.44)$$

we introduced a frequency $\omega_m = \gamma\sqrt{D_x M_s H_0(t)}$ that at $t = 0$ coincides with the frequency of fast oscillations ω . Substitutions $\varphi(L, t) \sim \tilde{A}(t)e^{i\omega t}$ and $M_x \sim \tilde{W}(t)e^{i(\omega-\pi/2)t}$ corresponding to $\pi/2$ -shifted harmonics are also solutions, and the initial conditions determine the linear combination of two envelope functions, *i.e.* the beating pattern of two hybridized polariton modes [9]. When initially all energy is stored in one degree of freedom, M_x is $\pi/2$ shifted from $\varphi(L, t)$ and $A_2(t) = 0$. Eqs. (4.44) describe a (damped) harmonic oscillator with frequency $\sqrt{g\bar{\omega}_m\omega} \ll \omega$ when $D_x W/4 \ll MH_0$ (since ω_m does not change much we replaced it by averaged $\bar{\omega}_m$). Such oscillatory behavior persists for general angles (except for motion with very large angle cones close to the antiparallel configuration). This is illustrated by Fig. 4.10 which shows a numerical simulation of Eq. (4.22) for an undamped system excited at $t = 0$ by a magnetic field \mathbf{H}_0 at an angle $2\pi/3$ with the initial magnetization. The number of periods necessary to transfer all energy

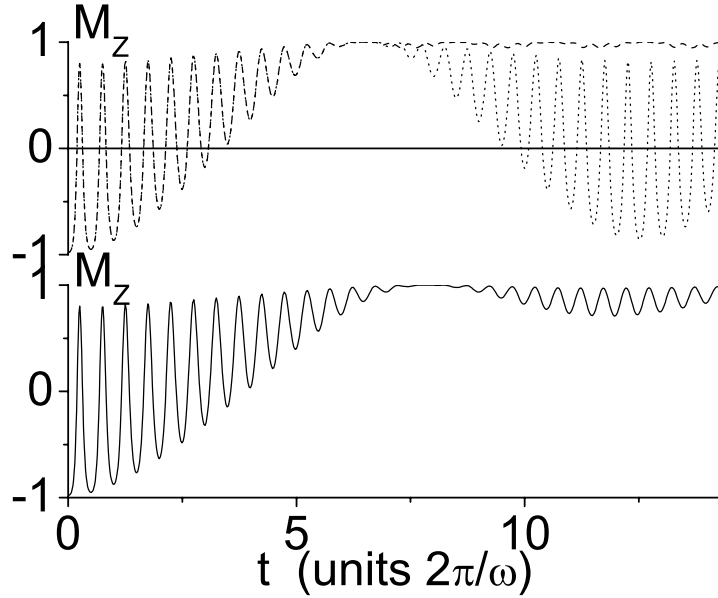


Figure 4.11: Time-dependent response of the magnetomechanical system to an external magnetic field switched on at $t = 0$ ($D_x M = 10H_0$, $\alpha = 0$). The importance of mechanical damping can be seen by comparing the dotted line ($\beta = 0$) with the full line ($\beta = 0.02$). The dashed line illustrates the dynamics when the subsystems brought out of resonance by reducing the external magnetic field to half of its initial value at $t = 6.5$ ($\beta = 0$).

from one subsystem to the other is therefore given by $\sim 1/(4\sqrt{g})$. Eq. (4.44) also shows that for damping constants $\alpha > \varphi_0/\pi$ or $\beta/\omega > \sqrt{g}/\pi$ the beating is suppressed.

Fig. 4.10 illustrates that the mechanical system absorbs energy from the magnetic subsystem and gives it back repeatedly in terms of violent oscillations that are modulated by an envelope function on the time scale derived above in Eq. (4.44) as plotted by dotted line. When the envelope function vanishes the magnetization is reversed and the systems seems to be at rest. However, since the energy is not dissipated, the momentarily silence is deceptive, and the beating pattern repeats. An efficient coupling requires that the frequencies of the subsystems are close to each other at each configuration, which was achieved in the simulation by the adiabatic modulation of the magnetic field H_0 according to Fig. 4.3. However, the reversal process is robust; an estimate from Eqs. (4.43) for the necessary proximity of the resonant frequencies of the mechanical and the magnetic subsystems is $\Delta\omega \sim \sqrt{g}\omega$. In that case, the above estimates still hold.

Let us now consider the magnetization reversal by an antiparallel magnetic field $H_0(t)$ that undergo slow change of amplitude to keep the subsystems at resonance. This method of magnetization reversal by oscillating demagnetizing field due to mechanical oscilla-

tions is strongly analogous to the reversal by time-dependent magnetic fields [25]. However, in contrast to the time-dependent field reversal, we vary the field $H_0(t)$ but not the rf fields so avoiding complicated time dependence of rf fields [25]. We can calculate the dependence $H_0(t)$ in advance for a specific sample, or we can create feedback circuit by connecting metallic contacts to the magnetic film, thus monitoring the dynamics. Since we assume zero temperature, the dynamics in Fig. 4.11 is initiated by assuming a tiny angle of magnetization at $t = 0$. We wish to illustrate here that making use of the magnetoelastic coupling can accelerate the reversal importantly. We can suppress the backflow of mechanical energy for example by a sufficiently damped mechanical subsystem, as evident in Fig. 4.11 by comparing the two curves for $\beta \sim 0$ and $\beta \sim 0.02$ with vanishing Gilbert damping, $\alpha = 0$. Alternatively, we may detune the external magnetic field out of the resonance precisely after the first reversal, effectively rectifying the energy flow from the magnetic into the mechanical subsystem. We observe that even without any intrinsic damping ($\alpha = \beta = 0$) the unwanted “ringing” can be strongly suppressed (dashed line in Fig. 4.11).

The experimental realization of such magnetization reversal will be a challenge since the cantilever has to preferably work at high frequencies ~ 1 GHz. In the resonant reversal, a significant coupling strength of $g \sim 10^{-3}$ requires that one tenths of the cantilever volume is a ferromagnet. We investigated here the non-linear dynamics of coupled magnetic and mechanical fields for a cantilever with a ferromagnetic tip. Employing the new dissipation channels, we propose new strategies for fast magnetization reversal and suppressed “ringing”. We can make use of the additional mechanical damping or shape the external magnetic field pulses, thus quickly channeling-off magnetic energy when damping is weak.

4.5.2 Non-resonant magnetization oscillations and reversal

We propose a non-resonant mechanical reversal scheme analogous to “precessional” switching [13]. The effective field \mathbf{H}_{eff} (see Eq. (4.22)) has a component perpendicular to the plane of the film $H_x \sim M\varphi$. Under a sudden mechanical twist this component acts like a transverse magnetic pulse about which the precessing develops. Alternatively, we can suddenly release a twist preinstalled on the cantilever. This could be achieved by an STM tip bonded to an edge of the cantilever at (L, d) and pulling it up slowly to the breaking point. The mechanical response should be fast, *i.e.* react on a time scale $(\gamma\varphi\nu M)^{-1}$, but there are no resonance restrictions now. We integrate the equation of motion numerically for a strongly damped cantilever $\beta/\omega \sim 0.15$ initially twisted by $\varphi = 0.2$ and suddenly released at $t = 0$. We reintroduce an easy axis anisotropy described by $DM_z\mathbf{z}$. Adopt $D = 0.05$, $\alpha = 0.01$ and no external fields. Fig. 4.12 displays the desired reversal. The rather severe overshoot, as in the case of the precessional switching technique, can be

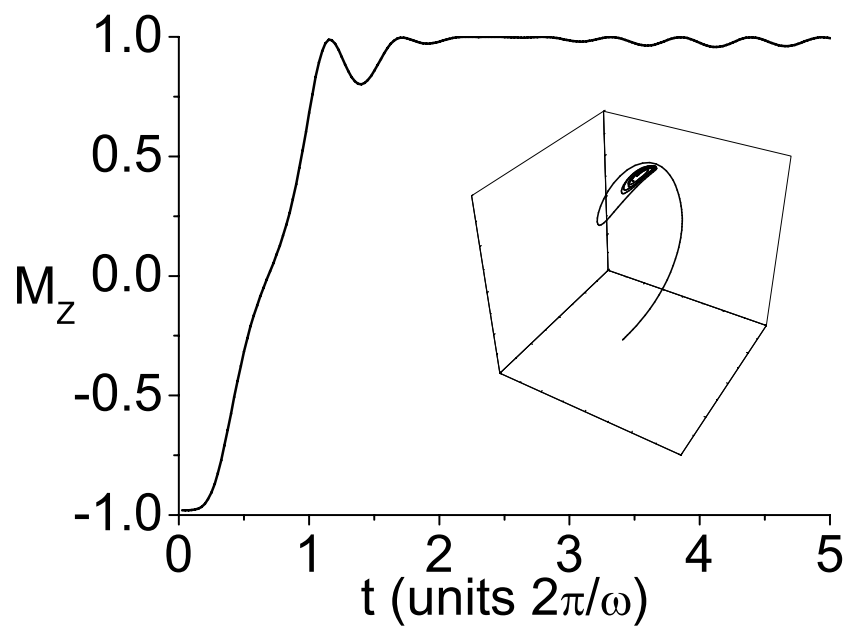


Figure 4.12: Magnetization switching without external field by an initially twisted cantilever that is released at $t = 0$. The inset shows the corresponding magnetization trajectory on the unit sphere.

minimized by carefully engineering the mechanical actuation to be closer to the optimum “ballistic“ path between $M_z = \pm 1$.

Summarizing, we demonstrate here a precessional reversal scheme based on the mechanically generated out-of-plane demagnetizing field without applied magnetic fields. In this reversal scheme, the sharp control of the resonance condition is not required, however, the cantilever has to be fast determining the reversal time.

4.6 Conclusion

This paper reports a detailed study of magnetomechanical effects in small magnetic cantilevers, summarizing some old results [9, 10] and making several generalizations. We proved that for small magnetization oscillations close to the mechanical resonance frequency, a ferromagnetic cantilever behaves like the dielectric cantilever with a small magnet at the tip analyzed before. Such a ferromagnetic cantilever has an enhanced coupling of mechanical and magnetic degrees of freedom and thus is more suitable for observation of magnetomechanical effects. A metallic ferromagnetic cantilever can be integrated into magnetoelectronic circuits as shown in Section 4.4 . Such an integrated device has the potential as a fast transducer of mechanical motion as an alternative to previous designs that take advantage of magnetomotive forces. In our case, the magnetomotive forces are supplanted by spin-transfer torques. Our strategy; that is to say to avoid magnetic fields, is similar to what happens in the field of random access memories in which there is a considerable effort to replace magnetic fields by employing spin-transfer torques. The technique presented in this paper strongly relies on resonant magnetovibrational coupling in which the magnetic torques can be effectively transformed into mechanical torques and *vice versa*. In order to see magnetomechanical torques in experiment, one needs to be able to handle small structures on micro and nano scale, the magnets have to be small enough to form a single domain. We believe that the integration of magnetoelectronics and magnetomechanics is possible and should lead to devices with new functionalities.

Acknowledgment

We thank Yaroslav Tserkovnyak for helpful discussions. This work has been supported by the Dutch FOM Foundation and the Research Council of Norway.

References

- [1] M. L. Roukes, Phys. World **14** (2), 25 (2001).

- [2] K. C. Schwab and M. L. Roukes, *Phys. Today*, July 2005.
- [3] J. A. Sidles, J. L. Garbini, K. J. Bruland, D. Rugar, O. Zuger, S. Hoen and C.S. Yannoni, *Rev. Mod. Phys.* **67**, 249 (1995).
- [4] X. M. H. Huang, C. A. Zorman, M. Mehregany, and M. Roukes, *Nature (London)* **421**, 496 (2003).
- [5] C. Friedsam, A. K. Wehle, F. Kühner and H. E. Gaub, *J. Phys. Condens. Matter* **15**, S1709 (2003).
- [6] K. L. Ekinci, Y. T. Yang, M. L. Roukes, *J. Appl. Phys.* **95**, 2682 (2004).
- [7] D. Rugar, R. Budakian, H. J. Mamin and B. W. Chui, *Nature* **430**, 329 (2004).
- [8] I. Bargatin and M.L. Roukes, *Phys. Rev. Lett.* **91**, 138302 (2003).
- [9] A.A. Kovalev, G.E.W. Bauer and A. Brataas, *Appl. Phys. Lett.* **83**, 1584 (2003).
- [10] A. A. Kovalev, G.E.W. Bauer and A. Brataas, *Phys. Rev. Lett.* **94**, 167201 (2005).
- [11] B. Hillebrands and K. Ounadjela (Eds.), *Spin Dynamics in Confined Magnetic Structures*, (Springer, Berlin, 2003); S. Maekawa and T. Shinjo (Eds.), *Applications of Magnetic Nanostructures*, (Taylor and Francis, New York, 2002).
- [12] M. Jamet, W. Wernsdorfer, C. Thirion, V. Dupuis, P. Mélinon, A. Pérez and D. Maily, *Phys. Rev. B* **69** (2), 024401 (2004).
- [13] Th. Gerrits, H.A.M. van den Berg, J. Hohlfeld, L. Bär, and Th. Rasing, *Nature* **418**, 509 (2002).
- [14] C. H. Back, D. Weller, J. Heidmann, D. Mauri, D. Guarisco, E. L. Garwin and H. C. Siegmann, *Phys. Rev. Lett.* **81**, 3251 (1998).
- [15] H. W. Schumacher, C. Chappert, P. Crozat, R. C. Sousa, P. P. Freitas, J. Miltat, J. Fassbender and B. Hillebrands, *Phys. Rev. Lett.* **90**, 0117201 (2003).
- [16] J.C. Slonczewski, *J. Magn. Magn. Mater.* **159**, L1 (1996); L. Berger, *Phys. Rev. B* **54**, 9353 (1996).
- [17] M. Tsoi, A. G. M. Jansen, J. Bass, W.-C. Chiang, M. Seck, V. Tsoi and P. Wyder, *Phys. Rev. Lett.* **80**, 4281 (1998).
- [18] T. Valet, unpublished.

- [19] A. Yamaguchi, T. Ono, S. Nasu, K. Miyake, K. Mibu and T. Shinjo, Phys. Rev. Lett. **92**, 077205 (2004); G. Tatara and H. Kohno Phys. Rev. Lett. **92**, 086601 (2004); S.E. Barnes and S. Maekawa, cond-mat/0311039.
- [20] J-E Wegrowe, D. Kelly, Y. Jaccard, Ph. Guittienne, J-Ph Ansermet, Europhys. Lett. **45**, 626 (1999).
- [21] J.Z. Sun, J. Magn. Mater. **202**, 157 (1999).
- [22] E. B. Myers, D. C. Ralph, J. A. Katine, R. N. Louie, R. A. Buhrman, Science **285**, 867(1999).
- [23] S. I. Kiselev, J. C. Sankey, I. N. Krivorotov, N. C. Emley, R. J. Schoelkopf, R. A. Buhrman and D. C. Ralph, Nature **425** (6956), 380 (2003).
- [24] A. V. Kimel, A. Kirilyuk, A. Tsvetkov, R. V. Pisarev and Th. Rasing, Nature **429**, 850 (2004).
- [25] Z. Z. Sun and X. R. Wang, preprint (2005).
- [26] T.L. Gilbert, Phys. Rev. **100**, 1243 (1955); IEEE Trans. Magn. **40**, 3443 (2004).
- [27] C. Serpico, I.D. Mayergoyz and G. Bertotti, J. Appl. Phys. **93**, 6909 (2003).
- [28] L.D. Landau and E.M. Lifshitz, *Theory of Elasticity*, 2nd ed. (Pergamon, Oxford, 1959).
- [29] M. G. Simmons and H. Wang, Single crystal elastic constants and calculated aggregate properties, MIT Press, 1975. J. D. Bass, Elasticity of Minerals, Glasses, and Melts, pp.45-63, in Mineral Physics and crystallography: a handbook of physical constants, edited by T. J. Ahrens, AGU, Washington, DC., 1995.
- [30] W. K. Hiebert, G. E. Ballentine, L. Lagae, R. W. Hunt and M. R. Freeman, J. Appl. Phys. **92**, 392 (2002).
- [31] J. Moreland, M. Lohndorf, P. Kabos, and R. D. McMichael, Rev. Sci. Instrum. **71**, 3099 (2000).
- [32] M. Lohndorf, J. Moreland, and P. Kabos, Appl. Phys. Lett. **76**, 1176 (2000).
- [33] G. F. Cochran, R. W. Qiao, and B. Heinrich, Phys. Rev. B **39**, 4399 (1989).
- [34] U. Rabe, K. Janser, and W. Arnold, Rev. Sci. Instrum. **67**, 3281 (1996).
- [35] A. A. Kovalev, A. Brataas, and G. E. W. Bauer, Phys. Rev. B **66**, 224424 (2002).

- [36] T. Ono, H. Miyajima, K. Shigeto, K. Mibu, N. Hosoi, T. Shinjo, *Science* **284** (5413), 468 (1999).
- [37] M. Tsoi, R.E. Fontana, S.S.P. Parkin, *Appl. Phys. Lett.* **83**, 2617 (2003).
- [38] D. Atkinson, D. A. Allwood, G. Xiong, M. D. Cooke, C. C. Faulkner and R. P. Cowburn, *Nature Materials* **2**, 85 (2003).
- [39] I. N. Krivorotov, N. C. Emley, J. C. Sankey, S. I. Kiselev, D. C. Ralph, and R. A. Buhrman, *Science* **307**, 228 (2005).
- [40] A.N. Cleland, *Foundations of Nanomechanics* (Springer-Verlag, 2002).
- [41] P.B. Visscher and X. Feng, *Phys. Rev. B* **65**, 104412 (2002).
- [42] S. Wolf, D. D. Awschalom, R. Buhrman, J. Daughton, S. von Molnar, M. Roukes, A. Chtchelkanova, and D. Treger, *Science* **294**, 1488 (2001).
- [43] S. S. P. Parkin, *Applications of Magnetic Nanostructures* (Taylor and Francis, New York, 2002), p. 237.
- [44] A. Jander, J. Moreland, and P. Kabos, *Appl. Phys. Lett.* **78**, 2348 (2001).
- [45] O. Benda, *IEEE Trans. Mag.* **5**, 921 (1969).

Summary

Electrical and mechanical magnetization torques

Only charge degree of freedom is utilized in most electronic devices. The use of the spin degree of freedom is relatively recent. The discovery of the Giant Magnetoresistance (GMR) effect initiated the development of magnetoelectronics - the field that studies effects on electron transport involving the spin degree of freedom. GMR is a very large change in electrical resistance observed in ferromagnet/nonmagnet multilayer structures when the relative orientations of the magnetizations in ferromagnetic layers change as a function of applied field. The development of magnetoelectronics was very rapid leading to useful applications already within several years. For example, the GMR effect is presently routinely used to sense magnetic fields of data in read heads of magnetic hard disk drives.

Whereas in GMR the relative direction of the magnetizations defines the current flowing through the system, an opposite effect of current on the magnetizations is also possible. Slonczewski predicted this effect - the spin transfer torque. In a ferromagnet/normal metal/ferromagnet structure with one magnetization free and the other fixed, the magnetization dynamics of the free layer can be driven by a current through the system as a result of spin-transfer torques. The magnetization dynamics in small magnetic clusters and films is a basic problem of condensed matter physics and is also important for applications: the spin-transfer effect may find applications in the so-called magnetic random access memories in which the direction of the magnetization is used to store the data and the rewriting process can be done by spin-transfer torques. Magnetoelectronics is a rapidly developing field at the moment and this thesis deals with some aspects of it related to magnetization dynamics and torques.

The main subject of the thesis is torque, i.e. a change of angular momentum in time. We deal with torques that arise in spin valves and small magnetic cantilevers; spin-transfer torques in the former and magnetomechanical torques in the latter case. In order to describe spin-transfer torques we develop an approach based on the diffusion equation with quantum mechanical boundary conditions. With some simplifications this leads to magnetoelectronic circuit theory. This allows us to treat arbitrary diffuse spin valves and other

devices.

Magnetomechanical torques arise in small magnetic cantilevers. An example is a cantilever with one end fixed and the other covered with a magnetic film. It is important that the magnetic film has strong crystal or shape magnetic anisotropy, which provides coupling between vibrations and the magnetization dynamics. The anisotropy in the film leads to magnetomechanical torques that affect both the magnetization dynamics and the mechanical motion of the cantilever. This can open new possibilities for Magnetic Resonance Force Microscopy in imaging and sensor applications.

In Chapter 1 of this thesis we introduce the basic concepts of magnetoelectronics such as the spin-polarized current, the GMR effect, the spin-transfer torque and the magnetization dynamics. We introduce also magnetomechanical torques and analyze an example of a nanomechanical system that can be used for detecting magnetomechanical torques.

We introduce magnetoelectronic circuit theory that can be used to describe spin-transfer torques. Furthermore, we give a short account of the derivation of the Landau-Lifshitz-Gilbert equation. In generalized form this equation allows us to describe the magnetization dynamics as a result of magnetic fields and/or spin-transfer torques. Finally, applications of the magnetomechanical torques in Magnetic Resonance Force Microscopy is mentioned, and a design for a novel "spin-transfer motor" is proposed.

In Chapter 2, we apply the diffusion equation to electronic transport in disordered ferromagnet (F) - normal metal (N) spin valves and show its equivalence to the magnetoelectronic circuit theory. The spin-transfer torque appears naturally in the diffusion approach from the boundary conditions at N-F interfaces; spin currents polarized perpendicular to the magnetization are absorbed at the interface of the ferromagnet. We obtain analytical expressions for the spin transfer torque and the angular magnetoresistance in asymmetric F1-N-F2 spin valves. The effect of spin-flip processes in the normal metal and ferromagnet constituents are obtained analytically as well. In an N1-F1-N2-F2-N3 system, spin-flip in the center metal N2 reduces the spin-transfer, whereas spin-flip in the outer normal metals N1 and N3 can increase it by effectively enhancing the spin polarization of the device.

In Chapter 3, magnetoelectronic circuit theory is employed to analyze perpendicular spin valves with ultra-thin ferromagnetic layers. We consider two finite size effects in transport through magnetic multilayers. The first effect arises when the magnetic layer thickness in spin valves becomes of the order or smaller than the spin-flip diffusion length. In this case the spin valve can become effectively asymmetric, which affects the transport properties and spin-transfer torques. The second effect arises in magnetic layers with thickness approaching the magnetic coherence length. In this case spin currents polarized perpendicular to the magnetization can pass through the thin ferromagnetic layer (the coherence length in transition metals is of the order of several atomic layers; much smaller than the spin-diffusion length and mean-free path). We investigate both effects on the

angular magnetoresistance (aMR) and spin transfer torque. The spin-flip diffusion length in the ferromagnet as well as the interface spin-mixing conductance are determined by a fit to recent aMR experiments. At the end, we propose a three terminal device to measure the ferromagnetic coherence length.

In Chapter 4, we study a small magnetic cantilever (e.g. a Si cantilever covered by a magnetic film or an entirely ferromagnetic cantilever). Such cantilevers can serve for observation of magnetomechanical torques, which, for example, leads to hybrid magnetovibrational (“polaritonic”) modes and line splittings in ferromagnetic resonance spectra. Magnetomechanical torques can even cause a complete magnetization reversal. It is still very difficult to make nanoelectromechanical systems working at microwave frequencies, but many new possibilities arise. We propose to build nanoelectromechanical systems propelled by spin-transfer and magnetomechanical torques. Such systems can extend the limits of detecting and exciting motion at the nanoscale and can serve as electric transducers of nanomechanical motion.

Samenvatting

In de meeste elektronische toepassingen wordt alleen de ladingsvrijheidsgraad gebruikt. Het gebruik van de spinvrijheidsgraad is relatief recent. De ontdekking van het reuze-magnetoweerstand effect (Giant Magnetoresistance, GMR) was het begin van de ontwikkeling van de magnetoelectronica - het vakgebied dat de effecten van de spinvrijheidsgraad op electronentransport bestudeert. GMR is een zeer grote verandering van de elektrische weerstand die wordt waargenomen in ferromagnetisch/niet-magnetische multilaagstructuren als de relatieve oriëntatie van de magnetisaties in ferromagnetische lagen verandert als functie van een aangelegd magnetisch veld. De ontwikkeling van de magnetoelectronica leidde zeer snel tot nuttige toepassingen. Het GMR effect wordt op dit moment bijvoorbeeld gebruikt om magnetische velden van data in leeskoppen van magnetische harde schijven te detecteren.

Terwijl bij GMR de relatieve richting van de magnetisaties de stroom door het systeem bepaalt, is het omgekeerde effect van stroom op de magnetisaties ook mogelijk. Slonczewski heeft dit effect voorspeld -het spinoverdrachtsmoment. In een ferromagneet/normaal metaal/ferromagneet structuur met één vrije magnetisatie en één vaste, kan de magnetodynamica van de vrije laag bepaald worden door een stroom door het systeem als gevolg van de spin-overdrachts momenten. De magnetisatiedynamica in kleine magnetische clusters en films is een fundamenteel probleem in de fysica van gecondenseerde materie en is ook belangrijk voor toepassingen: het spinoverdrachtseffect zou toegepast kunnen worden in de zogenaamde magnetische random-access geheugens (MRAM) waarbij de magnetisatie wordt gebruikt om data op te slaan en het herschrijfproces uitgevoerd kan worden met spinoverdrachtsmomenten. De magnetoelectronica is op dit moment een zich snel ontwikkelend veld en dit proefschrift behandelt sommige aspecten ervan die gerelateerd zijn aan magnetisatiedynamica en momenten.

Het hoofdonderwerp van dit proefschrift is moment, d.w.z. een verandering van impulsmoment in de tijd. We behandelen momenten die ontstaan in zogenaamde "spinventielen"(spin-valves) en kleine magnetische cantilevers; spinoverdrachtsmomenten in het eerste en magnetomechanische momenten in het tweede geval. Om de spinoverdrachtsmomenten te beschrijven ontwikkelen we een aanpak gebaseerd op de diffusievergelijking met quantummechanische randvoorwaarden. Met enige vereen-

voudigingen leidt dit tot de magnetoelectronische netwerktheorie. Dit stelt ons in staat willekeurige diffuse spinventielen en andere systemen te behandelen.

Magnetomechanische momenten ontstaan in kleine magnetische cantilevers. Een voorbeeld is een cantilever waarvan één eind is vastgezet en het andere is bedekt met een magnetische film. Het is belangrijk dat de magnetische film een sterke kristallijne of magnetische vormanisotropie heeft, die zorgt voor een koppeling tussen vibraties en de magnetisatiedynamica. De anisotropie in de film leidt tot magnetomechanische momenten die zowel de magnetisatiedynamica als de mechanische beweging van de cantilever beïnvloeden. Dit kan nieuwe mogelijkheden bieden voor Magnetische Resonantie Kracht Microscopie voor afbeeldings- en sensortoepassingen.

In hoofdstuk 1 van dit proefschrift introduceren we de basisconcepten van de magnetoelectronica zoals spin-gepolariseerde stroom, het GMR effect, het spinoverdrachtsmoment en magnetisatiedynamica. We introduceren ook magnetomechanische momenten en analyseren een voorbeeld van een nanomechanisch systeem dat gebruikt kan worden om magnetomechanische momenten te detecteren.

We introduceren de magnetoelectronische netwerktheorie die gebruikt kan worden om spinoverdrachtsmomenten te beschrijven. Verder geven we een korte samenvatting van de afleiding van de Landau-Lifschitz-Gilbert vergelijking. In gegeneraliseerde vorm kunnen we met deze vergelijking de magnetisatiedynamica beschrijven die het gevolg is van magnetische velden en/of spinoverdrachtsmomenten. Tenslotte worden toepassingen van de magnetomechanische momenten in Magnetische Resonantie Kracht Microscopie genoemd en wordt een ontwerp voor een nieuwe "spin-overdrachts motor" voorgesteld.

In hoofdstuk 2 passen we de diffusievergelijking toe op electronisch transport in wanordelijke ferromagneet (F)- normaal metaal (N) spinventielen en tonen we de equivalentie aan met magnetoelectronische netwerktheorie. Het spinoverdrachtsmoment volgt bij de diffusie-aanpak op natuurlijke wijze uit de randvoorwaarden bij N-F grensvlakken; spinstromen die gepolariseerd zijn loodrecht op de magnetisatie worden geabsorbeerd bij het grensvlak met de ferromagneet. We vinden analytische uitdrukkingen voor het spinoverdrachtsmoment en de hoekmagnetoweerstand (angular magnetoresistance, aMR) in asymmetrische F1-N-F2 spin valves.

Het effect van spinflip processen in het normale metaal en ferromagnetische onderdelen worden ook analytisch verkregen. In een N1-F1-N2-F2-N3 systeem vermindert spinflip in het middelste metaal N2 de spin-overdracht, terwijl spinflip in de buitenste normale metalen N1 en N3 het kan vermeerderen door de effectieve spinpolarisatie van het systeem te vergroten.

In hoofdstuk 3 wordt de magnetoelectronische netwerktheorie gebruikt om loodrechte spinventielen met ultradunne ferromagnetische lagen te analyseren. We beschouwen twee eindige grootte effecten in transport door magnetische multilagen. Het eerste effect ontstaat als de dikte van de magnetische laag in spinventielen van de orde van grootte of

kleiner dan de spinflipdiffusielengte wordt. In dit geval kan het spinventiel effectief asymmetrisch worden, wat de transport eigenschappen en spinoverdrachtsmomenta beïnvloedt. Het tweede effect ontstaat in magnetische lagen met een dikte die in de buurt komt van de magnetische coherentielengte. In dit geval kunnen spinstromen die loodrecht gepolariseerd zijn op de magnetisatie door de dunne ferromagnetische laag stromen (de coherentielengte in transitie metalen is van de orde van enkele atomaire lagen, veel kleiner dan de spindiffusielengte en de gemiddelde vrije weglengte). We onderzoeken het effect van beide op de hoekmagnetoweerstand en het spinoverdrachtsmoment. Zowel de spinflipdiffusielengte in de ferromagneet, als de grensvlakspinmenggeleiding worden bepaald met een fit aan recente aMR metingen. Tot slot stellen we een driecontactensysteem voor om de ferromagnetische coherentielengte te meten.

In hoofdstuk 4 bestuderen we een kleine magnetische cantilever (bijv. een Si cantilever bedekt met een magnetische film of een geheel ferromagnetische cantilever). Zulke cantilevers kunnen dienen ter observatie van magnetomechanische momenten, die bijvoorbeeld leiden tot magnetovibrationele ("polaritonische") vrijheidsgraden en lijnsplitsingen in ferromagnetische resonantiespectra. Magnetomechanische momenten kunnen zelfs een complete magnetisatieomkering veroorzaken. Het is nog steeds erg moeilijk om nanomechanische systemen te laten werken bij microgolf frequenties, maar er ontstaan veel nieuwe mogelijkheden. We stellen voor nanoelectromechanische systemen te bouwen die worden gedreven door spin-overdracht en magnetomechanische momenten. Dit soort systemen kan de grenzen voor detectie en opwekking van beweging op de nanoschaal verschuiven en kan dienen als elektrische overbrenger van nanomechanische beweging.

Curriculum Vitae

Alexey Alexeevich Kovalev

- 21-01-1976 Born in Kirov, USSR.
- 1983-1993 18th School and 35th Mathematical School in Kirov.
- 1993-1999 Engineer Physicist in Applied Mathematics and Physics,
Moscow Institute of Physics and Technology, Russia.
Graduate research in the group of Prof. A. F. Barabanov.
Subject: Spin-charge excitations in two dimensional Kondo
lattice model of high Tc cuprates.
- 2000-2001 Visitor in Uppsala University, Sweden.
Subject: Transport in double quantum wires.
- 2002-2006 Ph.D. Research at Delft University of Technology
under supervision of Profs. G. E. W. Bauer and A. Brataas.
Subject: Electrical and mechanical magnetization torques.
Including;
1. Transport and spin-transfer effects in ferromagnet-normal metal multilayers.
2. Dynamics of the order parameter in the presence of resonant
magnetovibrational coupling.
3. Nanomechanical systems in the presence of spin-transfer and
magnetomechanical torques.

List of publications

1. Alexey A. Kovalev, G. E. W. Bauer and A. Brataas, "*Spin-transfer nanomotor*", in preparation (to be published in Applied Physics Letters).
2. Alexey A. Kovalev, G. E. W. Bauer and A. Brataas, "*Magneto-electronic circuits with ultra-thin ferromagnetic layers*", accepted to Phys. Rev. B (cond-mat 0504705).
3. Alexey A. Kovalev, G. E. W. Bauer and A. Brataas, "*Magnetomechanical torques in small magnetic cantilevers*", accepted to a special issue of JJAP: Magnetization Dynamics in Spintronic Structures and Devices (cond-mat 0511548).
4. Alexey A. Kovalev, G. E. W. Bauer and A. Brataas, "*Nano-mechanical magnetization reversal*", Phys. Rev. Lett. **94**, 167201 (2005).
5. Alexey A. Kovalev, G. E. W. Bauer and A. Brataas, "*Magnetovibrational magnetization dynamics*", JMMM 272-276, e1593-e1594 (2004).
6. Alexey A. Kovalev, G. E. W. Bauer and A. Brataas, "*Magnetovibrational coupling in small cantilevers*", Appl. Phys. Lett. **83**, 1584 (2003).
7. Alexey A. Kovalev, A. Brataas and G. E. W. Bauer, "*Spin transfer in diffusive ferromagnet-normal metal systems with spin-flip scattering*", Phys. Rev. B **66**, 224424 (2002).
8. A.F. Barabanov, A.A. Kovalev, O.V. Urazaev, A.M. Belemouk and R. Hayn "*Evolution of the Fermi Surface of Cuprates on the Basis of the Spin-Polaron Approach*", JETP **92**, 677 (2001).

9. S.V. Korepov, A.A. Kovalev, M.A. Liberman, "*Transport properties of double quantum wires with correlated disorder*", Solid State Communication **117**, No. 5, 291-296 (2001).
10. A.F. Barabanov, A.A. Kovalev, O.V. Urazaev, A.M. Belemouk, "*Spin-polaron excitations in the two-dimensional Kondo lattice with spin frustration*", Physics Letters A **265**, 221 - 224, (2000).
11. A.F. Barabanov, O.V. Urazaev, A.A. Kovalev, L.A. Maksimov, "*On the Structure of the Spin Polaron in a Two-Dimensional Antiferromagnet*", Doklady Physics **44**, No. 5, 286-289, (1999).
12. A.F. Barabanov, O.V. Urazaev, A.A. Kovalev, L.A. Maksimov, "*On the splitting of the lower band of charged elementary excitations of a two-dimensional antiferromagnet*", JETP LETTERS **68**, No. 5, 412-416, (1998).

